MULTIFUNCTIONAL NANCOMPOSITE FOAMS FOR SPACE APPLICATIONS

By

Diandra J Rollins

A DISSERTATION

Submitted
to Michigan State University
in partial fulfillment of the requirements
for the degree of

Materials Science and Engineering–Doctor of Philosophy

2016

ABSTRACT

MULTIFUNCTIONAL NANCOMPOSITE FOAMS FOR SPACE APPLICATIONS

By

Diandra J Rollins

Materials combined with a small amount of nanoparticles offer new possibilities in the synthesizing of multifunctional materials. Graphene nanoplatelets (GnP) are multifunctional nanoreinforcing agents consisting of stacks of graphene sheets with comparable properties to a single graphene layer at an overall lower cost in a more robust form. Such particles have been shown to have good thermal, mechanical and electrical properties. In addition, a low density multifunctional nanocomposite foam has the potential for multiple applications and potential use for the aerospace industry. This dissertation investigates two different microporous (foam) polymers that are modified by the addition of GnP to combat this density effect to improve the foam's macroscopic properties Three sizes of GnP with varying aspect ratio were used to improve the polymeric foams' dielectric, electrical and mechanical properties.

GnP was added to a water-blown polyurethane/polyisocyanurate (PUR/PIR) foam with a neat density of 0.16 g/cm^3. The largest aspect ratio GnP percolated to form a connected network to allow for the transfer of electrons, which resulted in a decrease of the electrical resistivity by 5 orders of magnitude. This same electrical contact improved the overall dielectric properties: increased the real permittivity by over double the amount of the neat foam, increased the electromagnetic interference (EMI) shielding effectiveness (SE) by about ten times by increase the nanocomposite's absorbance and reflectance capabilities. However, these large particles suffer from agglomerations reducing the mechanical performance even though the cell size decreased and demonstrated little interaction of the particles with the matrix by the similar glass temperature between the solid and the foam.

The edge groups on the GnP were successfully treated with either polymeric or molecular isocyanate to form urethane type groups as confirmed by x-ray photoelectron spectroscopy

(XPS). Edge treatment of the GnP only showed significant advantages for the smallest size of GnP with the highest edge density, and resulted in improved mechanical strength, and some improvements in the dielectric and shielding properties. These particles were also found to have the least effect on the molecular structure. The effect of treating the edges with polymeric or molecular groups was most dependent on the size of the GnP. The shorter urethane molecules that formed when reacted with toluene diisocyanate (TDI) on the edges had little to no effect on the mechanical strength, but was able to lower the electrical resistivity by about an order of magnitude over the same particle size treated using the same method but with a polymeric isocyanate. The larger particles treated with isocyanate demonstrated no improvement in the compressive strength over the neat particles and in general increased the electrical resistivity as well causing the dielectric performance to decrease in conjunction.

GnP was also added to a polydimethylsiloxane (PDMS) matrix, which is commonly used in aerospace applications due to its flexible properties at low temperatures and environmental resistance. The nanocomposite with the largest aspect ratio and highest loading of particles significantly improved the real permittivity and EMI shielding properties in the X-band over the neat PDMS including the reflectance and absorbance capabilities, but the GnP still showed significant agglomerations. A syntactic foam was used to improve the percolation of the GnP by first coating the hollow glass spheres (HGS) with smaller GnP prior to adding to the matrix. Although it is unclear from the SEM images if the GnP was able to stay adhered to the particles during processing, the dielectric and EMI shielding properties of the nanocomposite syntactic foam was similar to the neat while producing a foam that was 20% lighter.

This dissertation is dedicated to my family who have not only supported and encouraged me, but have been excellent role models in showing me how to get it done.

ACKNOWLEDGEMENTS

Eternal gratitude to my Savior Jesus who by His Spirit that lives in me has given me joy and peace to help me finish the race strong. Thank you to Dr. L. T. Drzal who has always been so patient in helping me develop my research skills. My gratitude goes out to my committee members: Dr. L. Matuana, Dr. R. Ofoli Dr. J. Sakamoto and Dr. Jayaraman, some have been with me a long time and others more recent, but all have been so helpful in getting to the end of this long journey. To all the CMSC staff Per Askeland, Brian Rook, Mike Rich, Ed Drown and Karen Lillis who were always so helpful in designing my experiments and answering my many questions no matter how inane they were. Special thanks to Dr. Rothwell and his graduate students, especially Jon, for being so patient with me and helping me learn so much about such unfamiliar EE concepts in a short amount of time. I also want to express my gratitude to Matt and his team at NASA LaRC, they were very accommodating and gave great feedback in regards to my project. To the past and current graduate students of the CMSC who have been my support, my friends and confidants, I look forward to seeing all the amazing things each one of you will do. Lastly I want to thank my family. Each one of you is blessing who taught me the joy of learning and I look forward to continuing to grow with each of you.

TABLE OF CONTENTS

LIST OF TABLES

LIST OF FIGURES

CHAPTER 1

INTRODUCTION

In the past several decades technology has focused on the pursuit of extremes, a striving to create products that are smaller, faster, lighter and will take people deeper and further than ever before. Meeting these challenges begins with materials and over the past decades there has been a major shift in the type of materials that have become available through research development and commercialization. Historically the evolution of materials has revolved around starting with what is readily available and modifying it with straightforward procedures to meet new demands. As our understanding grew, this resulted in the application of fundamental science to the development of new materials. From chemistry came the discovery of polymers and new formability methods, from ceramics came semiconductors and single crystals which paved the move from analytical engines to the digital computer [1] and the past few decades has seen the birth of high strength, high stiffness, lightweight fiber reinforced composites that has fundamentally changed the characteristics of materials.

As technology continues to grow and expand along with consumer expectations and inventiveness, the need for highly functioning materials becomes increasingly important. The creation of new material technologies must be weighed against the feasibility of such creations. Finding cost effective ways to synthesize these materials becomes increasingly more significant as the demands on their performance also increases.

The discovery of nanoparticles and the scientific community?s subsequent investigation of their corresponding properties added a new dimension for achieving technologies? material demands. Much research has gone towards investigating different ways of producing and utilizing nanoparticles. We have learned that with nanomaterials, many of the problems at the macroscale are greatly reduced or even eliminated at the nanoscale.. There are now many different types of nanoparticles that vary in atomic make-up, sources and morphology. The

more common ones are made from metals and metal oxides, cellulose, as well as from pure carbon. Their morphology can include spheres, particles, ribbons, solid cylinders, tubes, and platelets. The carbon-based nanoparticles have multiple promising qualities that make them desirable in polymers and composites.

Since the rediscovery of carbon nanotubes in 1991 interest in different types of carbon nanoparticles has expanded [2]. A large amount of research has been directed at synthesizing different types of carbon nanoparticles and investigating their corresponding properties. The most common types of carbon nanoparticles are carbon nanotubes, fullerene tubes, buckyminsterfullerene and graphene. These all consist entirely of carbon atoms, each with a different morphology and/or bonding structure with at least one dimension on the nanometer scale. Most of these particles are challenging to synthesize especially when a bottom-up approach is used, but such methods are still useful for understanding the fundamentals of their formation and properties, but are typically very expensive when it comes to commercialization. Some of these materials, however, can start with natural minerals and be produced with a top-down approach to yield nanoparticles, which are generally less expensive, but may also have slightly different properties.

1.1 Background

1.1.1 Polymer Nancomposites

The last half of the past century saw a revolutionary change in the materials manufacturing industry with the development of composites. Composites, as their name implies, combines two or more different materials in the hope of creating a new material with synergistic effects. One of the major material groups used in the synthesis of composites are polymers. Polymers were quite the novel material when first commercially introduced due to their high flexibility and subsequently formability, in addition thermoplastics are also recyclable and boast of relatively inexpensive production costs. This has led to them pervading all

society as everything from disposable containers, casing for electronics, furniture, sound dampeners and even in clothing. Their versatility make them an attractive material for a variety of applications, but polymers in general also suffer from poor mechanical properties, low transport properties, such as thermal and electronic, and poor thermal stability thereby limiting their applications. Polymers are utilized for composite manufacturing as the matrix and continue to be utilized as the matrix in applications were the combination of high performance and low weight are important as in the aerospace industry.

Different types of nanoparticles that have been successfully added to a variety of polymers as well for everything from electronics, bio-engineering, robotics, gas sensing, energy and aerospace applications. The application strongly dictates what type of polymer and nanoparticle to use. The type of nanoparticles include different types of metals [3, 4], metal oxides [5, 6], carbon-based nanoparticles [7, 8, 9, 10] and even nanoclays [11]. The types of polymers are just as varied; common ones include epoxy, polypropylene, polystyrene, vinyls, rubbers [12, 13, 14] and more specialized polymers including electrically conducive polythiophenes [3] and polyanilines [15]. The addition of nanoparticles to polymer foams has also been gained attention in research, the focus has been mainly on the addition of nanoclays, but also includes carbon nanotubes (CNTs), carbon black (CB) and even graphene has been utilized [16, 17, 18]. These research efforts successfully showed that low amounts of nanoparticles could be added to polymeric foams and affect everything from their mechanical properties, thermal degradation temperature, cell morphology, and even the electrical conductivity.

1.1.2 Graphene

One of the newest additions to the diverse array of researched carbon nanomaterials is graphene. Graphene consists of a single layer of sp^2 hybridized carbon atoms in a hexagonal arrangement. Graphene is the basis of many carbon nanostructures and is the base structure of graphite [19]. Graphite consists of individual layers of graphene bonded to other graphene layers through Van der Waals forces, which is the reason graphite makes such a good solid

lubricant. Although the chemistry and structure of graphite has been known for over 150 years, Geim and Novoselov from Manchester University were able to create a field effect transistor from a single layer of carbon atoms (graphene) and it allowed for the first time the characterization of a single graphene layer [20].

Graphene has been shown to have high thermal conductivity of around 3000 W/m K [21] and a Young's modulus of around 1 TPa[22]. Graphene also has unique electrical properties owing to its 2D structure including high carrier mobilities greater than 15,000 cm^2/Vs [19]. In addition, a single layer of graphene absorbs only about 2.3% of white light making it optically transparent [23]. The unique mechanical, thermal and electronic properties of single-layer graphene has resulted in an explosion in research regarding the different ways to synthesize graphene sheets. Originally graphene was thought to be unstable as historically 2D crystals were considered thermodynamically stable [19].The first successful methods resulting in single layer graphene sheets were done by removing the layer from highly oriented pyrolytic graphite with cellophane tape, which while effective for characterizing the properties of atomically thin graphene, is impractical because the yield on such a process is very low [20] and this has led to the development of other methods.

Although van-der-waals forces are weak compared to other types of chemical bonding, separating the graphene layers on a large scale proves to be a challenge. Different methodologies for making graphene include both top-down and bottom-up approaches. The most common type of top-down procedures use a combination of intercalation and exfoliation through either mechanical, thermal, chemical means, or in combination, to separate the layers. Such procedures suffer from such limitations as low through-put, inability to form single layers and/or low performance characteristics due to residual chemical groups adhering to the graphene basal plane. Bottom-up approaches focus on creating high quality, single graphene layers mainly for use in electronic devices. They tend to be expensive and time-consuming. The most popular bottom-up approaches are chemical vapor deposition and epitaxial growth, both of which grow carbon on a substrate. Some more exotic methods include the use of

polycyclic aromatic hydrocarbons (PAHs) [24] as a starting material, as well as other organic compounds, to form graphene nanoribbons [25]. The most common bottom-up and top-down approaches to graphene synthesis will now be discussed in more detail.

Some of the most utilized bottom-up approaches to making graphene include chemical vapor deposition (CVD) and epitaxial growth. Both use substrates to grow single-layer to few layer graphene on the surface. For CVD, transition metal substrates, typically single crystalline, are exposed to a hydrocarbon gas under low pressure or ultra-high vacuum (UHV) conditions. Carbon atoms deposit on the surface causing nucleation followed by growth into graphene films [26, 27]. The graphene is generally very ordered but is also typically small-scale due to processing times and rather expensive to produce due to the high costs from the substrates or the experimental environment that must be maintained that allows for such growth. Comparably 4H- and 6H-SiC is a hexagonal crystal structure with alternating layers of silicon and carbon. Treatments of SiC that focus on exposing certain faces of the crystal structure have been studied for many years [28]. Exposing the (0001) silicon face and $(000\overline{1})$ carbon face of the silicon carbide crystals to temperatures above 1300 °C in ultra high vacuum results in the formation of ultra thin graphitic films; if the films are grown in an environment that has a controlled background gas less stringent vacuum conditions are allowed [29]. Obviously both of these approaches result in thin high purity graphitic layers but due to the processing conditions result in high costs and low yield. While they show potential for high conducting electronic surfaces and lithographic patterning for circuits [30], these methods remain impractical for making cost-effective large amounts of graphene for use in nanocomposites.

As mentioned previously another less common approach to making graphene uses aromatic hydrocarbons to create segments of sp^2 bonded carbon atoms. These organic synthetic methods use polycyclic aromatic hydrocarbons (PAHs) to create highly aromatic structures or in some cases free-standing graphene nanoribbons. According to Wu et al., PAHs are considered to be "two-dimensional graphite segments composed of all sp^2 carbons" [24].

The most common method for creating ordered 2D graphene molecules uses PAHs that add flexible aliphatic chains to the aromatic cores. This causes a nanophase separation between the cores that stack due to the π-π attraction between the aromatic blocks, the alkyl chains then fill the periphery [24]. These supramolecules are then aligned into thin films for use in different electronic devices. To develop the graphene nanoribbons from start to finish the process results in a 65% yield and develops individual graphene sheets from 8 to 12 nm in length [31, 32]. These graphene sheets tend to align themselves into ribbons when cast onto a silica substrate with 2.5 nm between each ribbon producing objects with 100 nm in diameter and up to 5 μm in length [32].

As the exceptional properties of graphene became more widely known, there was a need for a cost-effective method for synthesizing graphene. Some of the potential applications for graphene involve using them as reinforcing agents. This required that the sheets be free-standing so the they could be easily added to a material matrix, but makes allowances for the purity and thickness of the particles outside of the stringent requirements for electronic devices. The most common commercial methods to make graphene flakes include chemical reduction of graphite oxide and thermal exfoliation of graphite intercalated compounds (GICs). These methods produce contrasting types of graphene particles, but both are able to produce robust flakes that are on the order of a μm or more.

The first top-down approach starts with converting graphite to graphite oxide (GO). This method is appealing because of its ability to produce thin carbon sheets, which is more commonly referred to as graphene oxide. Because GO contains multiple sp^3 bonds this material shows a much higher electrical resistance (films demonstrate 4 MΩ/square) and therefore must be reduced back to a material much more similar to graphene [33]. Natural graphite is used as the starting material and converted to GO using strong acids according to either the Hummers or Brodie method as the two most popular processes [34, 35]. Upon oxidation the graphite still has aromatic regions where the carbons are now sp^3 instead of sp^2 because a large number of the carbons are now bonded to oxygen and hydrogen groups.

This also results in a wrinkling of certain areas of the sheets along with the sections that still have a planar ring structure in addition to structural defects [36, 37]. To get single or few layer sheets the layers must be separated and the two most common methods use either thermal or mechanical means. For the thermal method, dried GO flakes are exposed to rapid heating, generally in excess of 1050 °C forming a fluffy like appearance or worms; this is important to note because changing the processing temperature affects the rate of reduction and allows for the option of tuning the electrical conductivity to desired levels [38, 39]. After the resulting worms are broken apart into single to few layer wrinkled graphene sheets [40]. Reduced GO using the thermal method has been successfully made into films that show a reduction in electrical resistivity down to less than 1 kΩ/square [33].The second method that uses mechanical energy takes advantage of the hydrophillic nature of GO and disperses the material in water using mechanical agitation to produce very thin sheets. These sheets are then commonly reduced using hazardous chemicals like hydrazine hydrate. The resulting wrinkled sheets are very thin and once solidified into films or paper show conductivities on the order 10^2 S/m [41, 42].

The second commercial top-down approach relies on using graphite intercalated compounds (GICs) as the starting materials. GICs are graphite compounds that contain acid molecules adsorbed between the layers, which when exposed to high heat the intercalated groups expand forcing the layers apart once again creating worms [43]. Just like the method for GO, the worms are pulverized resulting in graphene flakes many layers thick due to the inability of ensuring that intercalated groups are between every layer, but because there is no disruption of the basal plane structure as the intercalated molecules are adsorbed not bonded, there are less defects and no wrinkling. In general, the flakes tend to also be larger on the order of several microns in diameter. When these exfoliated graphene flakes are compacted into a 'paper' using vacuum filtration the electrical conductivities are easily 10 times greater than that reported using reduced GO [44, 38, 33]. A schematic approach of the process using GICs is shown in Figure 1.1.

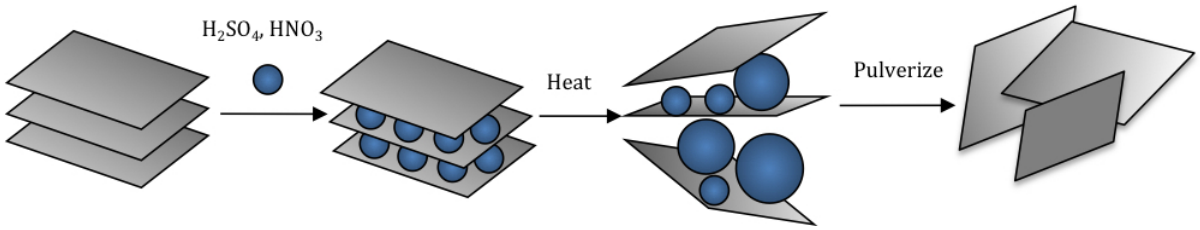

Figure 1.1: Schematic for synthesis of exfoliated multilayered graphene flakes from GICs

Due to the multifunctional properties of graphene, this material, sometimes in conjunction with other fillers, has been used extensively in the synthesis of high functioning polymer composites. This includes everything from high-density polyethylene, polyurethanes, polyetherimides, poly(p-phenylene sulfide), polypropylene and rubbers, just to name a few [10]. Most of the polymer nanocomposites have used graphene powders, either reduced GO or exfoliated graphene. The challenge with creating an effective resulting nanocomposite relies on there being a good interaction and dispersion between the graphene flakes and the matrix. If the interaction is poor agglomerations form which affect the composites' macroscopic properties, more specifically the mechanical performance. For this reason often the graphene is functionalized before adding to the composite. Reduced GO has epoxide and carboxylate groups readily available to functionalize, whereas, the exfoliated graphene flakes have a limited number of hydoxyl and carboxylate edge groups available. For reduced GO chemical functionalization is commonly and effectively employed to improve the dispersion [45, 41, 46]. For the exfoliated graphene flakes adding surfactants which interact with the $\pi - \pi$ bonds and the matrix is a more promising functionalization route as this method maintains the basal plane structure of the graphene [47, 48].

As mentioned previously, polymeric nanocomposite foams are gaining attention due to their great potential for a myriad of applications. Its most obvious advantage is that a cellular material has vastly lower density due to its cellular structure that increases the volume. In addition using a polymeric material generally decreases the material and processing costs and by combining such a material with a multifunctional nanoreinforcing agent such as graphene,

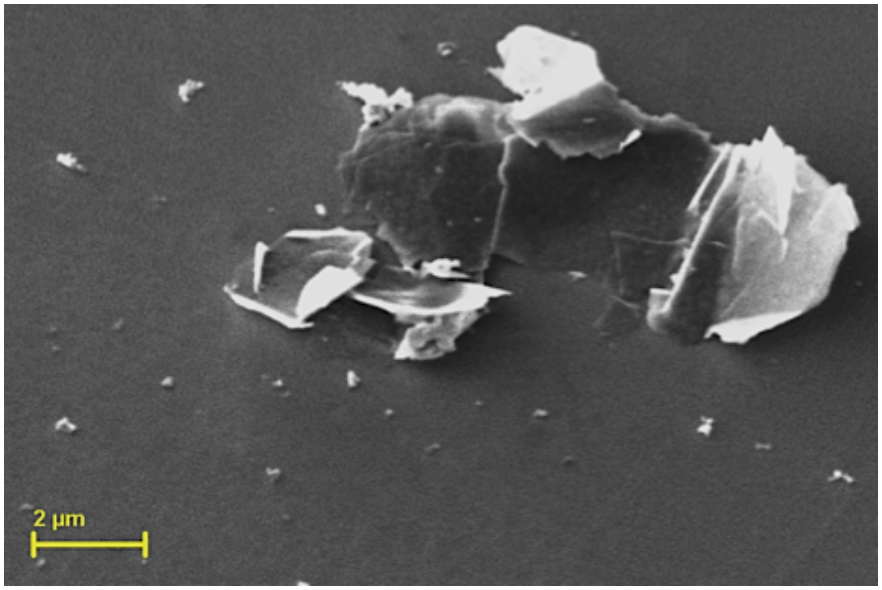

Figure 1.2: SEM image of XG Sciences' graphene nanoplatelets (GnP) which consists of multiple layers of graphene.

results in the synthesis of a multifunctional low-cost, light-weight material that could have many useful applications especially in the aerospace industry.

Aerospace technologies was the main focus of this research as it was funded by the NASA Space Technologies Research Fellowship (NSTRF), which is designed to identify graduate research projects that align with NASA's goals, specifically identified through their 14 Technology Roadmap [49]. A polymer nanocomposite foam was selected as the focus for this research and met the objects of TA (technology area) 10: Nanotechnology and TA 12: Materials, Structures, Mechanical Systems and Manufacturing [50]. For the nanoparticle, a commercial graphene nanoplatelet (GnP) was chosen from XG Sciences (see Figure 1.2) which is synthesized from GICs. It has a cost similar to that of high structured carbon black and consists of multiple layers of graphene giving them a thickness between 3-8 nm. They have high purity and include about 5 atomic percent of reactive edge groups, as confirmed by x-ray photoelectron spectroscopy (XPS).

1.2 Research Objectives and Goals

The goal of this research project is to create a multifunctional material using a porous polymer as a matrix and utilizing a graphene nanoplatelet (GnP) as a multi-functional additive to modify the foam. Using a porous polymer as a matrix results in further weight savings an important consideration in aerospace applications. The challenge with working with foams is that many properties decrease as the density does as well, thus the need for nanoreinforcement agent to combat that effect. Such a nanocomposite could potentially show improved thermal performance, electrical properties and dielectric properties while maintaining good mechanical performance. By adjusting the nanoparticle loading and type there is the potential that the foam properties could be tailored to specific applications. One objective is to gain a better understanding of how a 2D particle orients within a 3D structure, but also to determine methods to improve the interaction between the GnP and the matrix. The techniques are focused on cost-effective, readily available synthesis methods, and as a result of this research, the knowledge gained would help in the development of nanoparticle modified polymeric foam systems at a relatively low cost. This research involves the investigation of a multi-phase system and the knowledge gleaned could be applied to other composite systems. This investigation includes determining the validity of different techniques used to disperse nanoparticles in a polymer matrix, observing different types of dispersion and its effect on the overall properties, and is a step towards fully characterizing the ideal dispersion that needs to be achieved. Dispersion is important for the formation of the percolated network that allows for electron conduction. Thoroughly characterizing the dispersion is important for the determining the necessary parameters needed to create a conductive network that does not adversely affect the mechanical properties for the modeling of nanoparticle systems.

Two different polymer matrices were chosen, along with two different kinds of foam and multiple types of GnP to develop the nanocomposite foam. The first is a rigid polyurethane/polyisocyanurate (PUR/PIR) foam with a chemical blowing agent. Polyurethane

(PUR) is readily available and heavily utilized commercial material and its foam counterpart has been extensively studied. PUR foam is commonly used in everything from building insulation to sound proofing to furniture. It has been around for decades and heavily researched for commercial applications, which is why the material has a well understood processing-structure-property relationships. It was an ideal polymeric foam to characterize the changes the addition of nanoparticles makes on the molecular, microscopic and macroscopic scales of the foam with a breadth of potential applications. Polyisocyanurate (PIR) is the next generation of PUR; it has better thermal properties due to its higher cross-link density from the formation of trimer groups and better heat and flame resistance [51]. PIR is formed from polyurethane by adding a catalyst that causes cyclotrimerization reactions to occur [51].

The second polymer type is a flexible high performance polymer already utilized in the aerospace industry. Silicones are used as everything from caulking agents, in electronics and kitchen bakeware. It has very unique thermal properties due to its unusual inorganic/organic structure. There are many different types of silicone, but one of the most common is polydimethylsiloxane (PDMS). Like its name implies it has a silicon-oxygen backbone with methyl side groups. It is not as well understood as polyurethane and much of the research of silicones is protected by companies. However, its many uses and flexible properties up to low temperatures, generally less than -50 °C, suggests a material that could benefit from the use of multifunctional reinforcing agent. Silicon dioxide is already added to many different types of silicone to improve their mechanical properties. As mentioned earlier due to the proprietary nature of silicones this research will focus on the effect GnP has on a readily available commercial system. There are many different types of curing approaches available, but room-temperature-vulcanization (RTV), which allows for cure at room temperature, is commonly utilized. The PDMS elastomer comes in two-parts. One part contains the liquid rubber base and the other the curing agent (catalyst). Commercial PDMS foam systems commonly have large concentrations of silicon dioxide particles in them greater than 15 wt%. Since one of the properties the GnP could potentially improve is the electrical performance

having an insulting filler would disrupt the formation of the conductive network. For this reason PDMS elastomer with no fillers was chosen as the matrix and hollow glass spheres (HGS) were added to create a syntactic foam. The HGS are used as a template to form a percolated network by first coating each sphere with GnP before adding to the PDMS. Each sphere then acts as single conducive point in the network and when the HGS are close enough together electron conduction can occur.

Lastly for this research different types of GnP will be used to gain insight into the effect that the size has on the resulting polymeric foam. If electrical contact matters than aspect ratio is an important factor to keep in mind when trying to reach the percolation threshold at low loadings [52]. For this reason xGnP-M-25 was selected. All M-grade materials have a surface area between 120-150 $m/^2g$, and thicknesses between 6-8 nm, in addition xGnP-M-25 have an average particle diameter of 25 μm. These particles, though, are restricted to areas in the foam that accommodate their large size so a smaller particle is also used; xGnP-M-5 which has an average diameter of 5 μm. These M-grade particles are very similar in appearance as shown in Figures 1.2 and 1.3 (a). The larger particles have larger basal planes which are good for conduction, but can also cause the platelets to re-stack due to the Van-der-Waals attraction of the layers, so particles that have a distinctly larger edge density were added as well. The smallest particle grade available is the C-grade. They are high surface area platelets with thicknesses around a few nm. Their diameters are also < 2 μm and commonly on the scale of hundreds of nm, giving them dimensions similar to that of reduced GO, but still have better basal plane integrity as the total additional groups of oxygen and nitrogen make up only about 11 atomic % according to XPS, part of which is due to the higher concentration of edges. One of the main groups that form on GnP are hydroxyls, which is one of the reaction groups in the formation of urethane, in addition it is believed that one of the reasons silica disperses so well in silicone is due to the interaction with the hydroxyl groups on the silicon dioxide [53]. This means that there was the potential that the GnP could interact well with both matrices and even when the interaction is poor the edge-groups provide a way

to improve the dispersion through chemical means when the mechanical dispersion methods prove insufficient.

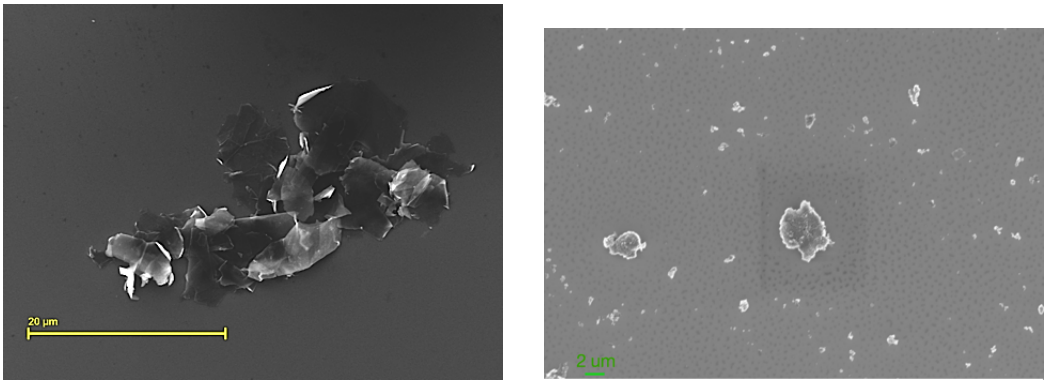

(a) (b)

Figure 1.3: SEM images of different grades of xGnP: (a) XG Sciences M-grade xGnP of average diameter of 25 µm and thickness of 6-8 nm(b) XG Sciences C-grade xGnP after ultrasonication in acetone.

The goal of this project is to create a multifunctional nanocomposite foam through the use of a multifunctional graphene filler. What follows in this dissertation is an investigation into the effect that GnP has on resultant properties of the foam. This is done by observing the effect GnP has on the local molecular structure, on the microscopic structure and finally the macroscopic properties; then utilizing different means to improve the interaction and thereby the dispersion. Chemical means through edge functionalization and coupling agents as well as more rigorous mechanical dispersion methods have both been employed. The effects of these methods was not only observed in changes in macroscopic properties, but images showing the particle dispersion in the foam with and without a template were also important tools for characterization. Different challenges came from working with a chemically blown foam versus a syntactic foam, but it was found that both were affected by the loadings and aspect ratio of the particles and the effect these had on the dispersion was a key part and will be discussed in this research.

CHAPTER 2

MATERIALS AND EXPERIMENTAL TECHNIQUES

2.1 Materials

2.1.1 Polymer Matrices

This research focuses on modifying two different types of polymer foams with the addition of a multifunctional reinforcing nanomaterial. The first foam has a polyurethane/polyisocyanurate matrix that utilizes a chemical blowing agent to polymerize and evolve gas simultaneously. The syntactic foam uses hollow glass spheres as the cells and the matrix is a flexible polydimethylsiloxane (PDMS). The multifunctional filler is both foams are graphene nanoplatelets (GnP).

2.1.1.1 Rigid Polyurethane/Polyisocyanurate Foam

Polyurethane (PUR) was chosen as the material matrix for the blown foam because it is a readily available commercial material used heavily in industry. It has been around for decades, heavily researched and characterized so there is a well understood process-structure-property relationship. It is a standard polymer of a relatively low cost, which means it has great potential for many different applications as a cost-effective alternative. However, it is currently limited in its applications due to the rather limiting performance properties that are characteristic of polymers, such as its low mechanical and dielectric performance as well as poor thermal stability and high electrical resistance. This material could then greatly benefit from the addition of multifunctional nanoreinforcement agent.

Polyurethane (-NCOO) is a result of the addition reaction between polymeric isocyanate (-N=C=O) and hydroxyl (-OH) groups [51]. The reaction for synthesizing polyurethane is shown in Figure 2.1 along with all other reactions of focus in this system. This material

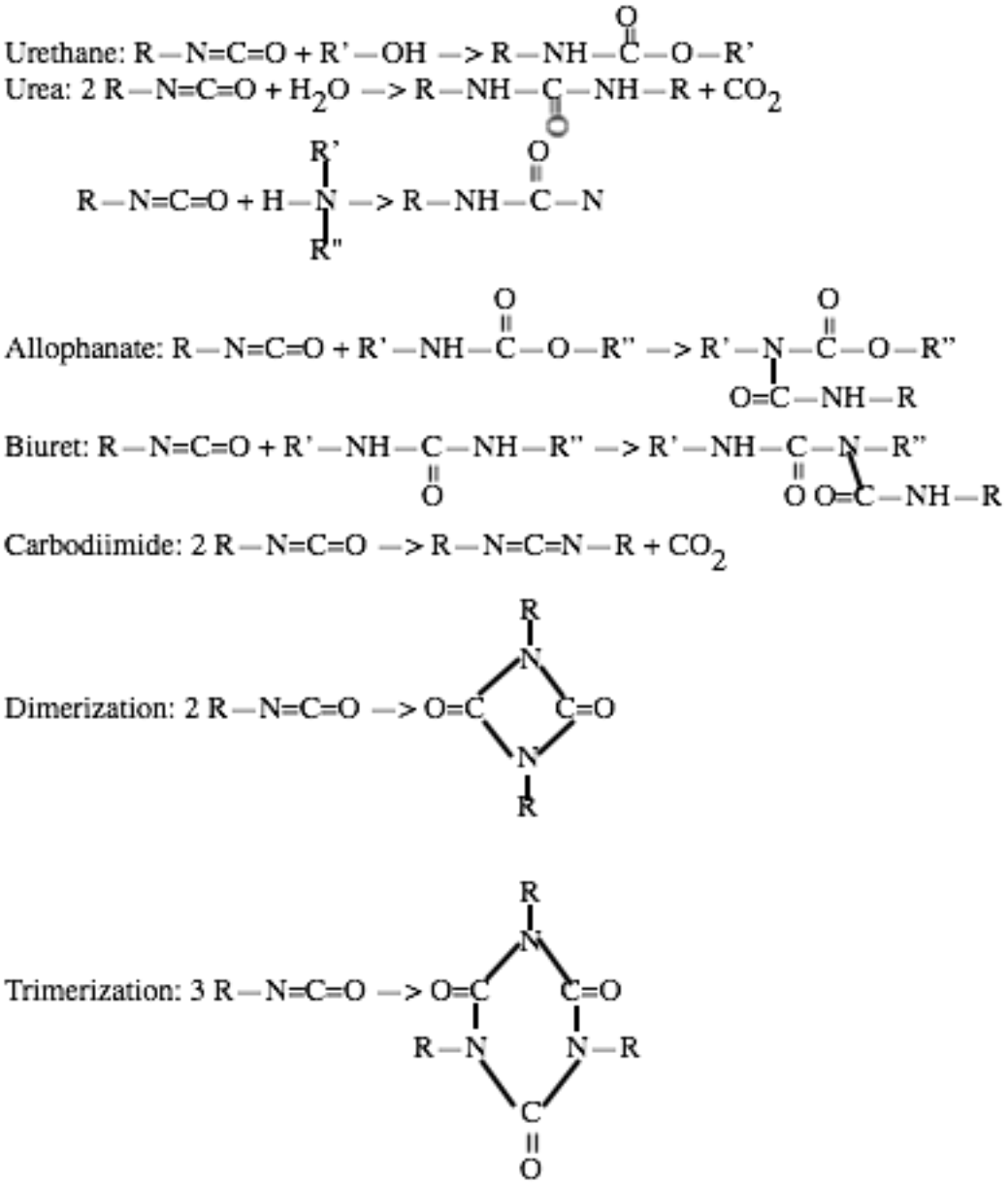

Figure 2.1: Chemical reactions for polymerization and gas evolution in PUR/PIR foam

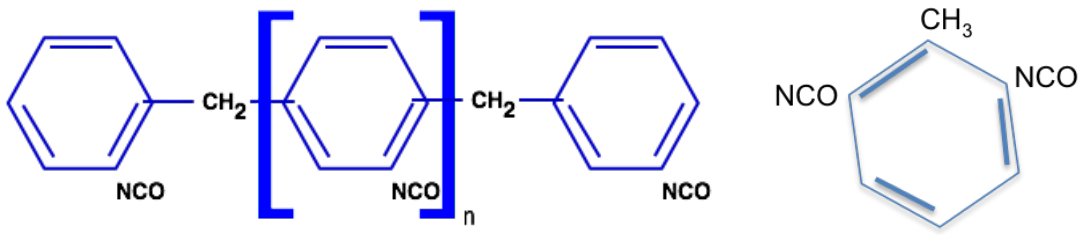

(a) (b)

Figure 2.2: Chemical structures of isocyanates used in the synthesis of PUR foams: (a) Polymeric diphenylmethane diisocyanate (pMDI) (b) 2,4'-Toluene diisocyante (TDI)

can be foamed using either physical or chemical blowing agents. For the physical blowing agent the polyurethane is synthesized and cured prior to infusing with a gas. A chemical blowing agent adds a chemical component to the polyol side prior to polymerization. The system in this researches utilizes an environmentally friendly chemical blowing agent, which is water. Isocyanate is commonly reacts with water and with the assistance of a blowing catalyst this reaction is accelerated to readily form carbon dioxide and urea. This is polyurethane/polyisocyanurate (PUR/PIR) mixture. PIR contains trimers that form from the isocyanate with the assistance of a catalyst to promote cross-linking giving the polymer better thermal stability [51].

Common isocyanates used for making polyurethane include toluene diisocyanate (TDI) and methylene diphenylene diisocyanate (MDI) both shown in Figure 2.2. Because the foam is a polyurethane/polyisocyanurate blend, polymeric MDI (pMDI) was chosen as the isocyanate due to the fact TDI is an unsuitable isocyanate for PIR foam preparation [51]. Polymeric MDI is a liquid mainly composed of 4,4'-MDI isomers and up to 10% of 2,4'-MDI and has the general structure shown in Figure 2.2 (a). Polymeric MDI (Rubinate M) has been supplied by Huntsman and has a viscosity of 190 mPa s^2, a specific gravity at 25 °C of 1.23 and an isocyanate content of 31.1 %NCO [54]. Huntsman also supplied two difunctional polyols Jeffol FX-31 and Jeffol G30-650. Jeffol FX-31 is a low viscosity at 25 °C (250 mPa s^2) polyol with a hydroxyl number of 240 %OH compared to Jeffol G30-650 which has a viscosity of

880 mPa s^2 and hydroxyl number of 650 %OH [54]. To keep the viscosity as low as possible ethylene glycol reagent from CCI (#216500) was utilized as one of the hydroxyl components as it has a water-like viscosity, and hydroxyl content of 181 %OH [55]. These isocyanate and hydroxyl values are used to determine the index as shown in the set of equations in Equation 2.1 [51]. The index number is used as a way to determine whether every NCO group has a corresponding OH group. A number above 100 means there is an excess of NCO, for rigid PUR foams this value is normally between 105 and 125 and for rigid PUR-PIR the index is generally between 180 and 135 [56].

$$\text{Amine Equivalent} = \frac{\text{Formula weight of } NCO * 100}{\%NCO} = \frac{42.02 * 100}{\%NCO} \tag{2.1}$$

$$\text{OH Equivalent} = \frac{\text{Formula weight of } OH * 100}{\%OH} = \frac{56.11 * 100}{\%OH} \tag{2.2}$$

$$\text{Isocyanate Index} = \frac{\text{Number of } AmineEquivalent}{\text{Number of } OHEquivalent} * 100 \tag{2.3}$$

For the PUR foam the additional components are the chemical blowing agent, polymerization and blowing catalyst, and the surfactant to promote uniform bubble formation. As mentioned before the chemical blowing agent is distilled water with an approximated hydroxyl value of 7 %OH. The surfactant and catalysts were all supplied by AirProducts. The surfactant is a polysiloxane (Dabco DC193) which helps in cell formation and has no hydroxyls [57]. The blowing catalyst is a commonly used commercial product (Dabco BL-11) with 200 %OH [57]. The polymerization/gelling catalyst (Dabco TMR-3) aids in the formation of trimers that are a key characteristic of PIRs, and has a large hydroxyl value of 2244 %OH [57]. Because it was desired that the foam matrix be a PUR, PIR mixture a value was chosen and the corresponding ratios of the individual components was then back-calculated from there taking into account that the desired density is around 0.16 g/m^3. Lastly, 2,4-TDI from TCI Chemicals (#T0264) was used to treat the edges of the GnP [58]. The concentration of each component in the system are shown in Tables 2.1 and 2.2.

Table 2.1: Ratio of concentrations of hydroxyl liquids used in PUR/PIR rigid foam formulation.

Polyol Components	**Concentration (parts)**
Jeffol FX31-240	70
Jeffol G30-650	15
Ethylene glycol	15

Table 2.2: Concentration of different components used for foam formulation normalized to parts per hundred of polyol (pphp).

PUR/PIR Components	**Concentration (pphp)**
Polyols	100
Polysiloxane surfactant	0.8
Blowing catalyst	0.05
Cyclotrimerization catalyst	0.6
Distilled water	0.4
pMDI	158

2.1.1.2 Flexible Polydimethylsiloxane

The second polymer matrix used in this research is a flexible polydimethylsiloxane (PDMS). It is a unique polymer consisting of an inorganic backbone (Si-O) and organic methyl side groups. This structure causes it to be flexible below room temperature as its glass transition temperatures is generally less than -50 °C. This high-performance polymer is used heavily in the aerospace industries and was identified as another polymer matrix that could greatly benefit from the addition of nanoparticles for this reason. The PDMS used in this experiment is from Momentive product RTV615 [59]. It is a consists of two-parts, a liquid rubber and catalyst that upon mixing cure to form a PDMS elastomer.

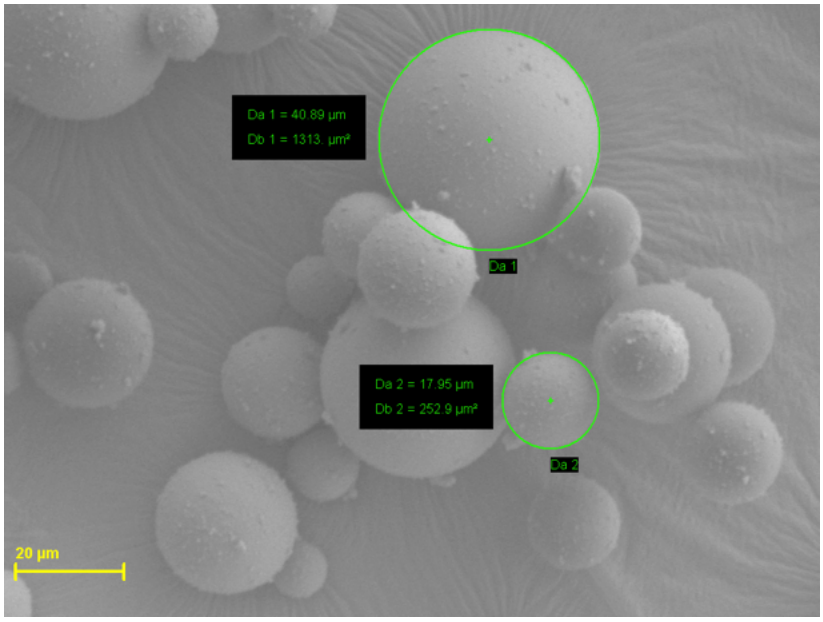

Figure 2.3: SEM image of 3M™ iM16K glass bubbles sprinkled with amorphous silica on surface and measured diameters

2.1.2 Hollow Glass Spheres

The glass bubbles iM16K (#98021327964) were donated by 3M™. The white powder contains soda lime borosilicate glass spheres with an average diameter of 20 µm and contain less than 3% of a synthetic amorphous silica that is necessary to ensure the glass spheres flow [60]. The hollow glass spheres (HGS) that contain the amorphous silica granules can be seen in Figure 2.3 These glass bubbles were chosen for their high crush strength of greater than 110 MPa that makes them able to withstand the thermal expansion coefficient of the PDMS [60]. Lastly, as the glass spheres are hollow they have a density of 0.46 g/cm^2[60]. A silane coupling agent was used to adhere the GnP to the glass bubbles. The binder is a trimethoxysilylpropyl modified polylethenimine silane (tPEI) from Gelest (#SSP-060), a schematic of which is shown in Figure 2.4 [61].

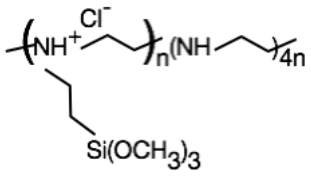

Figure 2.4: Chemical structure of trimethoxysilylpropyl modified polylethenimine, the silane coupling agent used to adhere GnP to HGS.

2.1.3 Nanofiller

The nanofiller used in this foam is a cost effective material sourced from XG Sciences, graphene nanoplatelets (GnP). Graphene consists of a single layer of hexagonally arranged of sp^2 carbon atoms. This unique bonding and structure gives single layer graphene very high in-plane properties. High tensile strengths of 1 TPa [22], high electrical conductivity of 10^4 S/m [62] and high thermal conductivity around 3000 W/m K [21]. It is made through the exfoliation of intercalated acid molecules between layers graphite, which upon heating force the layers apart, the process is described in Figure 1.1 on page 8. Because it is difficult to intercalate acid groups between each layer GnP generally consists of stacks of graphene sheets making it a much more robust nanoparticle, but has property similar to single graphene sheets. It comes in a variety of types and sizes. In this research both a M-grade product and C-grade product were utilized. The difference between the two are their surface areas and thicknesses. M-grade materials have surface areas of around 120 m^2/g and thicknesses of 6-8 nm, in addition two sizes were used that had average lateral dimensions of 25 (GnP-25) or 5 (GnP-5) μm[63]. The other C-grade type is a high surface area material of 750 m^2/g with average diameters of less than 2 μm (GnP-750), but the as-received material appears as sub-micron aggregates [63]. All as-received GnP is heated at 450 °C prior to adding to the nanocomposite foam.

2.2 Experimental Procedure

2.2.1 PUR/PIR Nancomposite Foam Synthesis

The foam synthesis is done according to the steps below:

1. The two polyols with ethylene glycol are combined and stirred for 2 h according to the ratios listed in Table 2.1.
2. The surfactant, catalysts and blowing agent are added to the polyol blend and stirred for one hour according the ratios in Table 2.2.
3. If GnP is required in the formulation it is then added to the polyol blend at the correct weight ratio.
    - 3 wt% of the 5 wt% total GnP-25.
    - 6 wt% of the 8 wt% total GnP-5 and GnP(750).
4. GnP is high-speed shear-mixed for 2 min at 1600 rpm and 1 min at 2400 rpm followed by ultrasonication at 100 W with a 2.54 cm probe from 5 to 20 min depending on the concentration and type of GnP.
5. Polymeric MDI is added into a separate container.
6. If GnP is required the remaining wt% is added into the pMDI so that the viscosities of the two components is kept as low as possible.
7. Polymeric MDI blend follows the same high-speed shear-mixing protocol and is then ultrasonicated with the same probe for the same conditions until blended generally for 5 to 15 min.
8. The two blends are combined with an immersion blender for 45 s.
9. The material is poured into a mold to free-rise and allowed to cure overnight at room temperature.

The dispersion of GnP in polyol blend is checked using an reflectance optical microscope to ensure that the particles are well dispersed. Samples were also synthesized that contained no blowing catalyst, agent or surfactant. The procedure and concentration of components stays the same except step two is modified to only stir for 30 min with only the addition of the polymerization catalyst. The mold is a stainless steel pan covered in non-porous teflon paper and has the dimensions: 5 cm x 15 cm x 25 cm.

2.2.2 Edge-Functionalization of GnP

As-received GnP contains hydroxyl-edge groups, which from the details of the chemistry stated in section one readily react with polymeric isocyanate to for form polyurethane. Polymeric MDI was added to the GnP in one of two ways. For the first method, GnP are heated to above 100 °C for an hour to removed adsorbed water molecules, enough pMDI is added to completely cover the GnP. This mixture is then heated to 140 °C either overnight or for one hour then cooled prior to removing the excess pMDI. The GnP is washed with acetone, centrifuged to collect the particles and the excess liquid is decanted and the process is repeated multiple times. The other procedure is much more involved and focuses on creating a monolayer of urethane type groups on the particle surface according to the following steps:

1. GnP is dispersed in acetone using a 2.54 cm ultrasonication probe at 100 W at a concentration of about 6 g of GnP per every L of acetone.

2. The solution is ultrasonicated for at least 1 h. The solution is drop cast onto a glass slide to observe the dispersion with an optical microscope.

3. A small amount of pMDI is added to the solution at a ratio of 64 μL for every 6 g of GnP.

4. Ultrasonication with the same probe and power is done for an additional hour.

5. The edge-functionalized GnP is then retained using the same washing-centrifuging-decant procedure detailed earlier in the chapter.

6. After the last decant the material is dried overnight at slightly elevated temperature.

This same procedure was also done used to treat the GnP with TDI in place of pMDI.

2.2.3 Nanocomposite PDMS

The neat PDMS elastomer is made by pouring part A then part B into a mixing vessel at a ratio of 10:1 by weight. The material is then hand mixed for 30 s followed by high speed shear mixing at 3000 rpm for 2 min. After mixing it is poured into a secondary container for degassing then cast into molds. The cast specimens are then baked at 100 °C for 1 h. For the samples that contain GnP, it is added after the hand mixing of part A and B and prior to the high speed shear mixing. The weight additions are determined relative to the neat sample. The GnP/PDMS is then mixed at 3000 rpm for 2 min followed by an additional minute after the material cools down to limit how hot the material gets during mixing to avoid curing.

2.2.3.1 Coating Glass Microspheres with GnP

The glass bubbles are coated with GnP-5 and GnP(750) prior to adding to the PDMS elastomer. The total weight percent (Wt%) of GnP needed to coat the spheres with 5 layers is given by equation 2.4 below:

$$(Wt\% = \frac{6 * t * \rho_{GnP}}{D_{iM16K} * \rho_{iM16K}}) * 5 \tag{2.4}$$

In this equation, t is the thickness, ρ_{GnP} and ρ_{iM16K} is the relative gravity of the GnP and glass bubbles, respectively, and D_{iM16K} is the average diameter of the glass bubbles. The total amount is multiplied by 5 as 5 layers was chosen to ensure a conductive coating forms on the surface. The resulting amount of GnP-5 and GnP(750) was divided by two since both types of GnP were simultaneously coated on the surface. The procedure is as follows:

1. GnP(750) is added to reverse osmosis (RO) water at a ratio of about 90 mg to 500 ml.
2. The solution is ultrasonicated with a 2.54 cm probe at 100 W for 1 h.
3. The GnP-5 is then added followed by additional ultrasonication for 1 h with the same parameters.
4. Add the tPEI binder to the solution at a ratio of 1:1 wt% to GnP.
5. Ultrasonicate for 4 min with a 2.54 cm probe at 50 W.
6. Slowly add the HGS while stirring
7. Continue stirring overnight
8. The GnP coated glass bubbles are then collected by filtration before drying.
9. After drying the GnP coated iM16K is high speed shear mixed at 1200 rpm for 30 s to break up the clumps.

The resulting glass bubbles are shown in Figure 2.5. Comparing the neat and GnP coated iM16K there is more fluffy platelet like appearance on the surface due to the GnP and especially the very thin GnP(750).

2.2.3.2 PDMS Syntactic Foam Procedure

The initial steps are the same for the neat PDMS sample where the two parts of the elastomer are combined by hand mixing for 30 s. The glass bubbles are added by volume percent to the PDMS elastomer prior to being high speed shear mixed at 3000 rpm for 2 min. The GnP coated glass bubbles are mixed for an additional min at 3000 rpm after cool down to ensure adequate mixing and to prevent the material from getting hot enough to start solidfying. The material is then poured into a secondary container for degassing, followed by casting into molds. The material is then heated at 100 °C for 1 h.

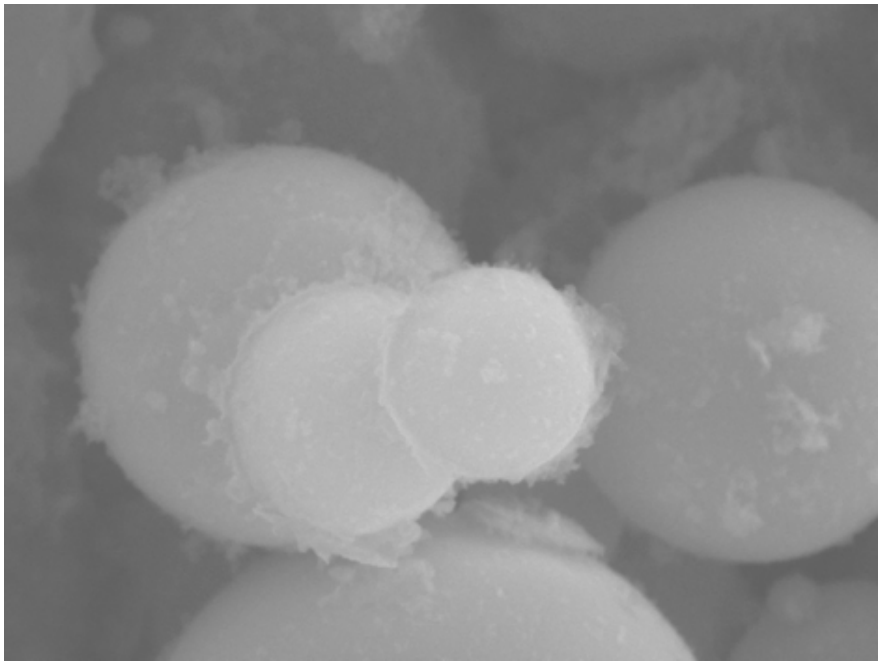

Figure 2.5: SEM image of HGS coated with GnP-5 and GnP(750) after drying. The sample was not coated prior to imaging.

2.3 Testing Procedures

The exothermic behavior of the foam was observed with a metered probe. After the foam was mixed and poured into the mold the probe was placed in the container, held in place at an angle with a binder clip. The temperature was then recorded for 500 s, which is the maximum number of data points the meter could hold.

2.3.1 X-ray Photoelectron Spectroscopy

Due to the small amount of functional groups expected to be on the surface GnP, x-ray photoelectron spectroscopy (XPS) was chosen to characterize the chemical groups. In addition to XPS being a surface technique, with a penetration depth of up to 1 μm, XPS measures the binding energies of the surface groups, which also can give insight then to the chemical groups as well as the elements on the surface. Because M-grade xGnP has no nitrogen groups prior to functionalization the nitrogen spectra was focused on to determine what type of functional

groups actually form on the surface after chemical treatment. First a scan was done on a neat PUR/PIR sample that contained no GnP. The only peak that appeared on the nitrogen spectra was a broad peak at 400 eV, which is then thought to be do to urethane-type bonds. The nitrogen spectra of the edge-functionalized GnP shows three peaks: the first is centered at around 399 eV and is commonly attributed to amine groups and probably represents urea [64], the second is the urethane peak and the third is centered at around 401.3 eV, the highest binding energy is probably due to pMDI groups. The pMDI could be from unreacted pMDI or simply to unreacted segments of the polymer chain.

2.3.2 Thermal Analysis

Thermogravimetric analysis (TGA) was used to determine how the material degrades with temperature at a rate of 20 °C/min in a nitrogen environment at a resolution of 4. Differential scanning calorimetry (DSC) was used to determine the glass transition temperature (T_g). The reference was an empty pan. The samples were run at 10 °C/min to 140 °C before being allowed to cool to 50 °C at a rate of 20 °C/min. Each sample was run twice and the T_g was determined from the cooling ramp.

2.3.3 Microscopy

An optical reflectance microscope was used to check the dispersion of GnP in the solution by dropping a drop of the solution onto a glass slide with a disposable pipette. In addition, scanning electron microscopy (SEM) was utilized to image the cell structure of the foam as well as the dispersion of the GnP. The samples are always adhered to the stub with conductive carbon paste. For the rigid PUR/PIR the samples are cut for imaging, whereas the PDMS samples the images were taken of the torn surface after a small cut on the surface. Field emission SEM, a high resolution SEM, in combination with focused ion beam (FIB) was able to cut sections of the PUR/PIR rigid foam to determine how well the platelets dispersed. FIB uses a stream of gallium ions to cut the material by rastering through the material.

Images of the cell structure were taken on the SEM. Sixty cells were measured with ImagePro software to determine each cell's maximum, minimum and average diameter.

2.3.4 Mechanical and Electrical

Four specimens were cut from the PUR/PIR foam samples with dimensions 25.8 c^2m by 2.54 cm thick. The specimens are then tested on a universal testing system (UTS) placed between two parallel platens compressed to 10% deflection at a rate of 2.5 mm/min. Electrical resistivity (AC) was done on three specimens either cut to the dimensions of 3 mm thick by 10 mm wide by 40 mm long or cast those dimensions for the flexible PDMS. A two-point probe with a distance of 1 cm between the probes was in contact with the specimen surface with the assistance of conductive silver paint, measurement was taken on the Gamry.

2.3.5 Electromagnetic Performance

The dielectric properties were determined using a transmission line system, which includes a vector network analyzer (VNA) connected to a waveguide. The waveguide dimensions were as follows: 10.5 mm by 22.9 mm by 7.4 mm thick. Three specimens were cut to this dimension for the rigid PUR/PIR foam or cast for the flexible PDMS. The NRW (Nicholson and Ross [65] and Weir [66]) algorithm was used to determine the complex relative permittivity and permeability according to the relationships below assuming the samples are isotropic. Relative refers the fact that the permittivity and permeability are a ratio relative to the permittivity

and permeability of free space. All testing was done at room temperature.

$$\mu_r^* = \frac{2\pi}{\Lambda\sqrt{k_0^2 - k_c^2}}\left(\frac{1+\Gamma}{1-\Gamma}\right) \tag{2.5}$$

$$\varepsilon_r^* = \frac{1}{\mu_r^* k_0^2}(\frac{4\pi}{\Lambda^2} + k_c^2) \tag{2.6}$$

$$\text{where, } X = \frac{S_{11}^2 - S_{21}^2 + 1}{2S_{11}} \tag{2.7}$$

$$\Gamma = X \pm \sqrt{X^2 - 1} \tag{2.8}$$

$$T = \frac{S_{11} + S_{21} - \Gamma}{1 - (S_{11} + S_{21})\Gamma} \tag{2.9}$$

$$\frac{1}{\Lambda^2} = -\left[\frac{1}{2\pi L}\ln(T)\right]^2 \tag{2.10}$$

and

$$k_c = \frac{2\pi}{\Lambda} \tag{2.11}$$

$$k_0 = 2\pi/\lambda_0 \tag{2.12}$$

k_0 is the wavenumber in air. It also used in applying a phase correction factor, $e^{-\gamma_0 L}$, for the transmission scattering parameter, $S_{12} = S_{21}$, to account for the transmission line length displaced by the sample of length L, where $\gamma_0 = jk_0$. In addition, S_{12} in this set-up is a measure of the respective voltages when a material is present and when it is not present, and is used in the definition of the shielding effectiveness according to the equation 2.13,

$$SE_T = 20\log\frac{V_1}{V_2} = 20\log|S_{12}| \text{ (dB)} \tag{2.13}$$

The total shielding effectiveness is the sum of the losses from reflection SE_R, absorption SE_A and multiple reflections SE_M as the wave propagates through the sample. The scattering parameters at each of the ports can be used to determine the fraction of the EM wave that is transmitted, reflected and absorbed. The transmittance (T), reflectance (R), which includes contribution from multiple reflections, and absorbance (A) with respect to the incident wave

is given by the following equations [67]

$$T = |S_{12}|^2 \tag{2.14}$$

$$R = |S_{11}|^2 \tag{2.15}$$

$$A = 1 - R - T \tag{2.16}$$

This concludes the details regarding the materials, experimental procedures and testing methods performed on the rigid PUR/PIR, rigid PUR/PIR foam and flexible PDMS samples. The mechanical, electrical, thermal and dielectric properties of the rigid PUR/PIR foam were tested. The only PDMS properties characterized were the dielectric and EMI shielding performance. Both nanocomposite foams were imaged on a SEM to determine cell structure and the dispersion of GnP.

CHAPTER 3

INTERACTIONS OF GNP IN RIGID PUR/PIR FOAM

3.1 Introduction

Technological advancements are always going to be limited by the materials that are available. And as technology progresses there are increasingly higher demands on the materials employed. It is no longer enough to have materials that are simply strong, tough, stiff or flexible. Certain applications require that they also be optically transparent, light, show high electrical conductivity, low heat transfer or high permittivity. Such multifunctional materials cannot be synthesized simply of polymers, ceramics or metals and require a mixture of the different properties of these materials thus leading to the development of engineered materials. These materials are vastly more complex and often combine different classes and as well as forms of materials and synthesis techniques to achieve the desired properties. One recent trend in the field of engineered materials is composites and with the discovery of nanoparticles, the evolution of nanocomposites.

Polymer nanocomposites are a relatively new field, but such materials show promising results as everything from thermal shielding [8] to energy applications [10], to electromagnetic interference (EMI) shielding devices [68, 69, 70, 71] to packaging [7] and beyond as new multifunctional polymer nanocomposites are being produced all the time. Carbon based nanoparticles show a great deal of promise as a component in the synthesis of multifunctional materials. But there are many challenges associated with the application of these materials from their manufacture, processing to characterization; as often these materials need to be tightly engineered at the molecular level to create materials that have the desired macroscopic properties.

One of the more promising carbon nanomaterials that is currently very popular in

nanocomposite research is graphene due its multifunctional properties. Graphene describes a single layer of sp^2 hybridized carbon atoms in a hexagonal arrangement. Single layer graphene has been shown to have good mechanical properties with a high Young's modulus of around 1 TPa[22], high thermal conductivity of about 3000 W/m K[21] and good electrical properties with carrier mobilities greater than 15,000 cm^2/Vs[19] due to its unique 2D structure. There are currently many methods to synthesize graphene, in general the purity and ability to create single sheets scales with cost. Considering that high loadings could be needed in a bulk nanocomposite to improve the overall properties, one common cost effective graphene synthesis method relies on exfoliating graphite into thin layers to create multilayered graphene particles that have similar properties to single layer graphene in a more robust form.

One desirable property of polymers is their relatively light weight that can be decreased even further as a foam. Of course polymeric foams suffer from many undesirable properties which limit their applications and thus the addition of a nanofiller to the polymeric matrix could be a great way to improve its properties. This chapter details the investigations done to characterize the effect that adding a nanoplatelet material has on the polymeric properties of a chemically blown foam. Since polymerization and gas evolution occur simultaneously in a chemically blown system there are many ways that adding nanoparticles could effect the resultant polymeric foam properties. Understanding the positive and negative effects adding nanoplatelets have on such a system will help in understanding the relationship between the gas, polymer and nano-reinforcement material; thereby making it easier to identify ways to improve the interaction. Focus was on the effect the nanomaterial has on the molecular formation, stabilization of the foam and on the behavior of the gas evolution. This research will help in understanding such three phase systems and how best to optimize their interactions to get the desired resultant properties.

This experimental study focuses on a polyurethane/polyisocyanurate (PUR/PIR) matrix. This material matrix was chosen for its well understood process-property-structure relationship due to its heavy use in industry as everything from building materials, furniture, and sound

dampeners. The reinforcing aid is a multifunctional graphene material that consists of stacks of graphene sheets. Because this product relies heavily on graphitic material to improve specific properties there is the potential for this nanomaterial to be adapted to other chemically blown polymeric system depending on the application. In addition, graphene nanoplatelets (GnP) are a relatively inexpensive nanoreinforcing agent so there is great potential that any resultant foam could be relatively affordable, have a low density, and multifunctionality, making for better, less expensive products.

3.2 Experimental Procedure

3.2.1 Materials

The polymeric matrix is a PUR/PIR free-rise closed-cell rigid foam and has a density of 0.16 g/cm^3. It utilizes water as the chemical blowing agent, where an addition reaction between water and isocyanate forms urea and evolves carbon dioxide. Huntsman supplied Jeffol FX31-240, Jeffol G30-650 and Rubinate M. Jeffol FX31-240 and G30-650 are diol polyols, with hydroxyl numbers of 240 and 650 mgKOH, respectively. Jeffol G30-650 has a molecular weight of 260 and a viscosity at room temperature of 880 cP-s. Jeffol FX31-240 has a molecular weight of 700 and room temperature viscosity of 250 cP-s. These two polyols are mixed with ethylene glycol from JT Baker according to the ratio shown in Table 2.1 to create a difunctional polyol system that still maintains a low viscosity. Rubinate M is a polymeric diphenylmethane diisocyanate (pMDI) that has an NCO value of 31.2 and room temperature viscosity of 190 cP-s. The structure of pMDI is shown in Figure 2.2 (a). The surfactant and catalysts were received from AirProducts; Dabco DC193 is a polydimethylsiloxane surfactant, Dabco BL-11 is the blowing catalyst and Dabco TMR-3 is a polymerization catalyst that forms the trimer groups found in the PIR. Distilled water is used as the blowing agent and all the components are mixed according to the ratio in Table 2.2. Toluene diisocyanate (2,4-TDI), an isocyanate also commonly used in the synthesis of polyurethane, is from TCI

Chemicals and its structure is shown in Figure 2.2 (b).

GnP are a multifunctional nanofiller sourced from XG Sciences. It is a cost effective thin graphite particle consisting of multiple layers of graphene, but with comparable properties to single graphene sheets in a more robust form. For this study three types were used from XG Sciences: the first two have 120 m^2/g surface area with lateral dimensions of either 5 μm, designated GnP-5, or 25 μm designation GnP-25; the last is a high surface area material of 750 m^2/g with an average diameter of less than 1 μm, designated GnP(750). All GnP is baked at 450 °Cfor 2 hours prior to use. An SEM image of as-received M-grade GnP is shown in Figure 1.2 on page 9.

3.2.2 Experimental Procedure

3.2.2.1 Rigid PUR/PIR Synthesis

Two types of rigid PUR/PIR material were synthesized; one a low density foam and the other a monolithic polymer that did not contain the surfactant, blowing catalyst or agent. The procedure is as follows: first the polyols were combined with ethylene glycol in a typical lab environment. Then the rest of the experiment is carried out in an environmental glovebox to reduce exposure of the chemicals to moisture which can absorb in certain chemicals decreasing the density. The polyols are mixed with a paddle-stirrer for 2 hours. For the foam the surfactant, catalysts and blowing agent are added into the system then mixed for one hour, whereas, for the monolithic polymer only the polymerization catalyst is added, followed by mixing for 30 minutes. As mentioned previously, Tables 2.1 and 2.2 on page 18 details the ratios used for the synthesis of both the monolithic and foam, if the components were not needed they were removed from the chemistry but the ratios were kept constant. If GnP is required it is added to the polyol blend up to 6 wt% for GnP-5 and GnP(750) or up to 3 wt% for GnP-25, the remaining amount of GnP required is added to the pMDI. Each blend is then high-speed shear mixed at 1600 for 1 min, then 2400 rpm for 2 min. Then proceeds

to be ultrasonicated with a one-inch probe at 100 W until well dispersed; the dispersion of the GnP in the polyol blend is confirmed using an optical reflectance microscope but takes anywhere from 5-20 min of ultrasonication depending on the loading and type of GnP. The two components are then allowed to cool before being combined, stirred with an immersion blender for 45 s and then poured into a mold and cured overnight. The mold is a 0.175 mL stainless pan lined with teflon paper and samples are cut from the cured sample.

3.2.2.2 Edge-functionalization of GnP

For the pMDI treated GnP, the baked GnP was poured into a beaker and heated to over 100 °C to remove any adsorbed water molecules on the GnP. Then enough pMDI is added to completely cover the GnP and is then reacted at 130 °C for 1 h or overnight. The material is then cooled and dispersed in acetone before centrifuging to collect the solids while the excess liquid is decanted. The washing procedure with acetone is repeated at least six times so that the majority of the excess pMDI is removed, followed by drying.

Another method focused on creating a thin layer of edge groups by reducing the amount of pMDI available for reaction, designated as "M". First, the GnP is dispersed in acetone by ultrasonication at low concentrations, about 6 g of GnP per every 1 L of acetone. This is followed by the addition of about 64 μL of pMDI. The solution is ultrasonicated with a 2.54 cm probe at 100 W for 1 hour to react. The majority of the acetone is then boiled off before the material gets washed multiple times using the same procedure with centrifugation detailed before to remove any unreacted polymer. This same procedure was repeated but with toluene diisocyanate (TDI) as the reactant instead. Both of these molecular groups are shown in Figure 2.2 on page 16.

3.2.3 Testing Procedures

The functional groups on the pMDI treated GnP is characterized using a x-ray photoelectron spectrometer (XPS) as the basal plane of the GnP is very inert and reaction would be limited

to the edges. XPS measures the binding energy of the atoms and therefore is able to get identify atoms and the molecular structure on the surface as the penetration depth for the instrument is less than 1 μm. The nitrogen spectra was used to identify the change in the edge characteristics of the GnP after reaction with the pMDI and TDI as M-grade xGnP contains no nitrogen prior to the treatment and C-grade contains only about 1 atomic percent. The thermal degradation was tested on a TA Instruments thermograviometric analysis (TGA) system at a ramp of 20 °C/min at a resolution of 4 under inert nitrogen gas to 750 °C. The glass temperature was determined using a TA differential scanning calorimetry (DSC). Three specimens were taken from each sample. Each specimen was ramped to 140 °Cat 10 °C/minand cooled to 30 °C at a rate of 20 °C/min and the cooling curve is used to determine the T_g. In addition, the exothermic behavior of two foam samples was measured by inserting a meter probe into the material right after it was poured into a pan for 500 s, the maximum count for the meter.

Images of the dispersion of GnP in the struts of the foam were taken on a field emission SEM, a high resolution SEM, in combination with focused ion beam (FIB) was able to cut sections of the PUR/PIR rigid foam to determine how well the platelets dispersed. FIB uses a stream of gallium ions to cut the material by rastering through the material. Lastly, the cells sizes were determined from images taken on a scanning electron microscope (SEM). The diameters of 60 cells were determined with the assistance of Image Pro Analysis software that measures the cell's mean diameter. A cell along with the other parts of the foam structure are highlighted in Figure 3.1. Since all of the histograms have at least two "peaks" due to the cells caused by the gas evolution and those caused by air bubbles due to the mixing the median cell size is given in addition to the average diameter and sample deviation.

3.3 Results

Tables 3.1 and 3.2 show the atomic percents of the nitrogen spectra on the treated GnP an example of which is shown in Figure 3.2. XPS was also performed on the neat PUR/PIR

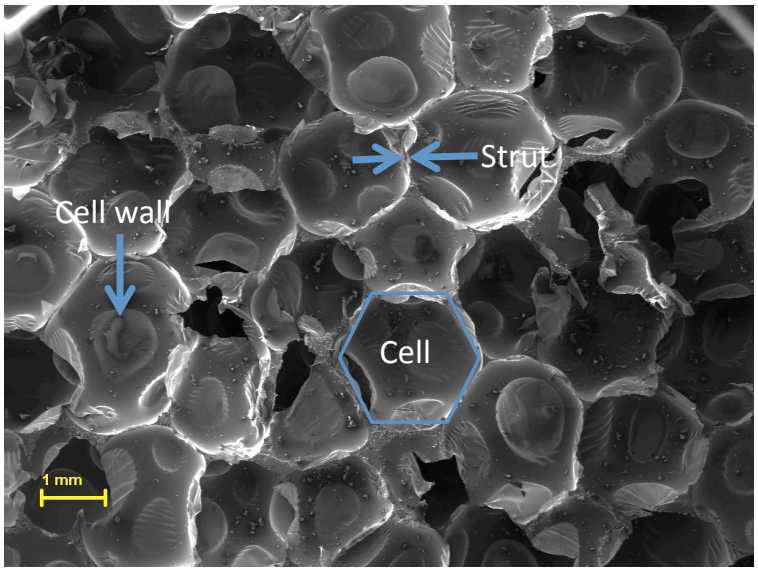

Figure 3.1: SEM image of PUR/PIR rigid foam highlighting the different parts in the cellular structure.

rigid foam and the only peak in the nitrogen spectra was a broad peak 300 eV so this binding energy is attributed to urethane-type groups (PUR, polyurea). The peak at 398 eV is commonly attributed to amines [64]. The peak at 401.3 eV is believed to be due to unreacted segments of pMDI or possibly excess that was not removed during the washing process.

Table 3.1: Atomic % of chemical groups on GnP after reaction overnight with pMDI as determined by XPS

Binding Energy (eV)	*pMDI GnP-25*	*pMDI GnP-5*
401.3	0.6 (12%)	0.6 (17%)
400	2.9 (57%)	2.5 (71%)
398	1.6 (31%)	0.4 (12%)
Total	**5.1**	**3.5**

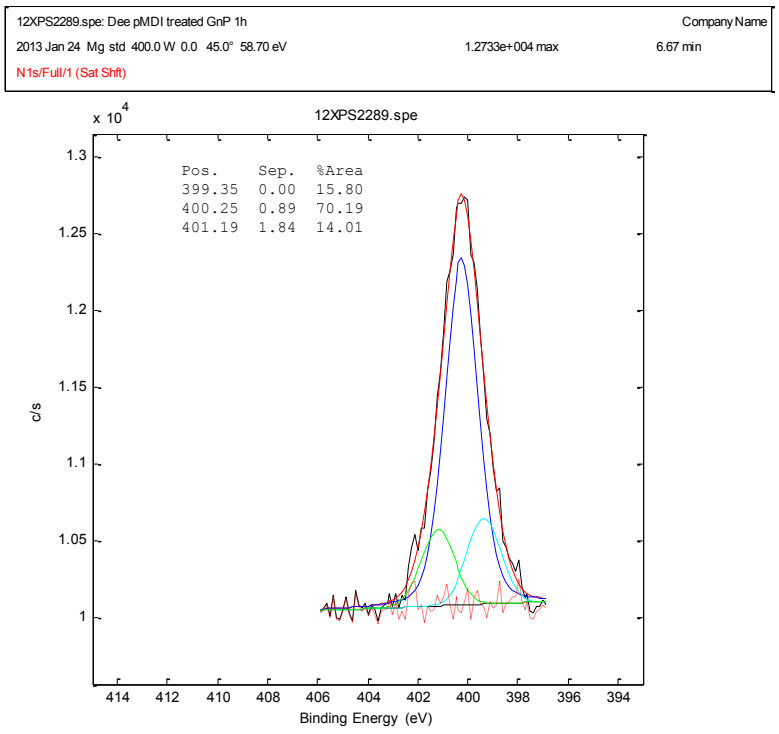

Figure 3.2: An example of the nitrogen spectra of pMDI treated GnP. A broad nitrogen peak suggests that the binding energy is not the same for all the nitrogen atoms and using FTT software the broad spectra can be broken down into their individual nitrogen groups.

Table 3.2: Atomic percent (at%) of chemical groups on GnP after reaction with pMDI and TDI as determined by XPS. *M* designates the monolayer method of reaction, for all others the reactant was in excess.

Binding Energy *(*eV*)*	*pMDI GnP-25*	*pMDI GnP-5*	*TDI M GnP-5*	*pMDI GnP(750)*	*pMDI M GnP(750)*	*TDI M GnP(750)*
401.5	0.3 (9%)	1.4 (22%)	0.2 (29%)	0.9 (15%)	0.6 (35%)	0.4 (22%)
400.1	2.7 (84%)	4.3 (69%)	0.3 (42%)	4.2 (69%)	0.9 (53%)	0.9 (50%)
398.9	0.2 (7%)	0.5 (8%)	0.2 (29%)	1.0 (16%)	0.2 (12%)	0.5 (28%)
Total	**3.2**	**6.2**	**0.7**	**6.1**	**1.7**	**1.8**

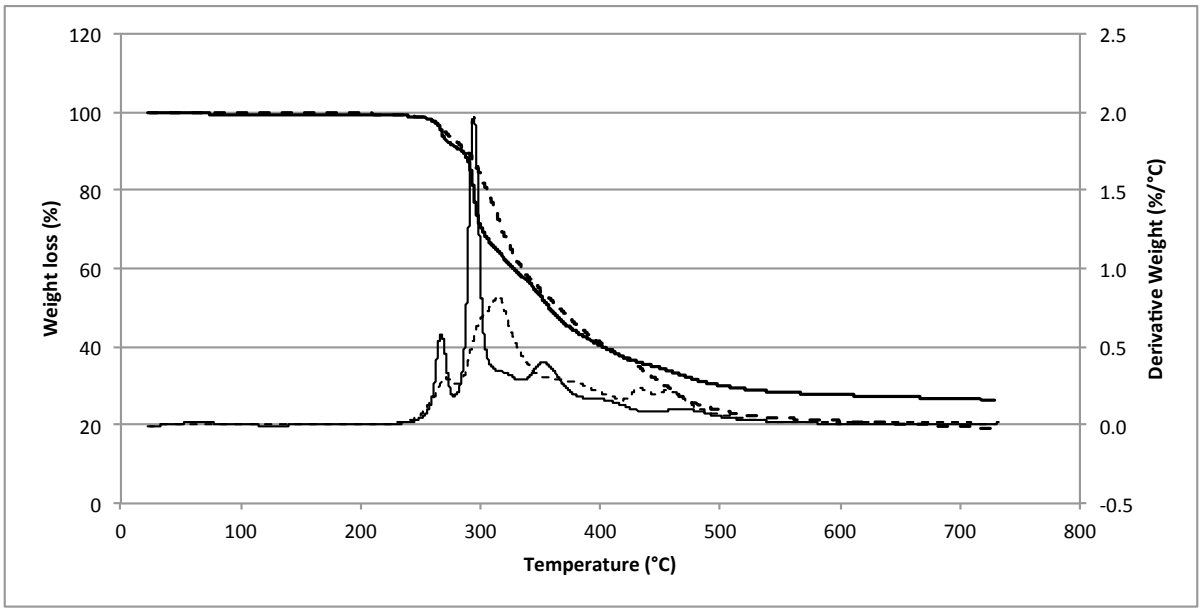

Figure 3.3: Thermal degradation profiles of PUR/PIR rigid foam and the monolithic polymer. The solid lines represents the rigid PUR/PIR foam and the dashed line is the for the monolithic rigid PUR/PIR.

Figure 3.3 is a comparison of the thermal degradation profiles for the neat rigid monolithic and foamed PUR/PIR samples with no GnP. It also shows how the derivative plots relate to the plots of weight loss. Figures 3.4 and 3.5 are overlays of the monolithic rigid PUR/PIR matrix with varying types of GnP. Figures 3.6-3.10 cover the TGA profile and derivative function of the rigid PUR/PIR foam samples.

The derivative plots of the weight loss highlight the fact that there are sharp changes in the rate of decomposition at certain temperatures that match the degradation temperature of certain molecular groups. The peaks that form then could be attributed to the decomposition or dissociation of different molecular groups in the polymer. Isocyanate is a very reactive molecule and Figure 3.11 shows some of the reactions that are occurring during the formation water-blown PUR/PIR foam some of which are reversible like the biurets and allophanates and some of which are prompted to form by certain catalysts such as the cyclotrimerization reaction that forms isocyanurate[51]. Urea can form from the reaction of isocyanate with

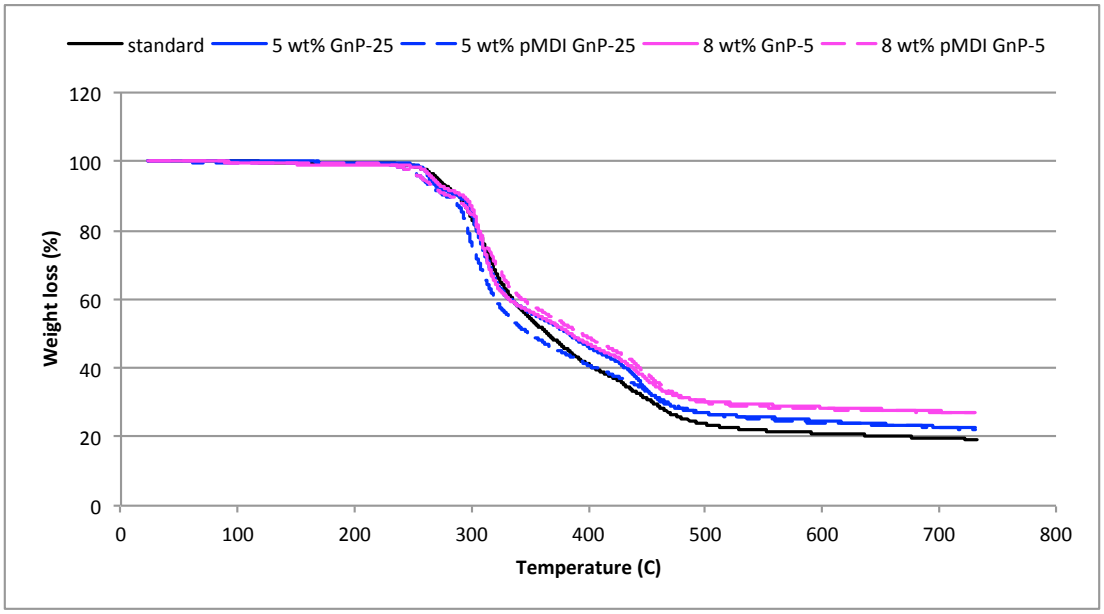

Figure 3.4: Graph overlay of the thermal degradation profiles of the monolithic rigid PUR/PIR with and without GnP ("standard").

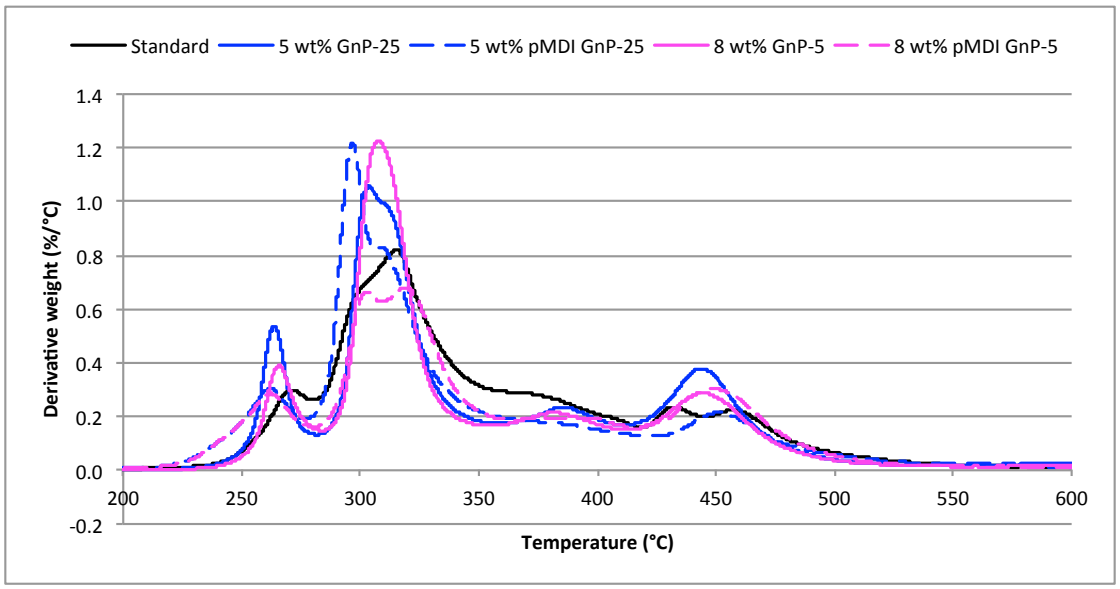

Figure 3.5: Graph overlay of the derivative thermal degradation profiles of the monolithic rigid PUR/PIR with and without GnP ("standard").

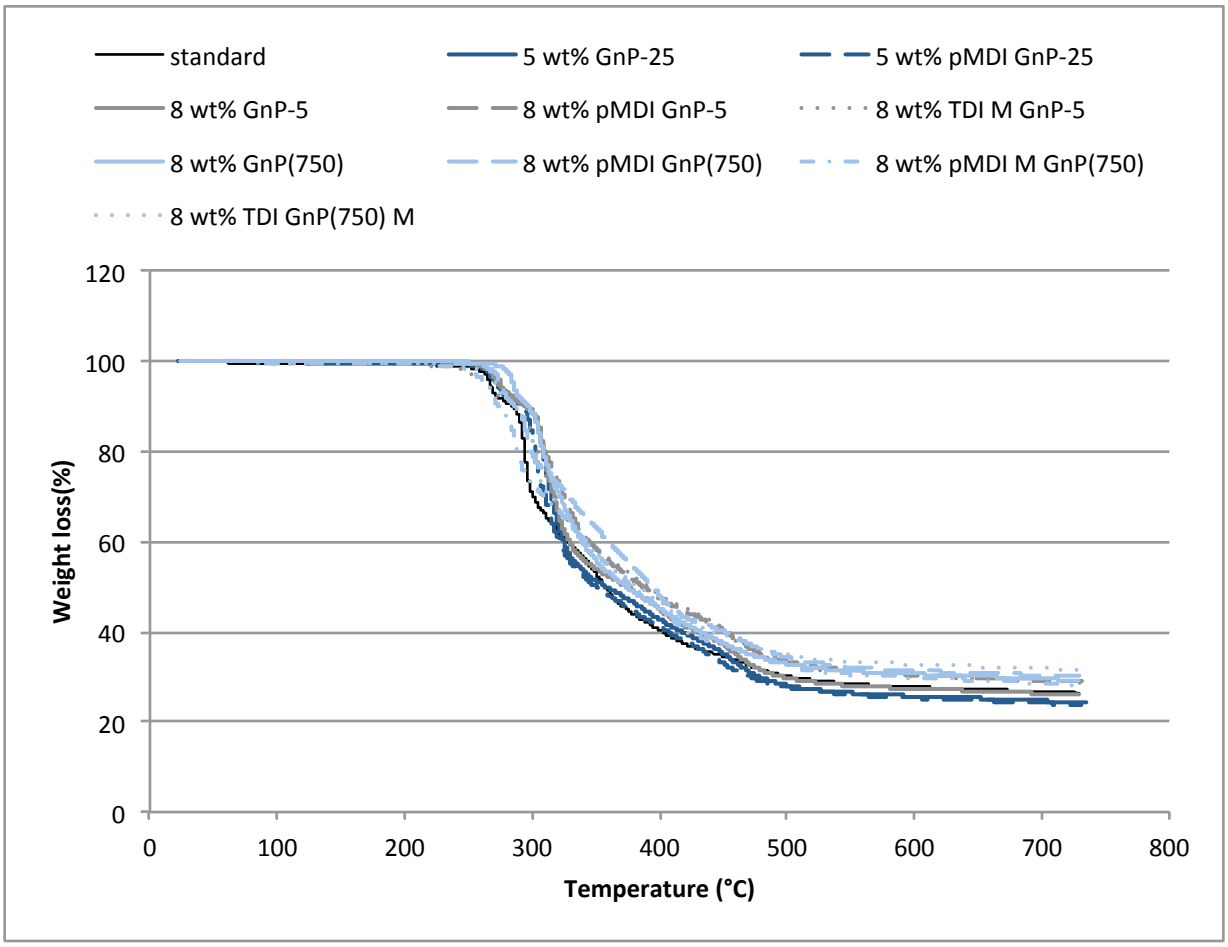

Figure 3.6: Thermal degradation profiles of PUR/PIR rigid foam before ("standard") and after the addition of different types and loadings of GnP.

primary and secondary amines and is also one of the byproducts from the reaction of isocyanate and water. The other product is carbon dioxide, and is therefore the main reaction responsible for the material expanding, the other is from a condensation reaction [51].

Previous research [72, 73, 74, 75, 76, 77] has investigated how the molecular groups in PUR decompose on their own and in PUR foams. Biurets and allophanates start to dissociate after 100 °C, but these reactions are somewhat reversible and so dissociate back to the groups they form from: polyurea, PUR and pMDI [74] and so do not necessarily appear in the decomposition profile and in fact, the derivate plots of the degradation show no weight loss below 200 °C. This matches other work done by Grassie and Mendoza [73] that confirmed

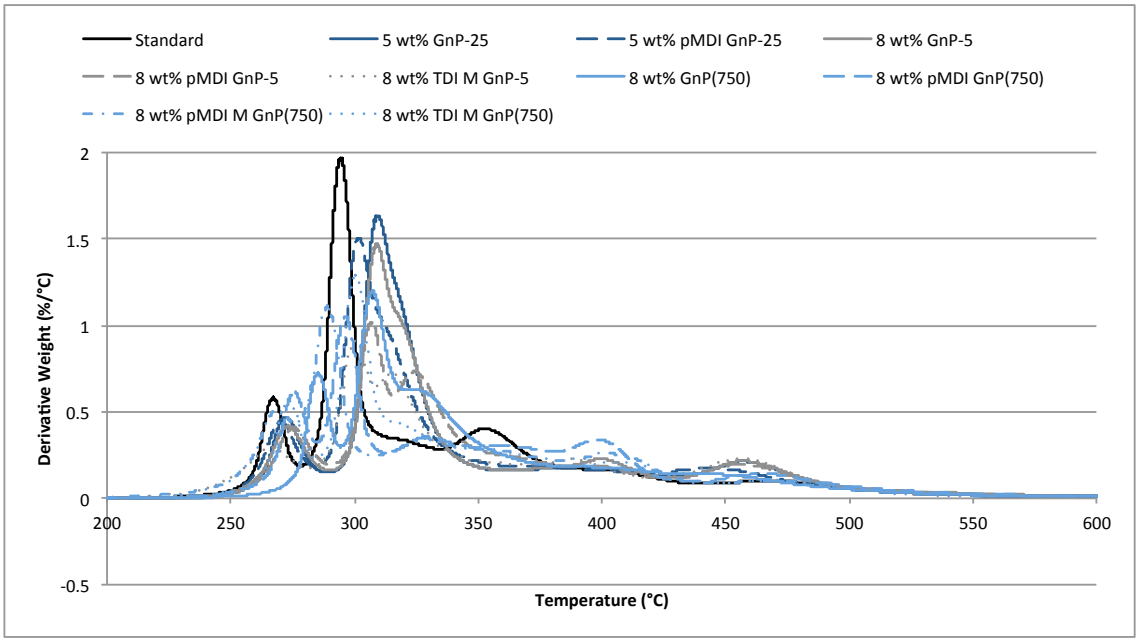

Figure 3.7: Graph overlay of the derivative weight of the thermal degradation profiles of PUR/PIR rigid foam before ("standard") and after the addition of different types and loadings of GnP.

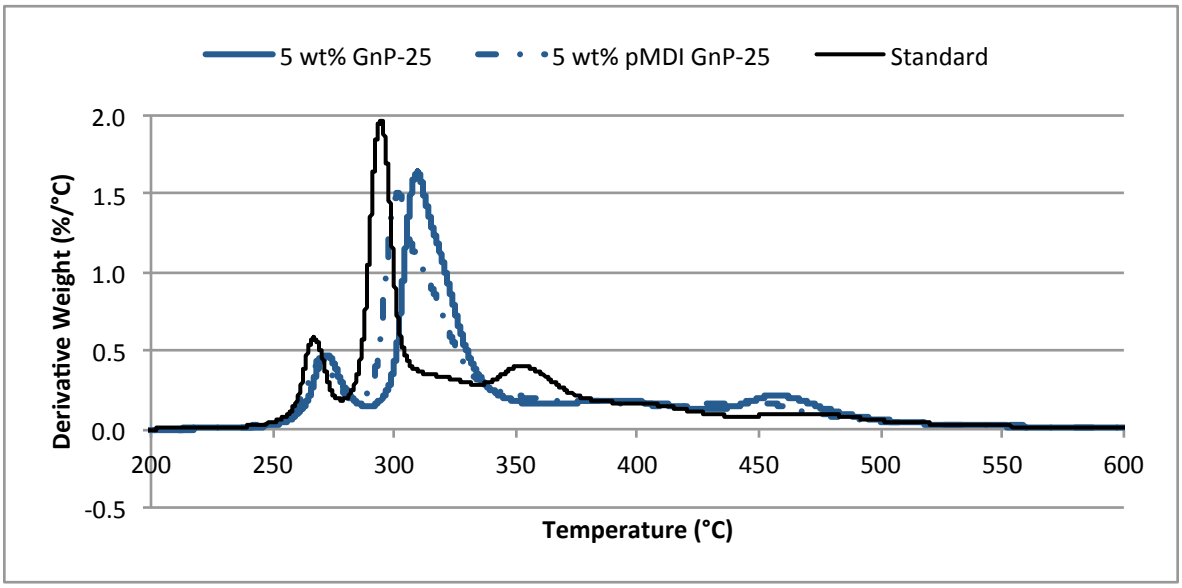

Figure 3.8: Comparison of the derivative weight thermal degradation profiles of rigid PUR/PIR foam of the neat ("standard") versus after the addition of 5 wt% baked GnP-25 and edge-functionalized pMDI treated GnP-25.

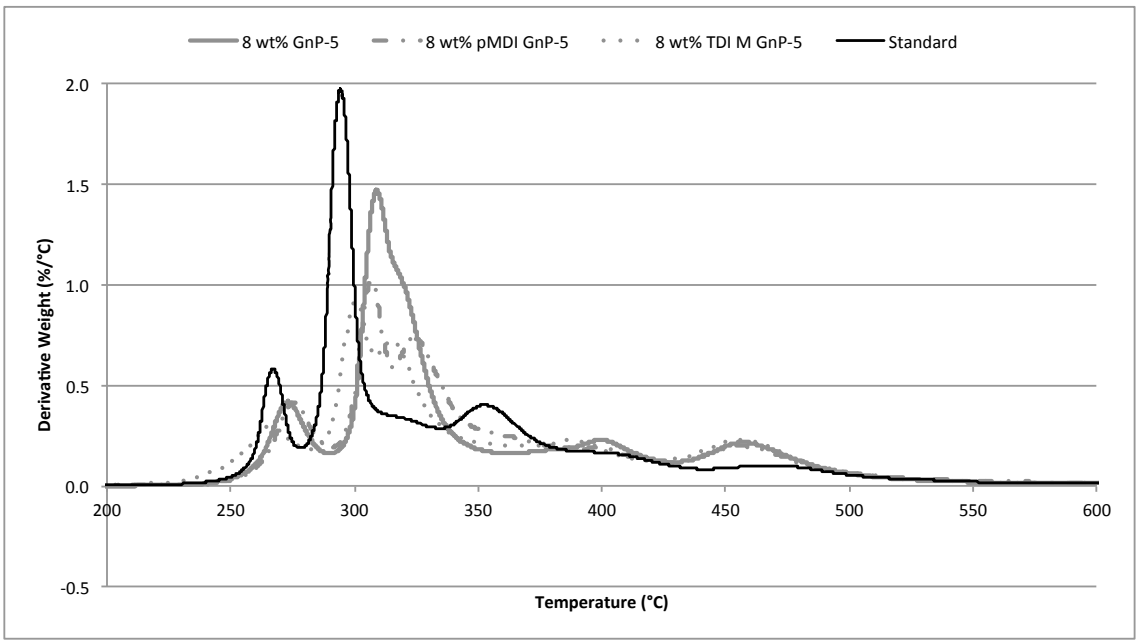

Figure 3.9: Comparison of the derivative weight thermal degradation profiles of rigid PUR/PIR foam of the neat ("standard") versus after the addition of 8 wt% baked GnP-5 and edge-functionalized GnP-5 with pMDI in excess or TDI using the monolayer method (M).

structural changes in the polymer below 250 °C, but did not result in degradation until 270 °C. They concluded that the first sharp peak above 250 °C is due primarily to the depolymerization of polyurethane [73, 74]. The second and generally largest peak includes the breakdown of the more thermally stable urea, as well as the decomposition of the now urethane monomer. Urethane in PUR foam decomposes at around 300 °C and urea has a decomposition temperature about 20 °C higher than that of urethane and forms from at least 2 reactions [78, 51]. Decomposition of polyurea could also behave similarly to PUR where polyurea breaks down to monomers prior to the decomposition. At about 400 °C the isocyanurate-urethane linkage begins to decompose [78, 51] at a much slower rate as shown by the peak centered around 400 °C on the derivative weight plots of the thermal degradation profiles. There is another peak centered at 350 °C that could be due to the decomposition of products that formed from the decomposition of urea [79].

Grassie and Mendoza found that under vacuum primary decomposition products can

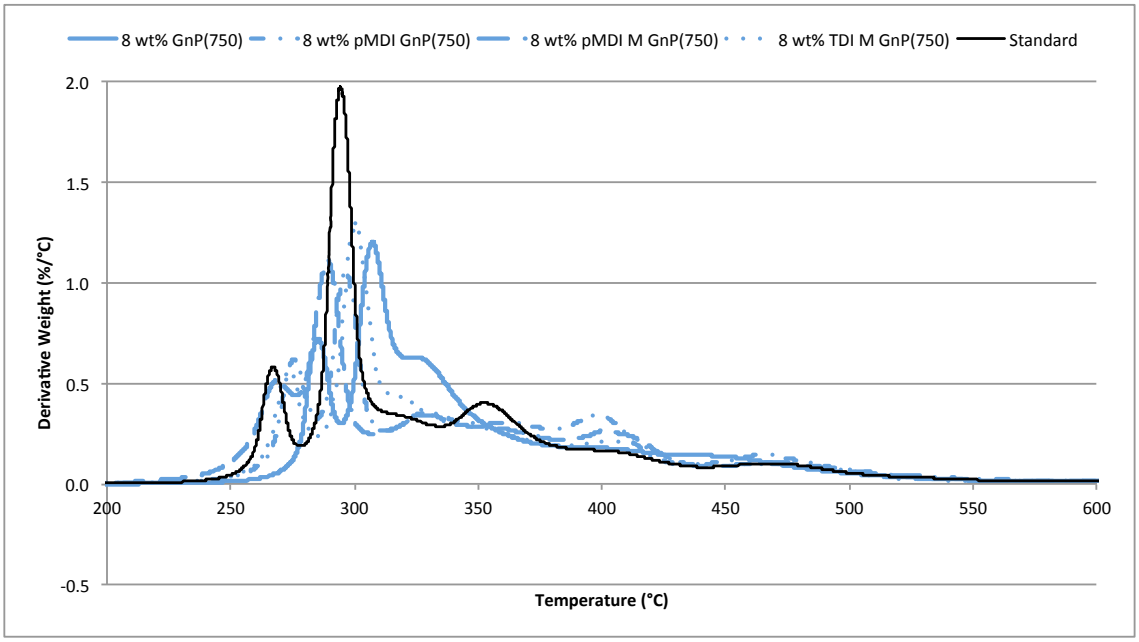

Figure 3.10: Comparison of the derivative weight thermal degradation profiles of rigid PUR/PIR foam of the neat ("standard") versus after the addition of 8 wt% baked GnP(750) and edge-functionalized GnP-5 with pMDI in excess, pMDI using the monolayer method or TDI using the monolayer method (M).

readily escape from the degrading polymer, but for higher pressures that escape is diffusion-controlled and if not fast enough allows for secondary reactions to occur, such as condensation reactions resulting in carbodiimide and amides that also release carbon dioxide [80, 73]. Other volatile products such as cyanic acid, butadiene, tetrahydrofuran and dihydrofuran and water are also being formed from secondary reactions taking place within the hot polymer [80, 73, 75]. So the subsequent molecular groups that are degrading could also come from secondary reactions that have taken place after the polymer starts to break down. Within all the decomposition profile there is a continued breakdown of previously unaccessible molecular groups as the temperature increases and the polymer becomes more fluid resulting in cascading secondary reactions as well [80]. As these molecules continue to dissociate and escape, less of the decomposed products are involved in secondary reactions but those products that did not escape react to form new molecules that become the contributing monomers to the

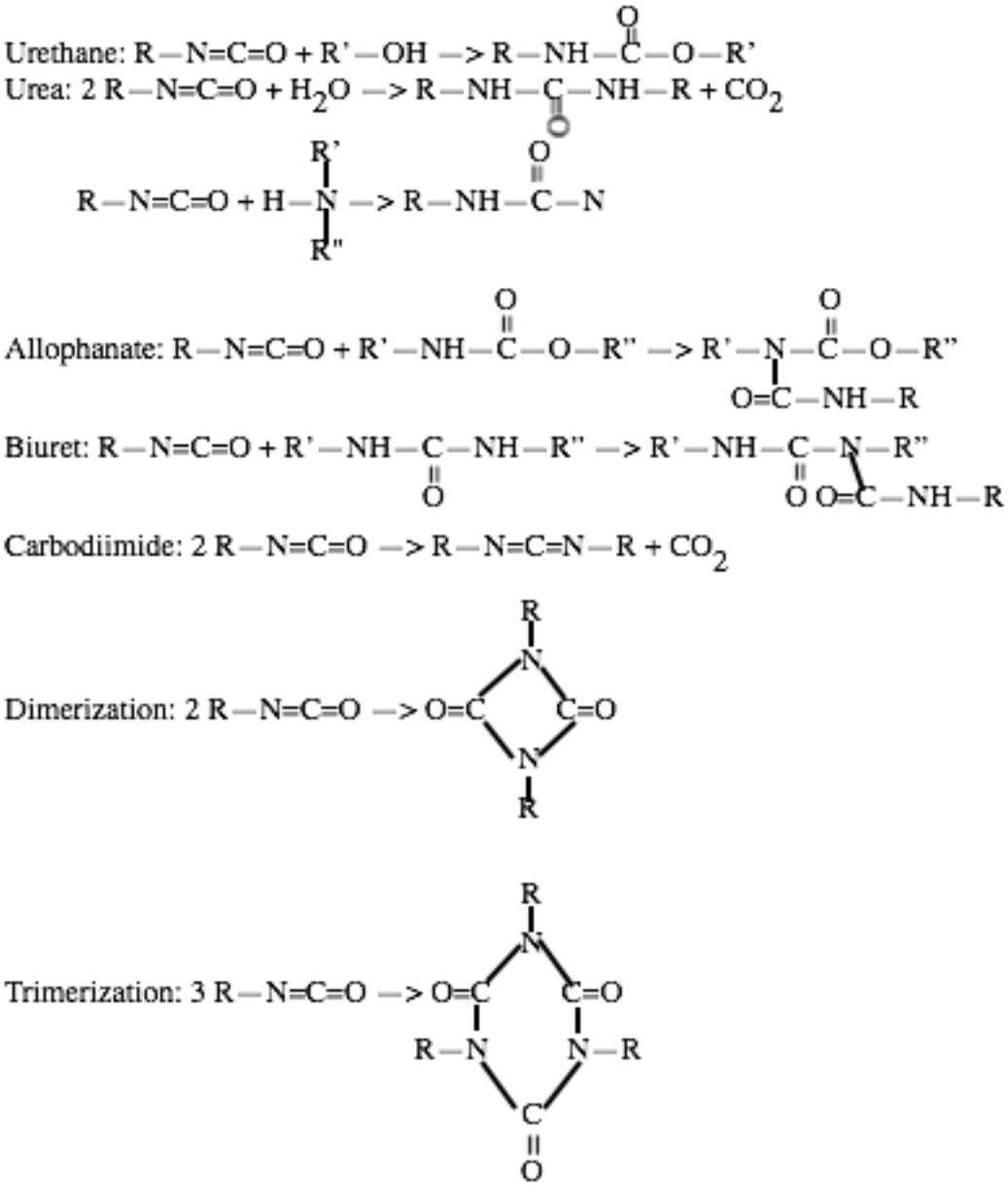

Figure 3.11: Some chemical reactions that occur during the foaming of a PUR/PIR water-blown foam.

Table 3.3: Glass transition temperature of monolithic PUR/PIR before ("standard") and after the addition of GnP from 3 specimens.

Rigid PUR/PIR	**T_g(°C)**	**Sample deviation**
Standard	105.9	0.3
5 wt% GnP-25	100.5	2.3
5 wt% pMDI GnP-25	103.5	2.0
8 wt% GnP-5	93.7	7.2
8 wt% pMDI GnP-5	92.8	5.0

polymer structure and begin to break down as well becoming the contributors to the chemical degradation above 450 °C. The TGA plots also show that there is still a residue at about 730 °C, which is common in polyurethane foams that do not have the assistance of removal of decomposed products from the hot polymer and is found to include a large amount of carbodiimide [73]. This is why the degradation is virtually nonexistent above 500 °C as the rate goes back to zero. The remaining decomposed products must be continually decomposing and reacting with each other.

The glass temperature (T_g) as determined by DSC is shown in Tables 3.3 and 3.4. In addition the exothermic behavior of the foam standard sample without GnP compared to the foam sample with 5 wt% GnP-25 is shown in Figure 3.12. Lastly, since this system uses a chemical blowing agent the cell size can be drastically affected by the addition of the nanoparticles. The average cell size shown with the sample deviation is detailed in Table 3.5. It is important to note that the mixing method inputs large air bubbles into the system, this is confirmed from the monolithic samples that still have a small amount of large cells. Therefore, cells larger than 300 μmare not believed to be from the nucleation and growth of the chemical blowing agent, but are still included in the cell count so the median cell size is also given as more accurate representation of the blown cells.

Table 3.4: The average glass temperature (T_g) and sample deviation of rigid PUR/PIR foam with and without ("standard") GnP and with treated GnP as measured by DSC taken from 3 specimens.

Rigid PUR/PIR foam sample	**T_g(°C)**	**Sample deviation**
Standard	107.4	1.0
5 wt% GnP-25	100.7	4.5
5 wt% pMDI GnP-25	103.6	3.9
8 wt% GnP-5	102.1	7.0
8 wt% pMDI GnP-5	97.8	4.5
8 wt% TDI M GnP-5	90.0	10.4
8 wt% GnP(750)	107.6	4.2
8 wt% pMDI GnP(750)	102.2	4.5
8 wt% pMDI M GnP(750)	105.3	1.2
8 wt% TDI M GnP(750)	106.4	1.6

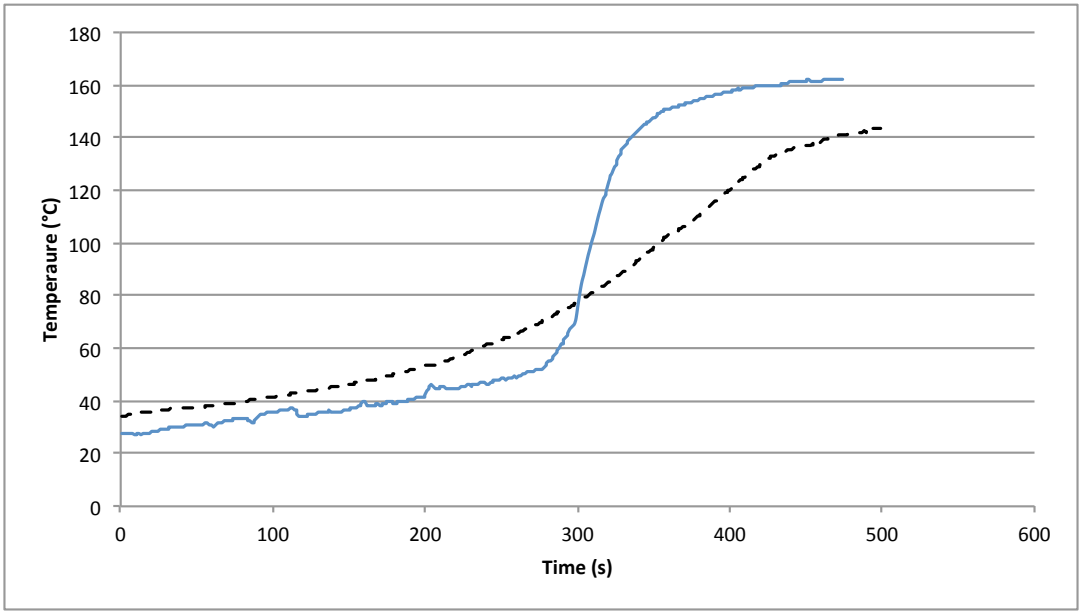

Figure 3.12: The amount of heat increase as the foam cures without GnP (solid line) and with 5 wt% GnP-25 (dashed line).

Table 3.5: Cell size of the mean and median diameter of PUR/PIR rigid foam with and without different types and loadings of GnP versus the neat rigid PUR/PIR foam ("standard".)

Rigid PUR/PIR foam sample	**Mean Cell Size (μm)**	**Sample deviation**	**Median Cell Size (μm)**
Standard	119.2	46.2	114.5
5 wt% GnP-25	82.7	41.5	76.0
5 wt% pMDI GnP-25	179.8	213.5	112.8
8 wt% GnP-5	168.5	148.8	95.7
8 wt% pMDI GnP-5	170.7	149.1	115.5
8 wt% TDI M GnP-5	213.9	113.4	218.5
8 wt% GnP(750)	177.8	142.1	127.2
8 wt% pMDI GnP(750)	231.7	113.4	218.5
8 wt% pMDI M GnP(750)	184.4	111.2	174.5
8 wt% TDI M GnP(750)	147.9	57.0	150.6

3.4 Discussion

3.4.1 Comparison of Monolithic Rigid PUR/PIR and Rigid PUR/PIR Foam with no GnP.

Remember that the monolithic polymer was synthesized without the blowing agent (water), surfactant or blowing catalyst that are used in the foaming process, but still in a dry environment, so one of the reaction mechanisms for forming polyurea was removed without access to water. This does not seem to not affect the molecular structure as the T_g between the monolithic and foam PUR/PIR are closely related. Where there is difference between the two is in the thermal degradation performance. Figure 3.3 shows that more weight is lost initially from the rigid PUR/PIR foam below 300 °C specifically from peaks 1 and 2, although peak 2 is the more significant showing a difference of around 15 wt%. As mentioned previously the temperature from 275 to about 325 °C is for the decomposition of urethane monomers followed by urea at about 20 °C higher. The more gradual weight loss at this temperature for the monolithic PUR/PIR could be due to a more significant amount of urea than the foam. However, the similar glass temperature between the two suggests another mechanism as polyurea has a higher T_g than PUR. It could also be that the broadness of the urethane/urea peak is due to the less efficient removal of the primary reaction products that form from the decomposition due to lower surface area compared to the foam. This is more likely because the weight loss at 325 °C matches between the two samples. The amount of polymer retained even at 500 °C suggests that the structure of the foam plays a significant part in the removal of the decomposed products preventing the occurrence of secondary reactions. The PUR/PIR foam retains about 50% more weight than the monolithic polymer at 750 °C even though the weight loss is initially higher for the foam. The crossover point occurs above 400 °C which includes the decomposition of products that formed from the decomposition of the primary molecules. It could be that initially the higher surface area cell structure increase the removal concentration, but this same structure can also aid in

retention of any decomposed products from the internal surface and this same high surface area allows for the possibility of more secondary reactions to occur as they escape.

3.4.2 Characterization of Monolithic Rigid PUR/PIR with Neat GnP

For the monolithic rigid PUR/PIR the addition of GnP results in a change in the amount of weight loss over certain temperature ranges. The onset of degradation seems to be similar between the neat polymer and those samples with the addition of the baked GnP. The rate of decomposition between the samples, however, varies. Starting at the end of the profile then going backwards at 750 °C the decomposition profile of the three samples are all parallel to each other. Since GnP can be stable up to 750 °C the variation in weight loss at the end point could be solely due to the addition of the GnP. There is about 4.5 wt% difference between the two samples of GnP and does not match the expected 3 wt%, however, when compared to the standard, the sample that is supposed to contain 5 wt% of GnP-25 is only showing a difference of 3.3 wt% at 750 °C which is lower than expected. Comparison of the neat polymer to that which contains 8 wt% GnP-5 there is 7.8 wt% difference at 750 °C the expected amount of GnP. This confirms that in the polymer the GnP is probably stable up to about 750 °C so the degradation plots are purely of the PUR/PIR. There also appears to be variability in the PUR/PIR sample with GnP-25 as the loading is lower than expected. It could be due the larger particles settling out of the liquid polymer.

A significant change in the thermal degradation occurs at about 350 °C where the standard PUR/PIR starts to experience a much more significant weight loss and separates from the nanocomposite samples with baked GnP as seen in Figure 3.4. This difference is confirmed by Figure 3.5 where the standard also has a higher rate of degradation that is maintained between 325 and 375 °C the temperature range that likely represents the decomposition of the products that formed from the decomposition of urethane and urea. It is possible that the neat GnP is making the thermally decomposed groups that formed from urea and urethane more thermally stable, shown by the higher rates of degradation above 400 °C for the neat

GnP-25 and GnP-5. This is confirmed in the thermal degradation profiles, which shows a significant drop in the absolute weight loss at this same temperature when compared to the standard profile.

The glass temperature is commonly related to cross-link density, the higher the T_g the more cross-linked the structure. However, there is another feature that can cause an increase in T_g and that is an important feature in PUR synthesis and that is the phase separation. PUR has been shown to phase separate into hard and soft segments either phase or both can be crystalline. In water-blown foams the hard segment is generally attributed to urea, which tends to have a high glass temperature [81]. The addition of nanoparticles has been shown to have a great effect on the kinetics and thereby the hard and soft domain formation in PUR whether their size or separation [82]. The addition of the GnP could be disrupting the microphase structure, a fact that would be more prominent with a higher loading of particles. In addition, this polymer is PUR/PIR mixture and what effect the addition of isocyanurate has on the phase-separated morphology is unclear. According to Table 3.3, in both cases the addition of the neat GnP resulted in a decrease in T_g that was more significant with the higher loading of GnP-5. When the difference in weight loss between 375 and 425 °Cis measured, there is a decrease in absolute weight loss when compared to the standard of 0.7% and 1.7% for the 5 wt% GnP-25 and 8 wt% GnP-5, respectively. It could be GnP is decreasing the concentration of trimer linkages resulting in a drop weight that is lost at the decomposition temperature suggesting that the PIR helps with crosslinking, now whether they are located in the hard or soft domain of the polymer is unclear. Otherwise the thermal profiles of the nanocomposite PUR/PIR closely match, which is why changes in the microphase structure is likely responsible.

3.4.3 Characterization of Foam Samples with Neat GnP

Figure 3.6 shows that the foamed PUR/PIR is more affected by the loadings of the baked GnP as demonstrated by the shifts in the onset of degradation of the subsequent nanocomposite

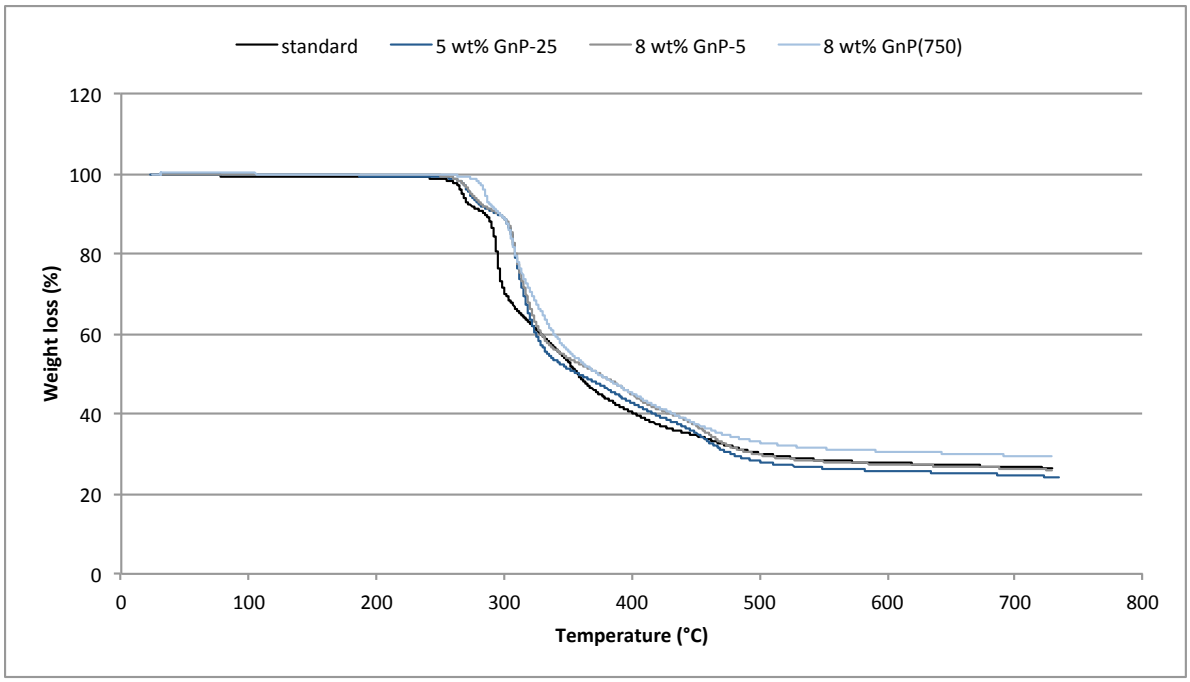

Figure 3.13: Degradation profile of rigid PUR/PIR foam with no GnP compared to foam with neat GnP.

foam samples in Figures 3.8 - 3.10. The addition of GnP seems to improve the thermal stability of the PUR/PIR molecular groups, this is likely due to the high specific heat capacity of that is closely that of graphite that would decrease the heat conduction to the polymer [83]. The rate of decomposition of rigid PUR/PIR with 5 wt% GnP-25 is much broader for peak 2 as shown in Figure 3.8, which results in a lower weight retention between 300 to 350 °C confirmed in Figure 3.13 suggesting that there are more urea groups that are decomposing at the higher temperature. The higher polyurea formation as compared to the standard are probably to compensate for the addition of the larger GnP. An unexpected feature is the amount of weight retained at compared between the samples at 750 °C. The sample with GnP-25 has lost more weight than the standard and this cross in profiles seems to happen at about 450 °C. A similar profile is seen in the foam sample loaded with 8 wt% GnP-5 and shows final weight loss that matches the standard. Even the sample with 8 wt% GnP(750) only shows a difference in weight loss of about 3% from the standard. The data suggests

that the foam samples with GnP-5 and GnP-25 have improved removal of the decomposition products and this could be due to the significantly reduced median cell size resulting in an increase in cell density for a higher surface area, but the cell size for the foam with GnP(750) is similar to the standard so the loss must be due to another mechanism for this sample.

The foam sample that contains GnP(750) is unique in comparison to the other types of neat GnP, but still shows effective decomposition. For the analysis it is easier to simply compare the GnP-5 to GnP(750) as both have the same loading of GnP. It appears that the addition of GnP(750) does result in a similar increase in the thermal stability of the different molecular groups, but what is different in the weight loss profile. Above 300 °C there is a much sharper decrease in weight loss until about 350 °C. This corresponds to the rate of decomposition for peak 2, which is definitely much broader and actually suggests two peaks which would correspond to the thermal degradation of urethane followed by urea. This is different than the samples with GnP-5 or GnP-25 where this feature is difficult to resolve and suggests that the GnP(750) is significantly affecting the formation of urea. Images taken comparing the dispersion of the GnP in Figure 3.14 show that smaller size of the GnP(750) is better for going into thin areas than the larger GnP resulting in more interaction between the polymer and the nanoreinforcing agent. This means that more molecular groups, in this case polyurea, would form bonds with the GnP resulting in an increase of these stable groups, whereas the limited dispersion of GnP-5 and GnP-25 due to agglomeration increasing the polyurea content only marginally. The effect of agglomerations will be discussed more soon. The GnP(750) is also smaller so the concentration of particles is higher, but are apparently too small to prevent bubbles from coalescing resulting in a larger median cell size (see Table 3.5 and a less significant decomposition at 450 °C.

Looking at the effect that the GnP additions have on the glass temperature of the foam shown in Table 3.4. First data point of note is that the effect of GnP-25 does not change between the monolithic polymer and the sample. This could be due to the heavy agglomeration of large particles that limit its interaction with the polymer (see Figure 3.15.

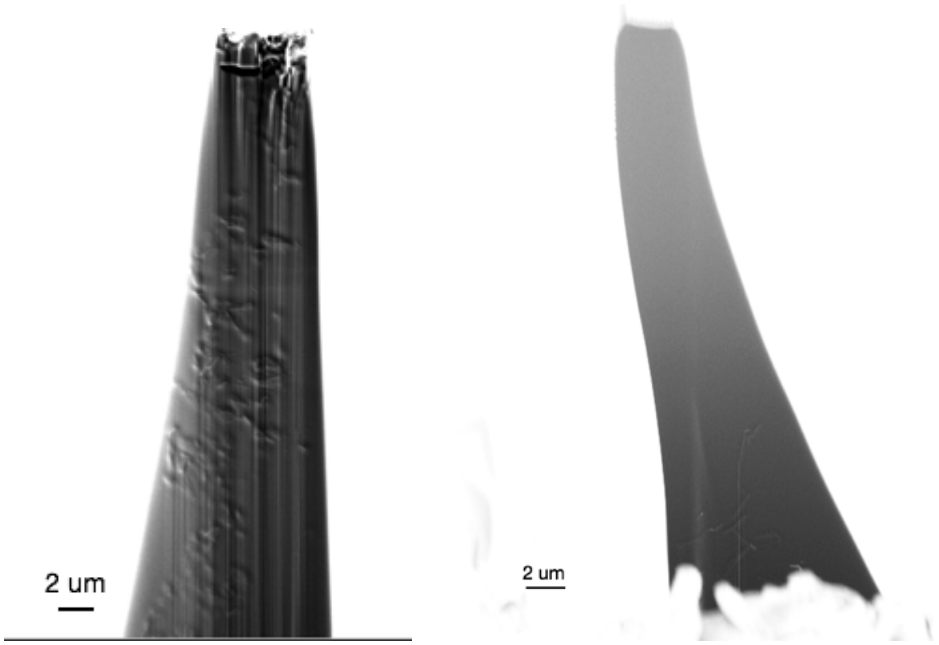

(a) (b)

Figure 3.14: SEM images of GnP dispersion in struts in rigid PUR/PIR foam: (a) FIB cut of foam with 8 wt% GnP(750); (b) FIB cut of foam with 8 wt% GnP-5

GnP-5 shows a lower T_g than the neat foam, but has a higher T_g than its counterpart in the monolithic polymer suggesting that the foaming allows the polymer to better adjust to the invasion of the GnP-5 to maintain more of its cross-link or possibly even hard segment structure. This seems to be the case as the even smaller GnP(750) particles have a similar glass temperature to the standard. In general it appears that the smaller size of the GnP is better for the molecular structure, but remember GnP-25 is better for decreasing the median bubble size in Table 3.5. Sterically this makes sense as it would be harder for the bubbles to move around and coalesce with the larger platelets especially as the viscosity increases and they agglomerate. Further evidence of the effect GnP has on the molecular structure and its foaming behavior is seen by the change in the exothermic profile in Figure 3.12. This plot demonstrates the effect that even the larger platelets can have on the foam as there is a more gradual rate of heat evolution and a likely decrease in the maximum temperature and gives further proof that GnP is interacting with the polymer on a molecular scale.

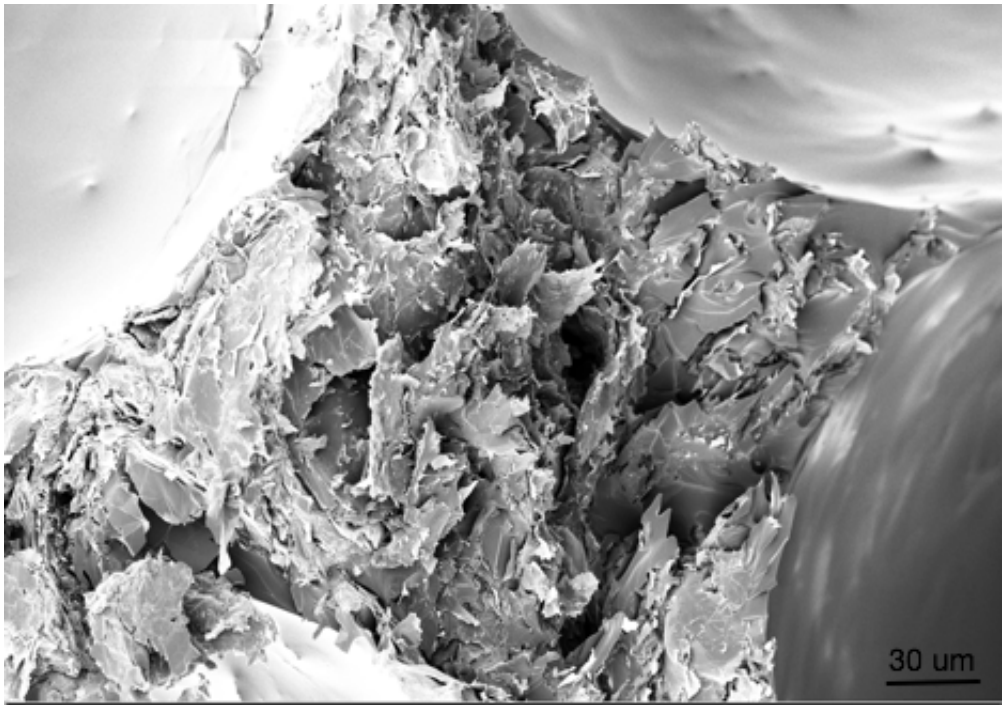

Figure 3.15: SEM image of GnP dispersion at the apex of struts in rigid PUR/PIR foam with 5 wt% GnP-25.

3.4.4 Characterization of treated GnP

Treatment of the GnP was done to improve the interaction of the GnP with the matrix and the resultant edge groups were characterized by XPS and the results are shown in Tables 3.1 and 3.2. The edges are the only points available for reaction as the basal plane of GnP is very chemically inert. The nitrogen plot was focused on for determining the amount and concentrations of functionalized groups since GnP is made up of mostly carbon and a small amount of oxygen, and only GnP(750) shows a small amount of nitrogen at all. Most of the oxygen groups are likely hydroxyls, which readily bond to isocyanate to form urethane molecules. XPS results confirmed that by allowing isocyanate to interact with GnP at elevated temperatures causes reaction to occur forming urethane groups. The heat was applied either externally or by the hot spots cavitation causes during ultrasonication [84]. The procedures where pMDI is added in excess results is designed to form the maximum amount of of polymeric groups forming on the edges, whereas, the reduced method seeks to

form only a single layer amount of polymer groups on the surface which is confirmed in the decrease in concentration of reacted groups shown in Table 3.2. The peak at 400 eV was assumed to be from urethane-like groups as a an XPS scan of PUR/PIR rigid foam was done and the only peak that appeared was a broad peak at 400 eV suggesting that it represents urethane bonds. The peak at 399 eV is commonly attributed to amines [64] as well. The highest binding energy is probably from un-reacted pMDI whether that is from excess pMDI or unreacted segments in the pMDI is unknown. Without a catalyst it is unlikely isocyanurate formed.

Since all the functional groups including hydroxyls are only on the edges, the GnP with the higher edge density should have more functional groups, specifically the concentration should go GnP(750)>GnP-5>GnP-25. The result of the overnight treatment with pMDI does not follow this pattern as shown in Table 3.1. Since the isocyanate is polymeric it could be that the larger basal plane allows more polymeric chains to wrap around the platelets given a sufficient amount of time resulting in a higher count of amine type groups forming. Compare Figure 3.16 which is the GnP-25 that has been reacted with pMDI for 1 h at about 130 °C to Figure 1.3 that clearly shows that even at a reaction time of 1 h and reaction only occurring at edges, the polymer still manages to wrap around the particle isolating it.

Compare to the results of the edge group concentration that formed after an hour of reaction time and there is a decrease in the concentration of reacted groups on the GnP-25 compared to the GnP-5, according to Table 3.2. However the at% of reacted groups on GnP-5 is similar to that on GnP(750). This is due to the fact that as-received GnP(750) is aggregated into sub-micron particles although the platelets are generally less than 1 μm in diameter so many of the edges are internal and unavailable for reaction. Correlate to the samples that have been treated with a small amount of TDI, but are ultrasonicated prior to coating to break up the particles to expose as much of the edges as possible. Now there is the expected higher concentration of edge groups on the GnP(750) compared to the GnP-5.

Functionalizing the edges of the GnP alters the affect it has on the molecular structure

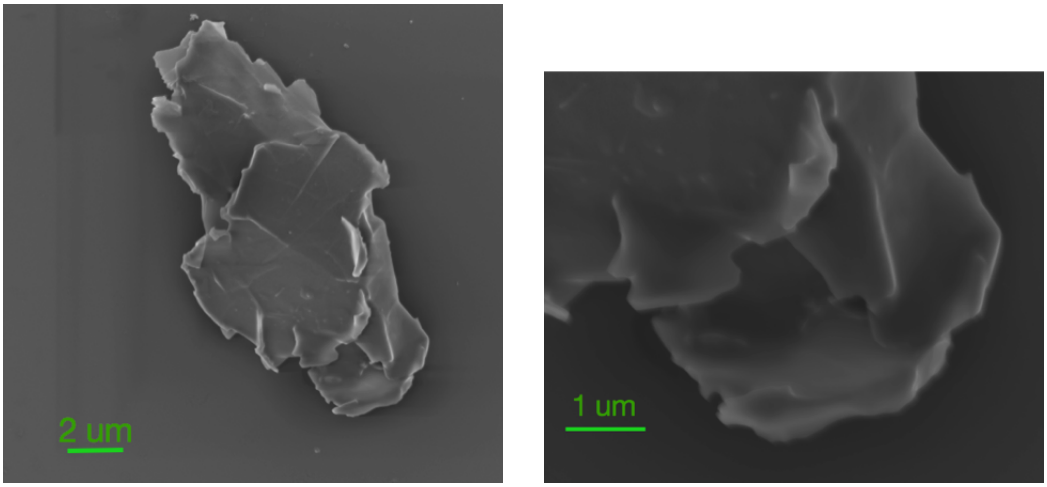

(a) (b)

Figure 3.16: SEM images of GnP-25 reacted with pMDI for 1 h at elevated temperature

as shown by the changes in the glass temperature in Tables 3.3 and 3.4. The greatest effect though in T_g, still seems to come from the size and loading of the particles. When comparing the change in T_g in the nanocomposites when neat GnP is used compared to treated GnP the glass temperature may only change a few degrees, but represents significant change in the cross-link density. The exception is the difference between the T_g in the nanocomposite foam with GnP-5 treated with excess pMDI and that treated with a small amount of TDI. However, the sample deviation is so large it suggests inconsistency in the local structure. The samples with GnP-25 show some unique behavior in the T_g as well. First, the glass temperature of the PUR/PIR solid with pMDI treated GnP-25 matches with that of the foam the same similarity was observed in the neat GnP-25 between solid and foam. Second the pMDI treatment of GnP-25 results in an increase in glass temperature when compared to the neat where all other nanocomposite samples show it remains constant or a decrease. Even though the concentration of atomic groups is different between the GnP-25 used in the monolithic polymer and that in the foam, the polymer that now surrounds the agglomerated particles must allow for cross-linking whatever phase this occurs in.

The nanocomposite foam with GnP(750) and a minimal amount of treatment, demon-

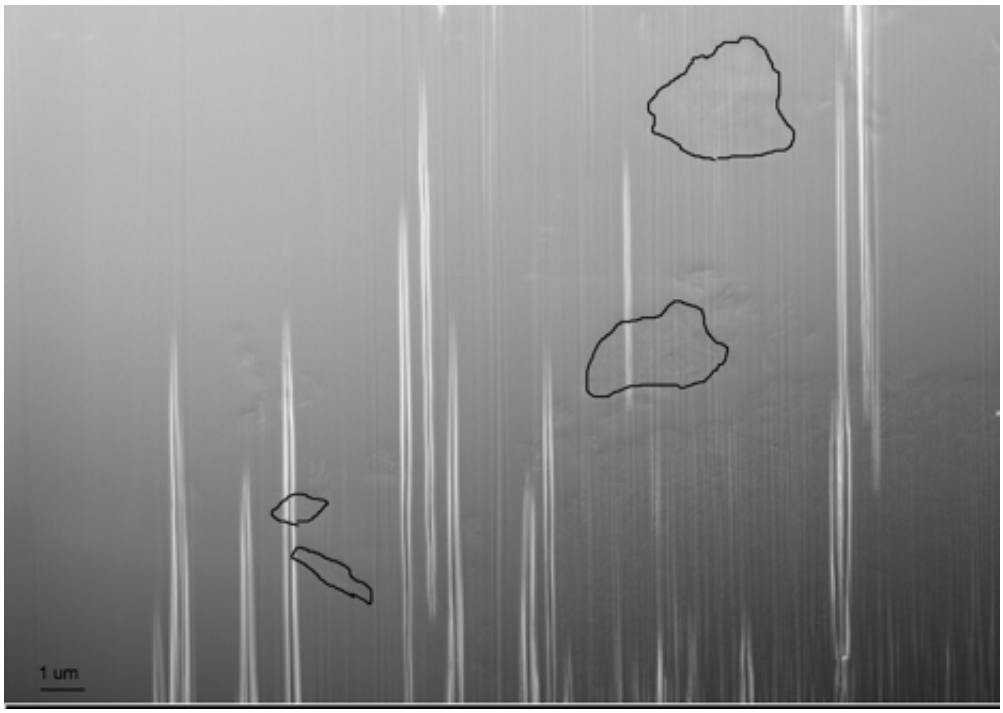

Figure 3.17: FESEM image of GnP dispersion in rigid PUR/PIR foam with 8 wt% pMDI treated GnP(750). Strut was prepared with the FIB and aggregates are outlined in black.

strated a similar glass temperature to the non-treated GnP(750). Since pMDI treated GnP(750) consists of much larger agglomerations as seen in Figure 4.16, whereas the neat and minimal treated GnP(750) do not; it appears that the small particles do a much better job at allowing the polymer to cross-link in the foam. The smaller GnP appear to tend not to disrupt the local molecular structure even when there is a edge-functionalization, which is slightly surprising due to its higher edge density, but probably has to do with the sizes of the particles being more on the scale of the microphase structure.

For the monolithic PUR/PIR adding the treated GnP causes some significant changes in the degradation profiles of certain molecular groups according to Figures 3.4 and 3.5. PUR/PIR with pMDI treated GnP-5 and GnP-25 show early onset for the depolymerization of urethane (peak 1) the opposite of the expected improvement due the GnP specific heat capacity. PMDI treated GnP-5 shows no improvement over the neat GnP-5 and a slight decrease in the amount of urethane and urea. In addition, the monolithic polymer with

pMDI treated GnP-25 also shows earlier onset for peak 2 representing the breakdown of urethane monomers. This gives further evidence that the GnP is coated with polymer as it prevents the GnP from absorbing the heat preventing it from transferring to the particle and causes a lower heat capacity. Urea in the same sample appears to have about the same thermal stability as there appears to be a second peak in the profile that has formed above 300 °C. The increased amount polyurea suggested by the significant increase in weight loss of the solid with neat GnP-25 is probably responsible for the higher T_g. There is a significant concentration of GnP-5 which seems to be the deciding factor along with the size that is affecting the cross-link density and likely the microphase morphology. One thing the pMDI treated GnP-5 does help is in the thermal stability and since it is only really at the end of peak 2 that suggests that it might be making polyurea more thermally stable.

Compared to the monolithic polymer there are significant changes in the thermal properties of the rigid PUR/PIR foam with the addition of the edge-functionalized GnP. The size however still seems to be the significant factor as the profile of the neat and treated GnP-25 overlap for the most part. Looking at Figures 3.6 - 3.10 the degradation profiles still show an increase in the thermal stability of the molecular groups in the foam samples with treated GnP when compared to the foams sample with no GnP; demonstrated by the shift in onset temperature, although the change is not as significant suggesting again that coating the GnP with polymer is decreasing its specific heat capacity. The peak starting at around 300 °C for the nanocomposite foam with pMDI treated GnP-5 follows the pattern of the monolithc polymer and clearly resolves two peaks, suggesting a more significant contribution from polyurea. Foam samples with pMDI treated GnP(750), both minimal and excess, do not show the two peaks and in fact the pMDI treated GnP(750) show a decrease in the thermal stability of the molecular groups suggesting a change in molecular structure that lowers the polymers heat capacity. The minimal treated pMDI treated GnP experiences constant weight loss from 300 to 400 °C, that is probably due to a decrease in PUR that has been compensated for with increased polyurea or PIR and explains why the T_g is similar to that of the neat

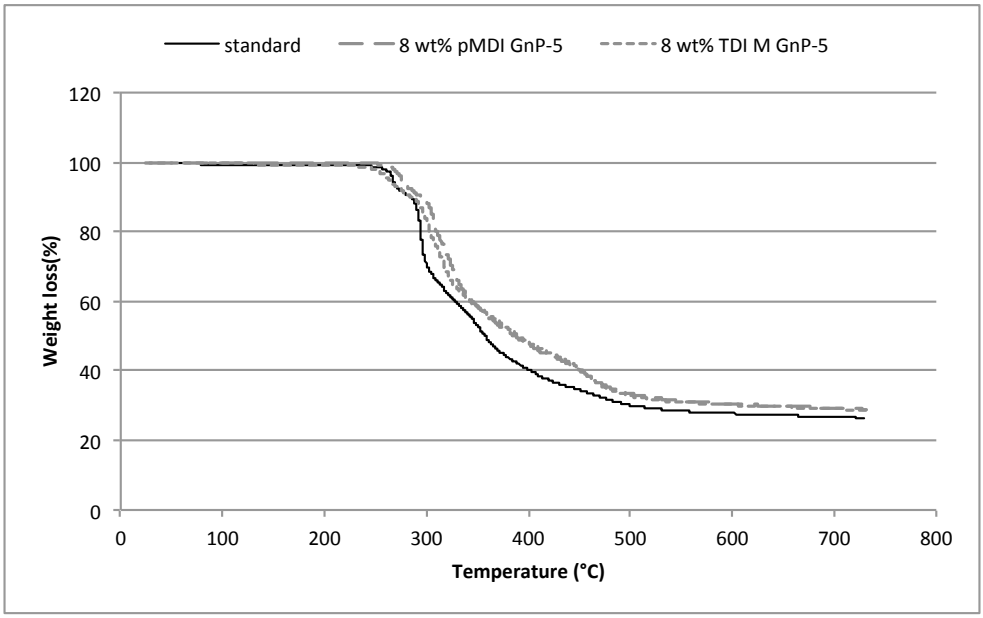

Figure 3.18: Thermal degradation profile of edge treated GnP-5 compared to the neat foam.

foam. Functionalizing the GnP(750) with the short TDI molecule instead of the polymeric isocyanate seems to not prevent the heat absorption of the particles. This is not the case for the foam that contains TDI treated GnP-5 that has a lower onset temperature when compared to the GnP treated with the polymeric isocyanate and in fact causes a slightly earlier degradation onset of the depolymerization of PUR compared to even the standard. In addition the treatment on the edges of the GnP-5 seems to prevent the formation of the PIR as seen as seen in the lower slope of the weight loss in Figure 3.18 and derivative weight loss profiles at 400 °C and this is confirmed by the significantly lower T_g, which is not compensated for with an increase in polyurea as was seen in other samples. Once again the loading and size of the particle seem to be the dominating factor.

There are definitive changes in the cell diameters due to the changes in the reinforcements except for the pMDI treated GnP-5 and GnP-25 which show similar cell size to the neat rigid PUR/PIR foam sample. It appears, however, that edge functionalization better accommodates polymer chain formation during foaming shown by the increase in T_g along with the cell size for the treated GnP-25 over the neat GnP-25. Adding the treated GnP(750) result in a

larger cell size compared to the neat GnP(750) no matter what type of treated GnP is used. Generally a decrease in glass temperature that correlates to a change in cross-link density would allow for more movable linear polymer chains to facilitate the coalesce of the bubbles causing larger cell sizes. But the samples with minimal amount of treated GnP(750) have similar T_g to the standard and significantly larger cells. So it appears that cross-linking in this case does not affect the cell size. It could be a different physical phenomenon as evidenced in the foam with treated GnP (750) and GnP-5 where a significantly higher concentration of particles could be prolonging the gelation of the foam allowing the bubbles to coalesce and stabilization of the larger air bubbles due to mixing [82]. These changes in viscosity and mobility affect the kinetics, which in turn affect the phase separation and could be a deciding factor in the cell structure. In general the samples that have a larger median cell size also have a higher count of bubbles sizes greater than 300 μm (see Appendix). Once again, the larger cells could be responsible for the significant decrease in weight loss that reduces the amount secondary reactions that occur as the decomposed products escape.

3.5 Conclusion

The addition of a nanomaterial to a chemically blown foam appears to disrupt the polymeric system on a physical and chemical level changing the resultant polymer's molecular and microscopic properties. The gas expansion process alone causes changes in the thermal degradation profile, but not in the crosslink density, as the expanded structure results in a larger surface area, but similar T_g. A large surface area is commonly more beneficial in a diffusion controlled process. It helps to assist in the removal of the decomposed products on the surface, which is confirmed by the much narrower rate peaks. This structure can also be disadvantageous as it seems to prevent the removal of the decomposed products of the internal structure resulting in all the foam samples having a higher rate retention than the monolithic polymer. In general the rate of decomposition is much broader for monolithic polymer structure due to the diffusion limitations in the solid polymer.

The addition of the nanoparticle's high specific heat capacity increases the foam's thermal degradation. The addition of neat GnP-5 and GnP-25 to the rigid PUR/PIR demonstrated a similar degradation profile except from 325 to 380 °C, which could come from more thermally stable hard segments. The addition of comparatively larger GnP-25, both neat and treated, resulted in a similar cross-link density between the monolithic polymer and the foam, which was significantly lower. The large particles then tend to interact the same with the polymer regardless of the structure. Although, the addition of the neat GnP-25 in the foam also resulted in a lower cell size so the larger particles helped to stabilize the bubbles and prevent coalesce. The GnP-5 helps in this regard as well, but not to as quite as small a cell size, and the smallest particles (GnP(750)) do nothing for the cell structure resulting in significantly larger cell sizes, but could also be that the microphase structure enables the coalesce. It does appear, however, that the foam is better able to adapt its molecular structure as the T_g of the neat GnP-5 and pMDI treated GnP-5 was significantly larger in the foam as compared to the solid. In addition, the foam samples with neat and treated GnP(750) show a similar T_g to the standard the only exception is the pMDI treated GnP(750), and images show they have large μm aggregates and could be reason it shows a similar T_g as the pMDI treated GnP-25. These agglomerations could be affecting the resultant properties even more than the particle sizes and moving forward methods to reduce the aggregates will have to be employed as functionalization of the edges is not significant enough especially for particles that have a low edge density. The smallest particles were the most effective at improving thermal stability while maintaining a similar cross-link density and were most affected by the edge treatment due to their higher edge density. The foaming action also compensated better on a molecular level with the addition of nanoplatelets to maintain the cross-link density. In general the addition of GnP tends to prevent the formation of isocyanurate, which the polymer compensates for by increasing the concentration of polyurea to maintain the cross-link density.

Adding a nanoplatelet reinforcing material to a chemically blown polymer foam affects the

resulting chemical bonding and molecular and cell structure and the result can be improvement of the thermal stability of certain molecular groups. When changing the resultant properties of the polymer, platelet size is significant along with loading and it is important that the interaction between the individual particles and the matrix is maximized. Any fillers added to such a system in the future will have to take into account the effect they have on the chemical reactions and structure to improve the resultant properties of the overall nanocomposite foam.

Appendix

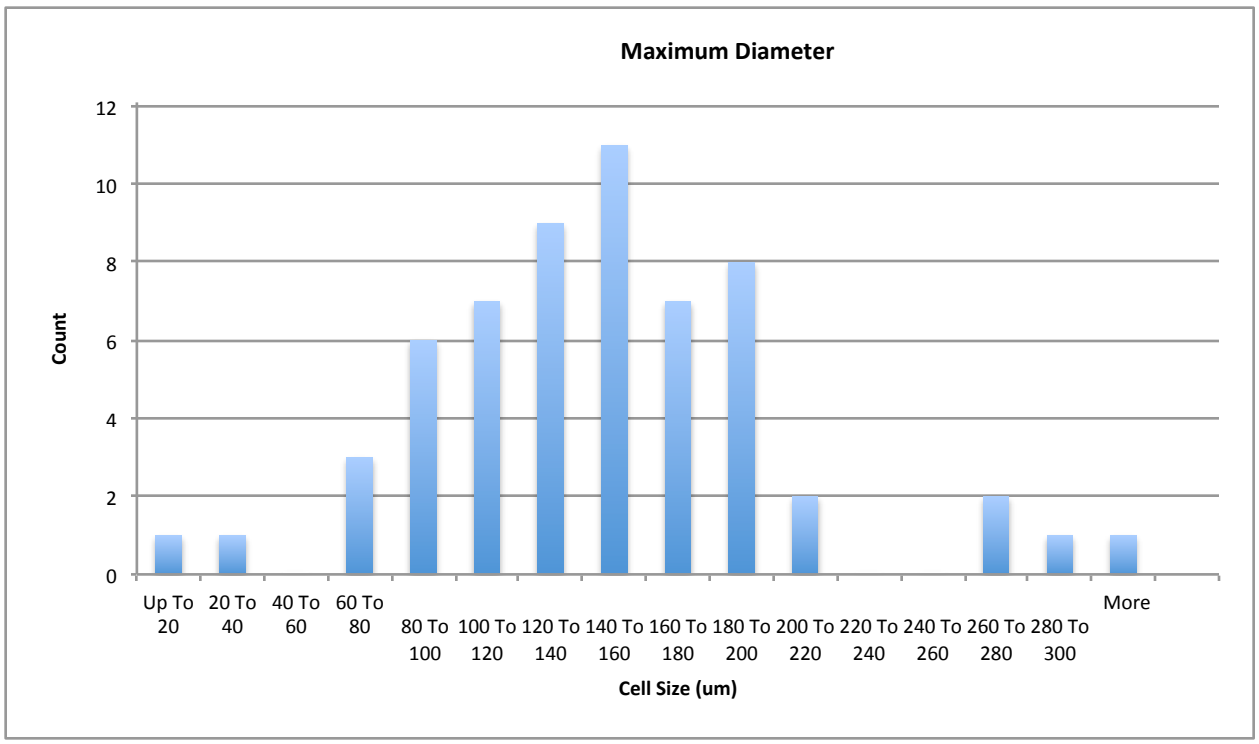

(a)

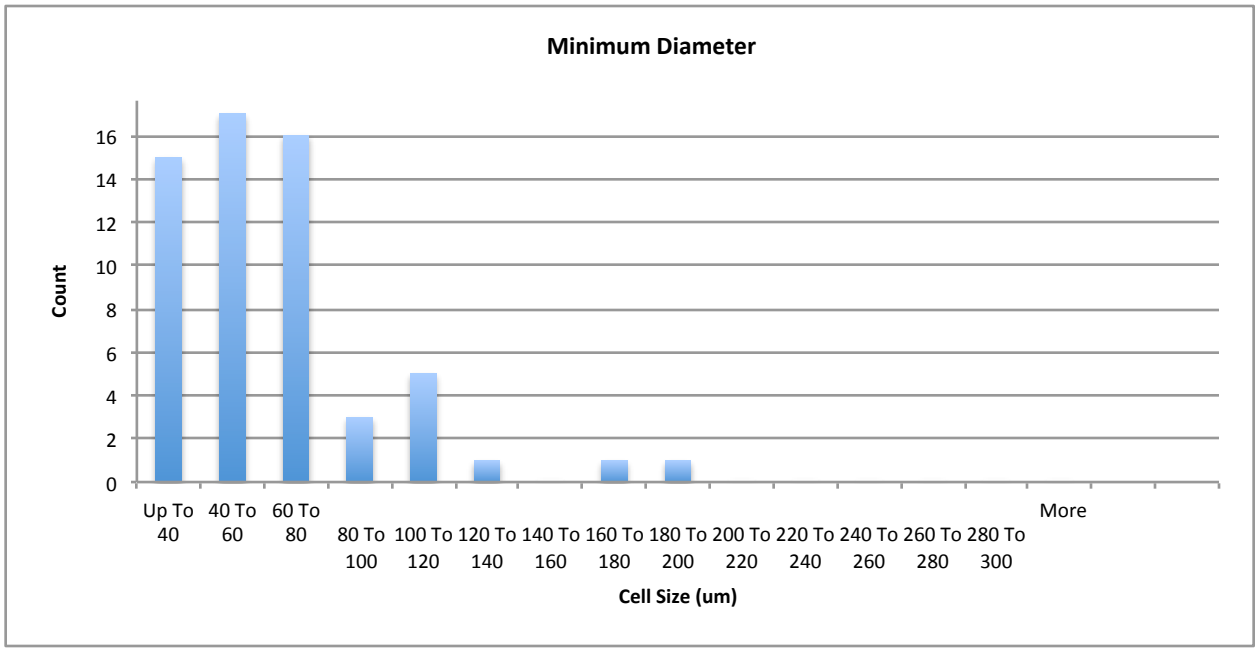

(b)

Figure 3.19: Max and min cell diameters of 60 cells in rigid PUR/PIR foam: (a) Histogram of maximum cell size (μm); (b) Histogram of minimum cell size (μm)

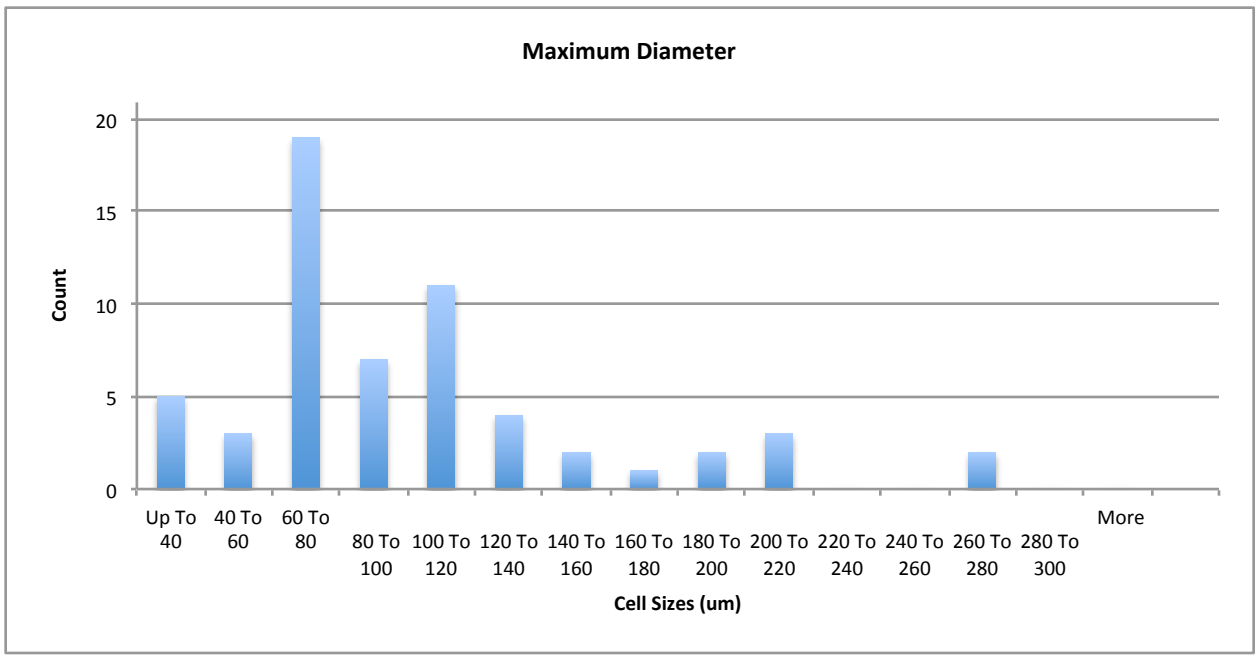

(a)

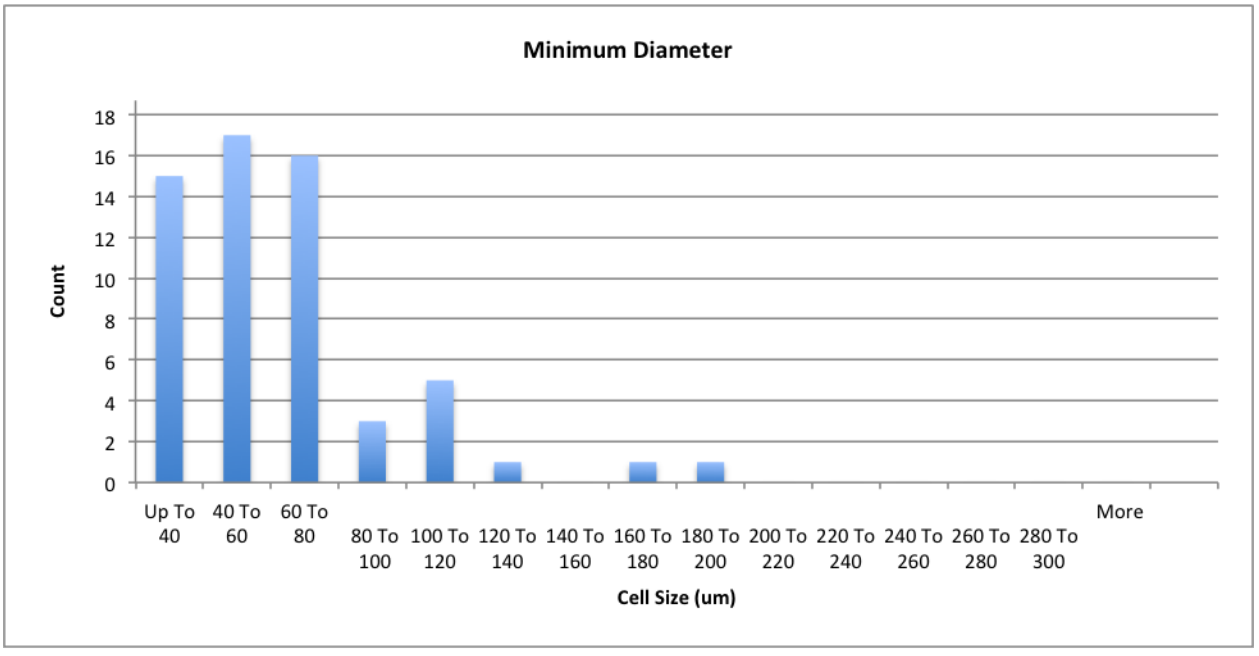

(b)

Figure 3.20: Max and min cell diameters of 60 cells in rigid PUR/PIR foam with 5 wt% GnP-25: (a) Histogram of maximum cell size (µm); (b) Histogram of minimum cell size (µm)

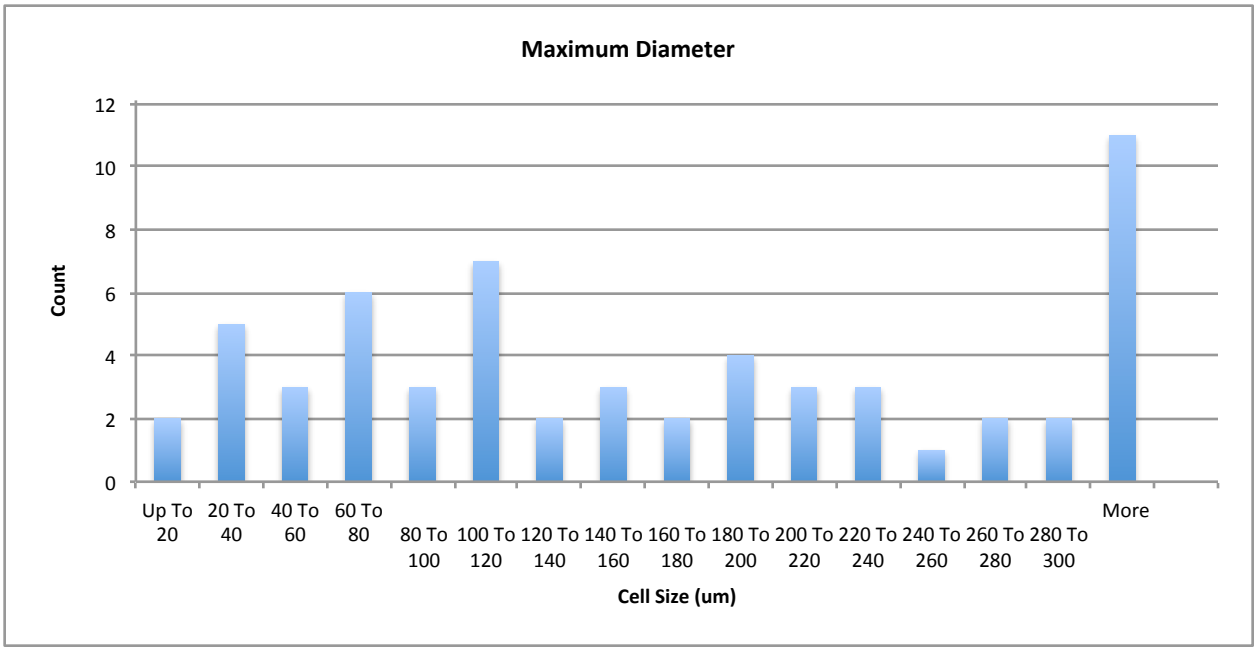

(a)

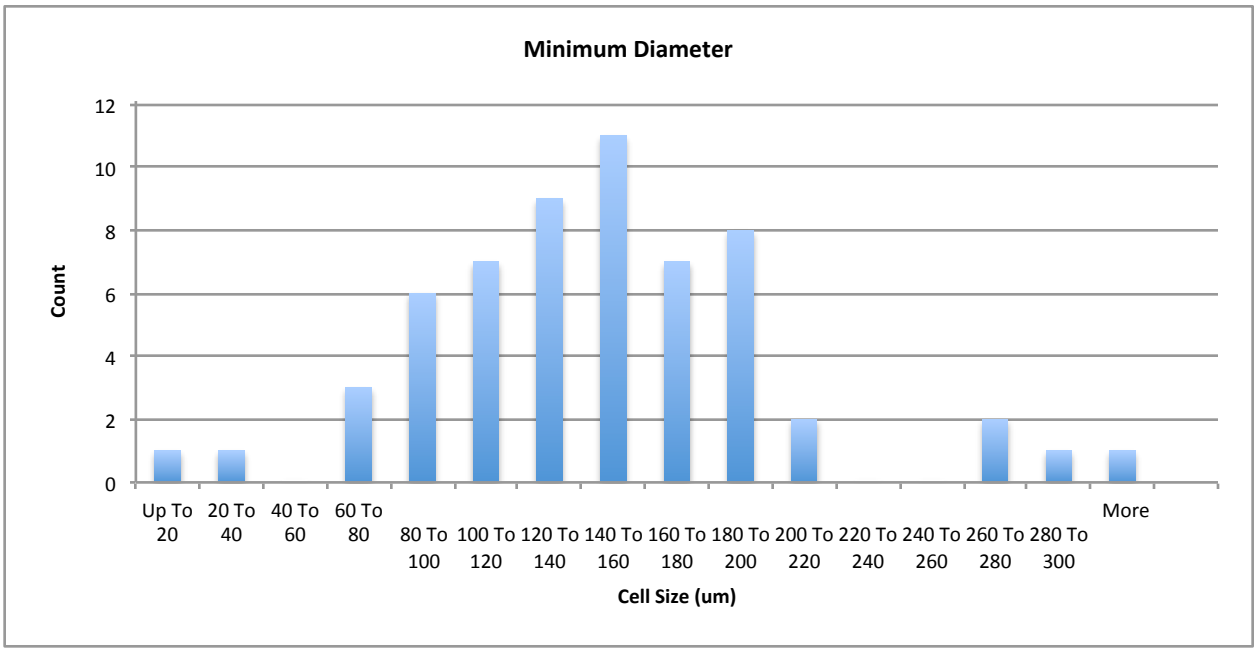

(b)

Figure 3.21: Max and min cell diameters of 60 cells in rigid PUR/PIR foam with 5 wt% pMDI GnP-25: (a) Histogram of maximum cell size (μm); (b) Histogram of minimum cell size (μm)

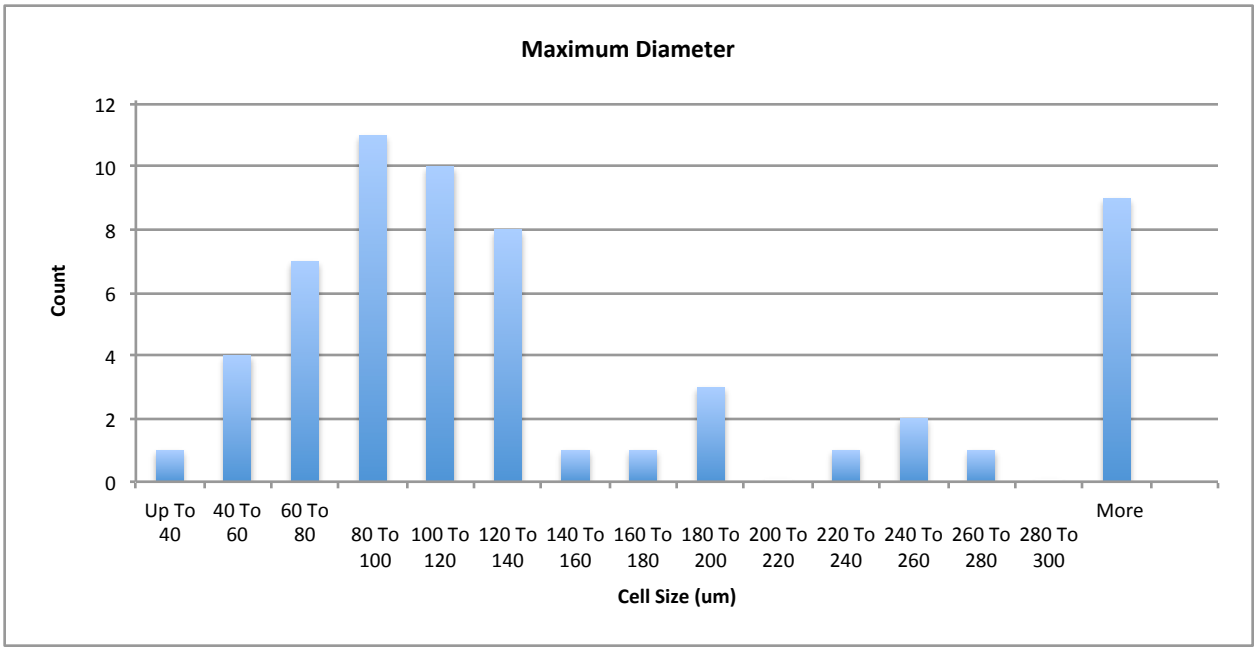

(a)

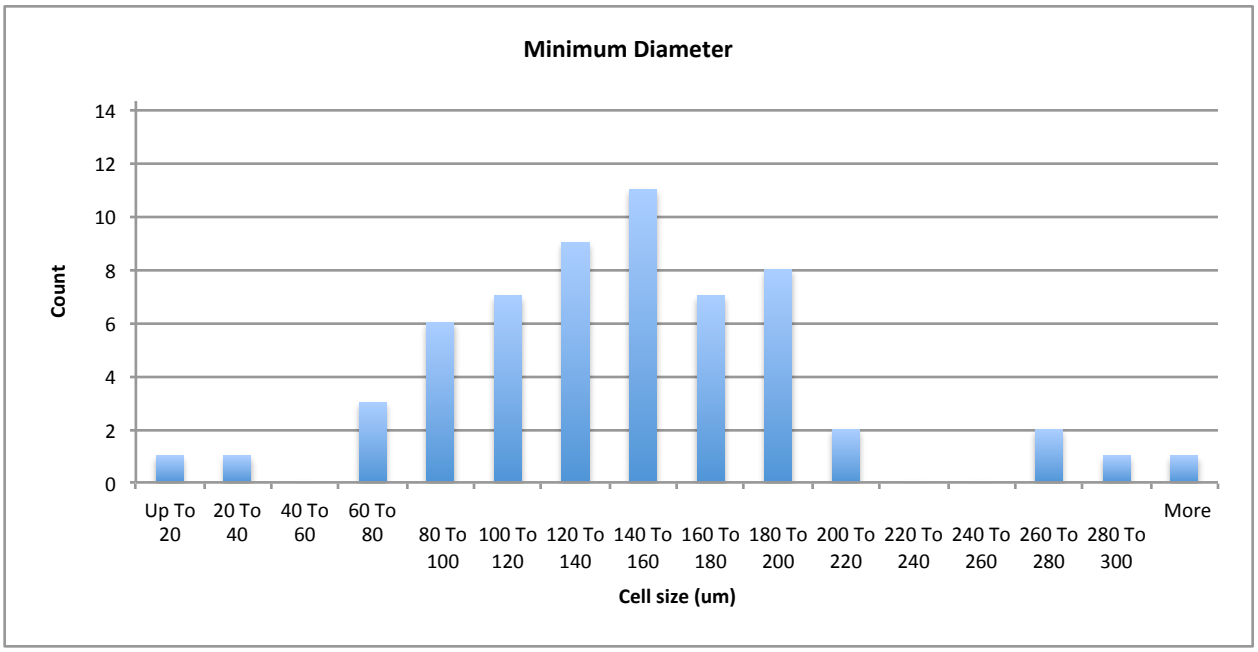

(b)

Figure 3.22: Max and min cell diameters of 60 cells in rigid PUR/PIR foam with 8 wt% GnP-5: (a) Histogram of maximum cell size (μm); (b) Histogram of minimum cell size (μm)

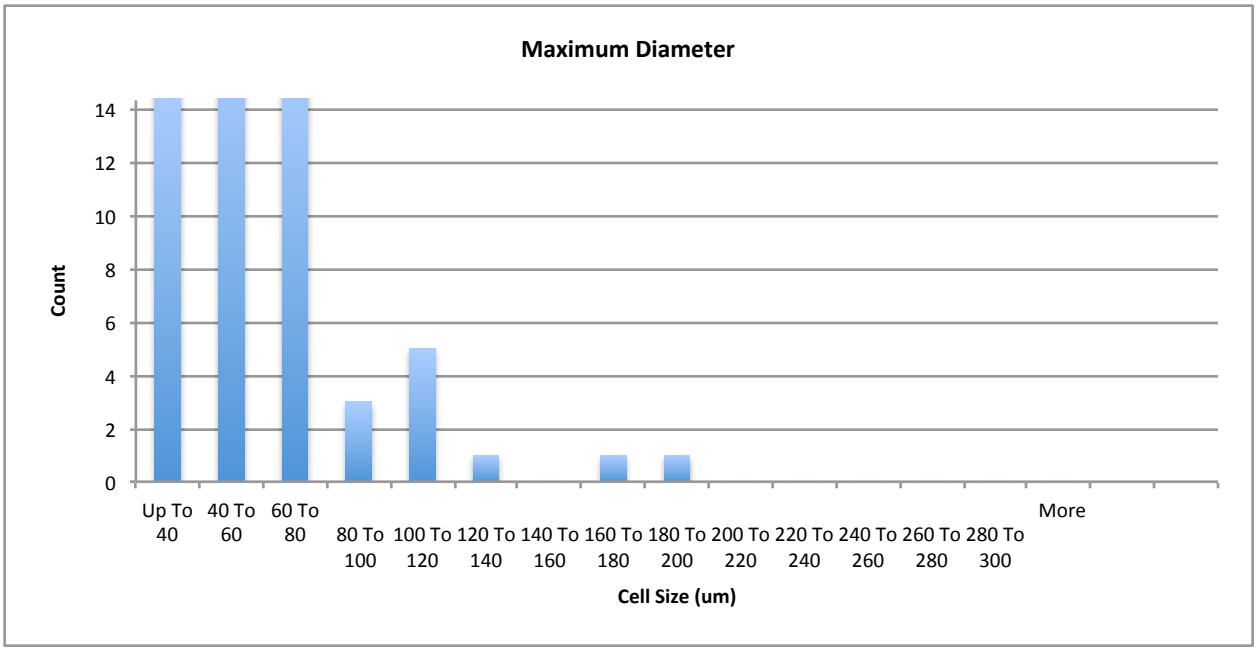

(a)

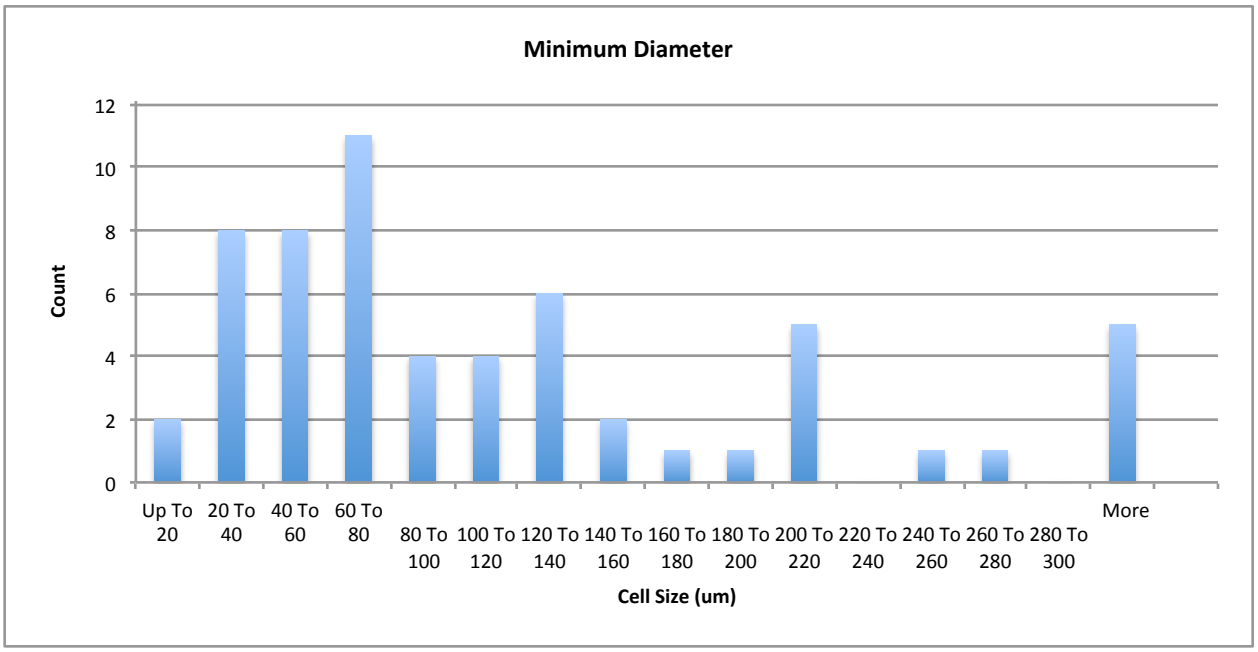

(b)

Figure 3.23: Max and min cell diameters of 60 cells in rigid PUR/PIR foam with 8 wt% pMDI GnP-5: (a) Histogram of maximum cell size (μm); (b) Histogram of minimum cell size (μm)

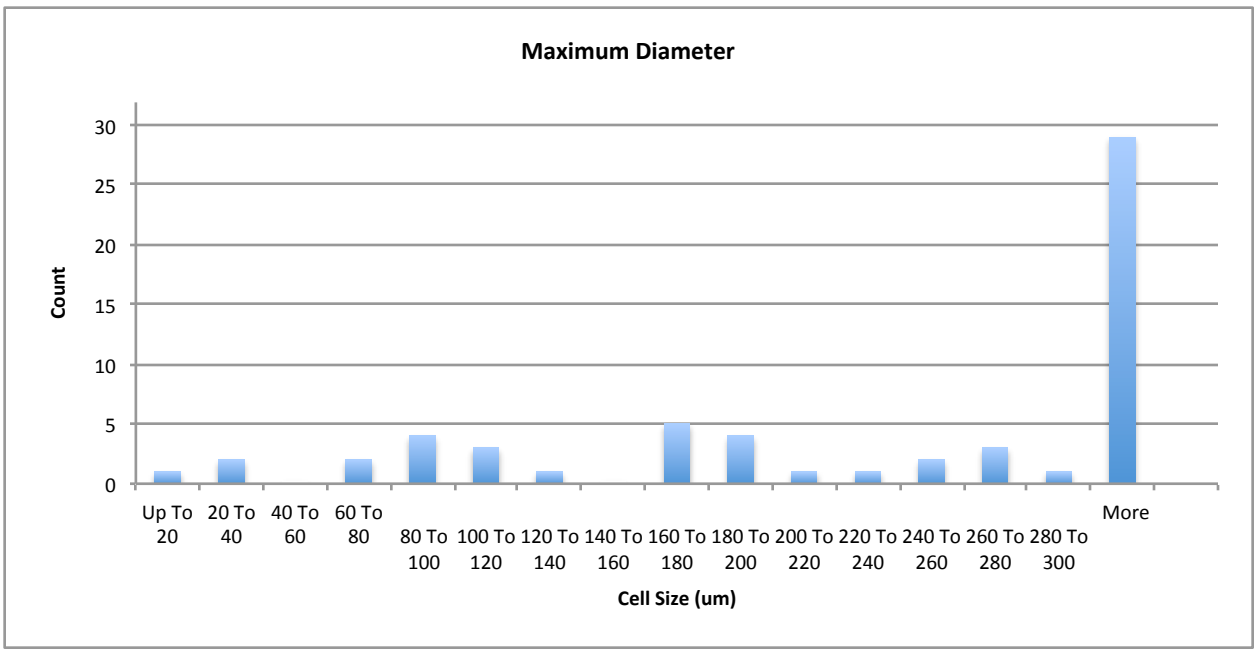

(a)

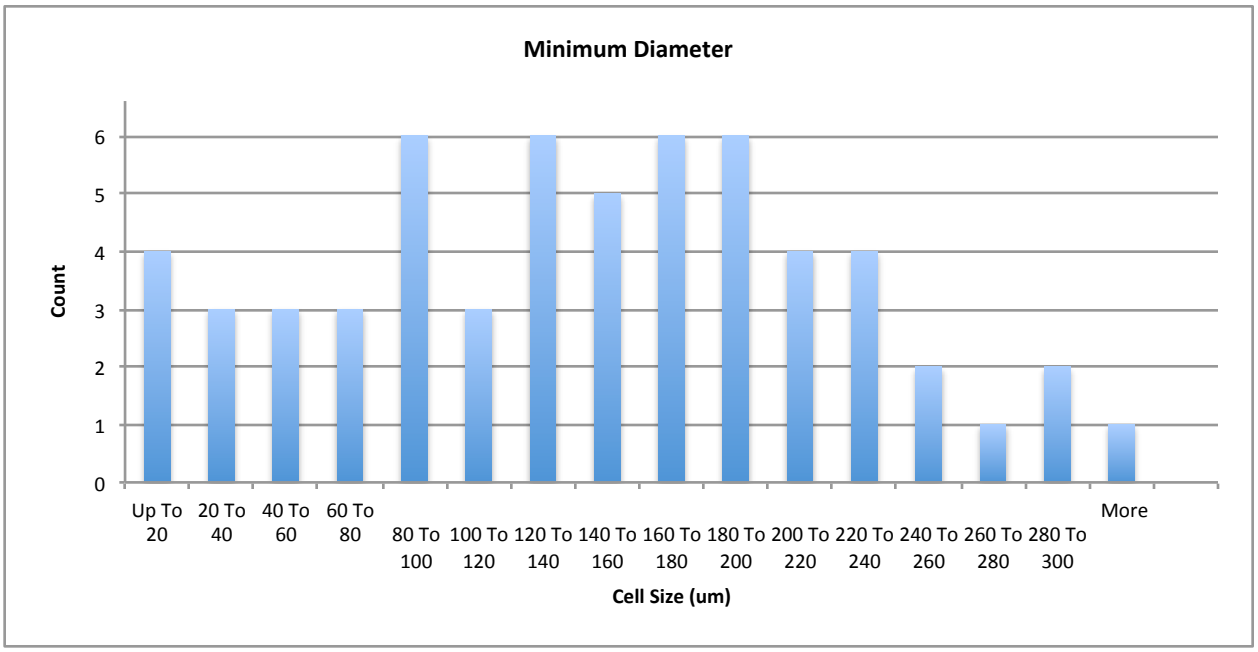

(b)

Figure 3.24: Max and min cell diameters of 60 cells in rigid PUR/PIR foam with 8 wt% TDI M GnP-5: (a) Histogram of maximum cell size (μm); (b) Histogram of minimum cell size (μm)

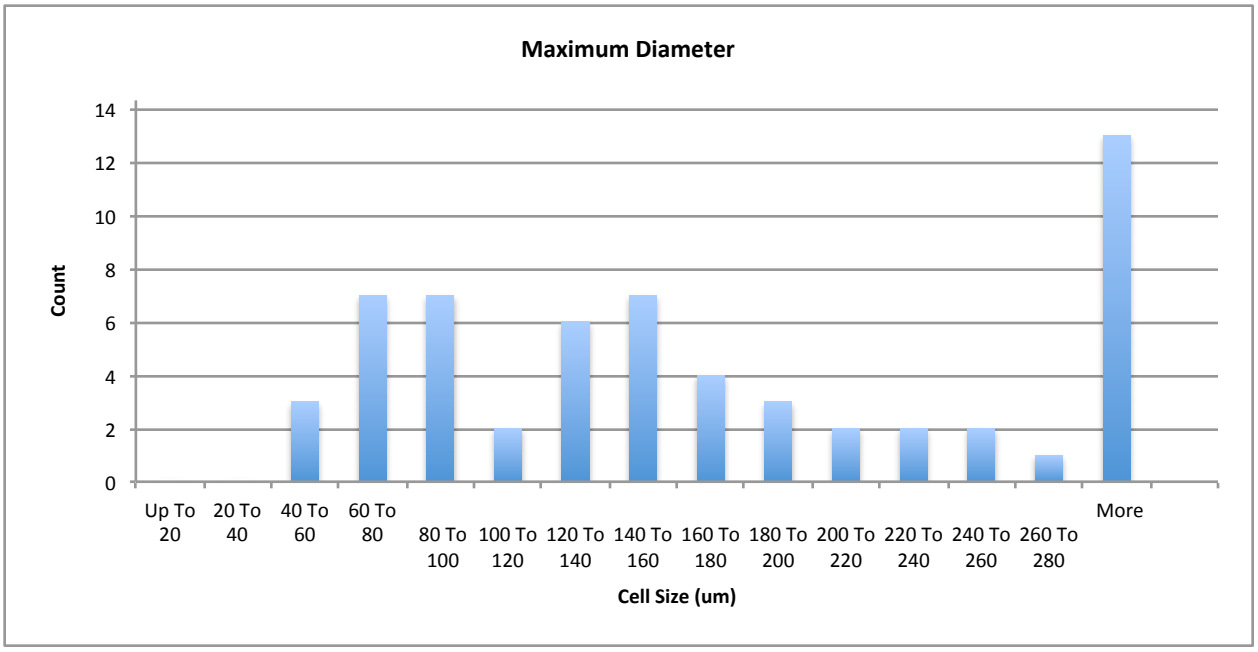

(a)

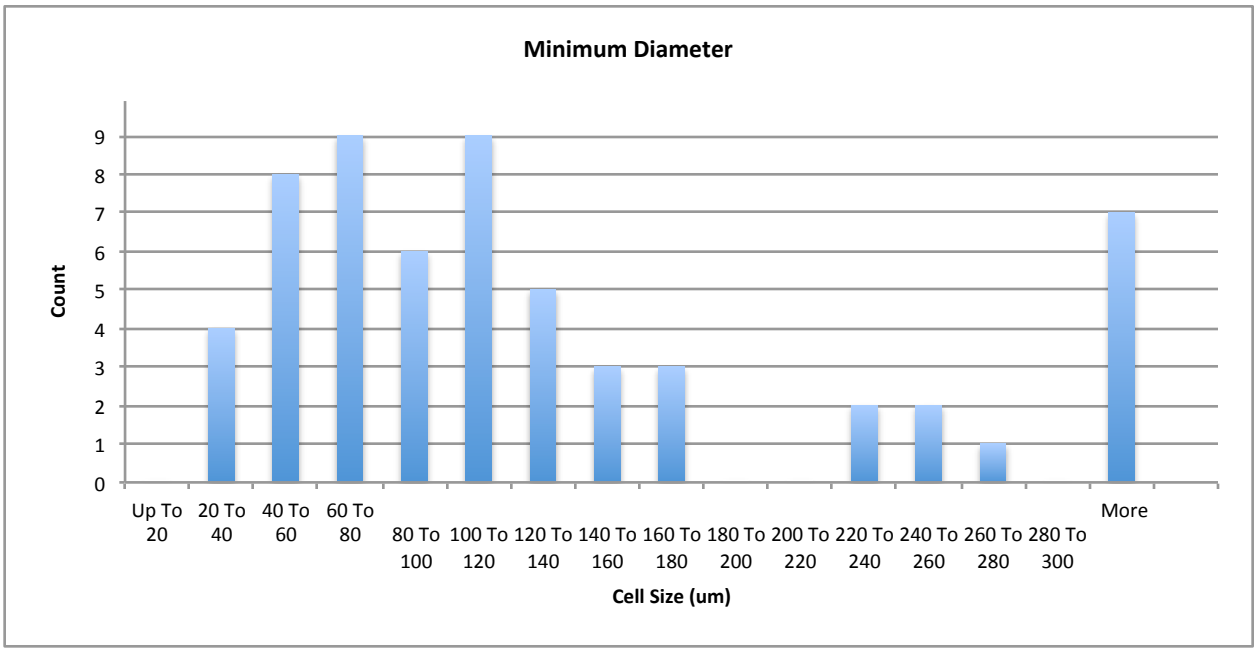

(b)

Figure 3.25: Max and min cell diameters of 60 cells in rigid PUR/PIR foam with 8 wt% GnP(750): (a) Histogram of maximum cell size (µm); (b) Histogram of minimum cell size (µm)

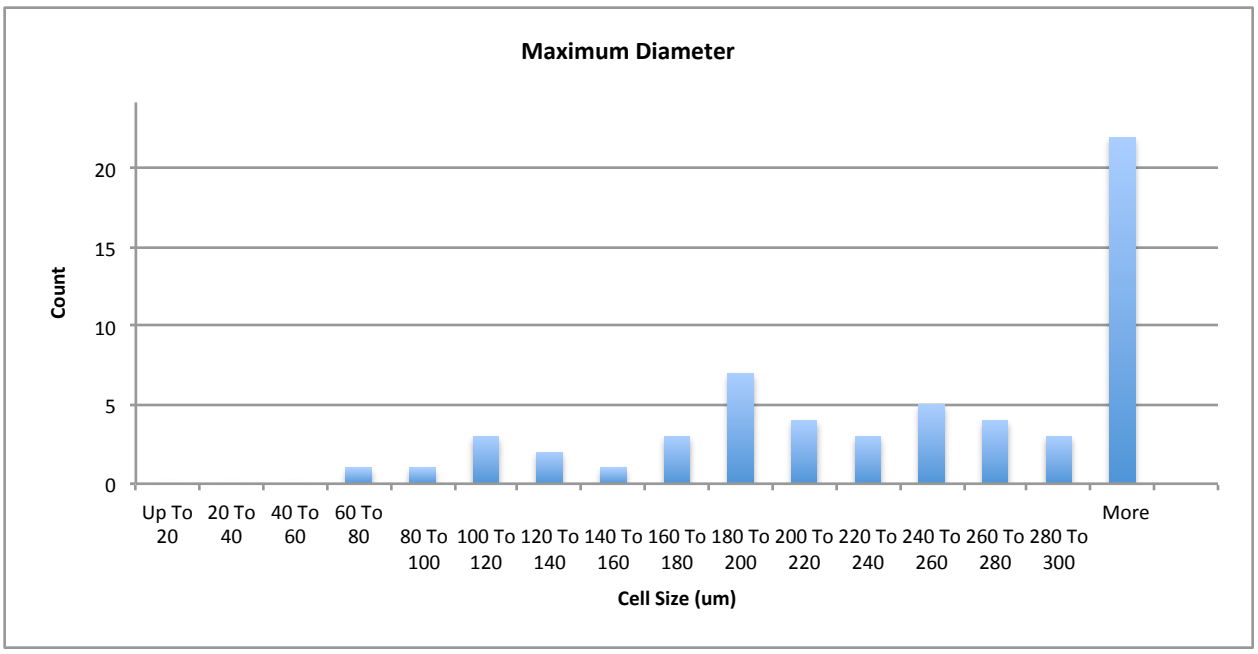

(a)

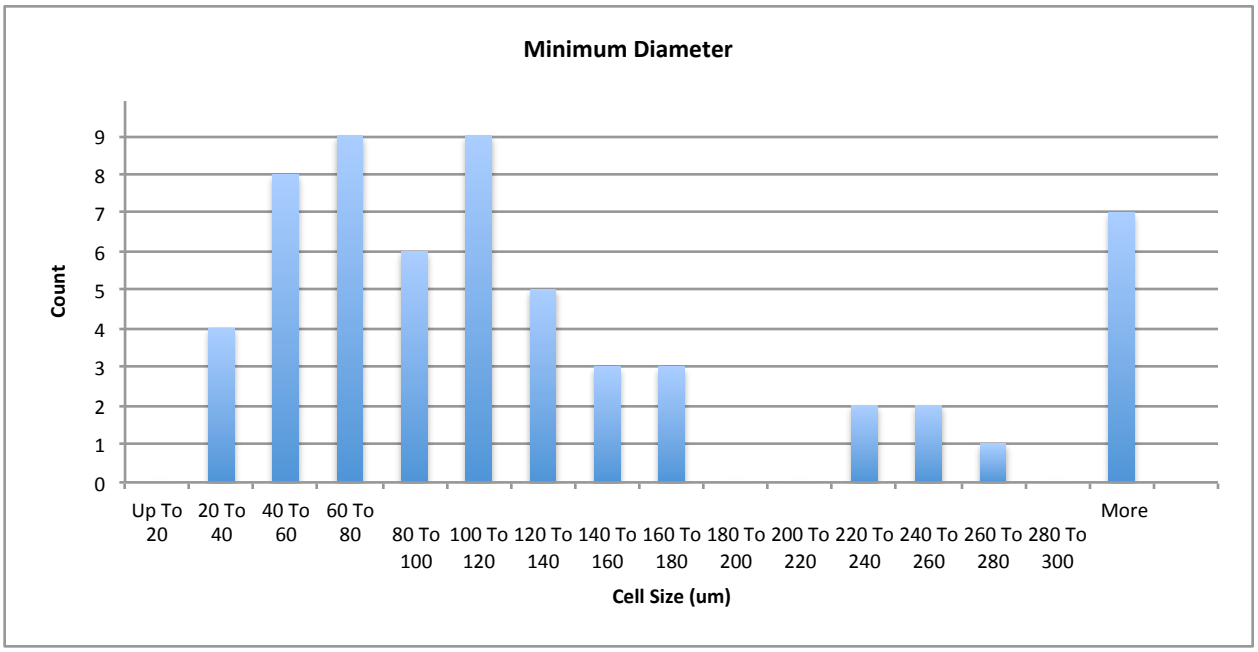

(b)

Figure 3.26: Max and min cell diameters of 60 cells in rigid PUR/PIR foam with 8 wt% pMDI GnP(750): (a) Histogram of maximum cell size (µm); (b) Histogram of minimum cell size (µm)

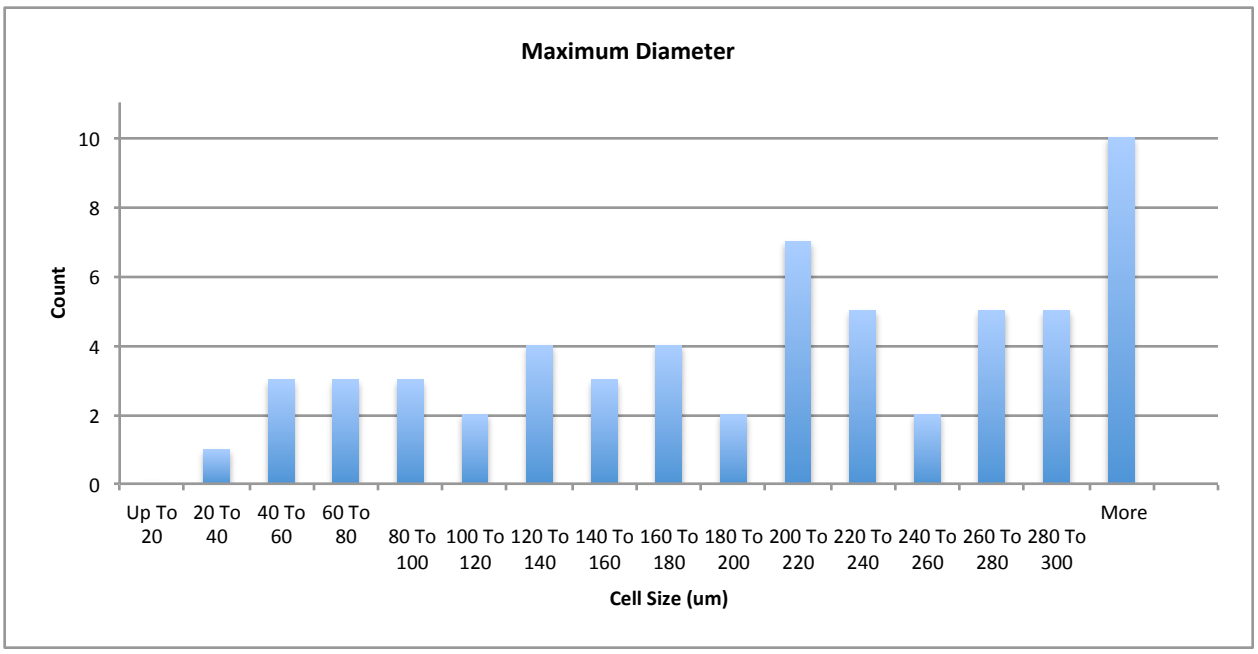

(a)

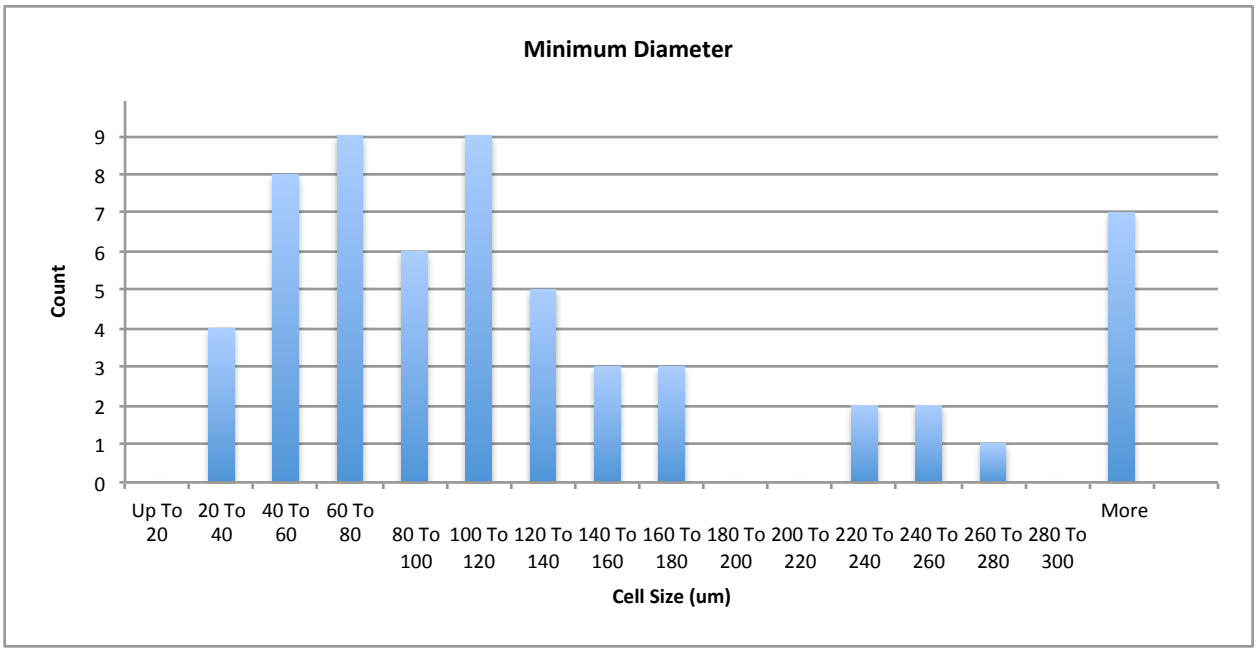

(b)

Figure 3.27: Max and min cell diameters of 60 cells in rigid PUR/PIR foam with 8 wt% pMDI M GnP(750): (a) Histogram of maximum cell size (μm); (b) Histogram of minimum cell size (μm)

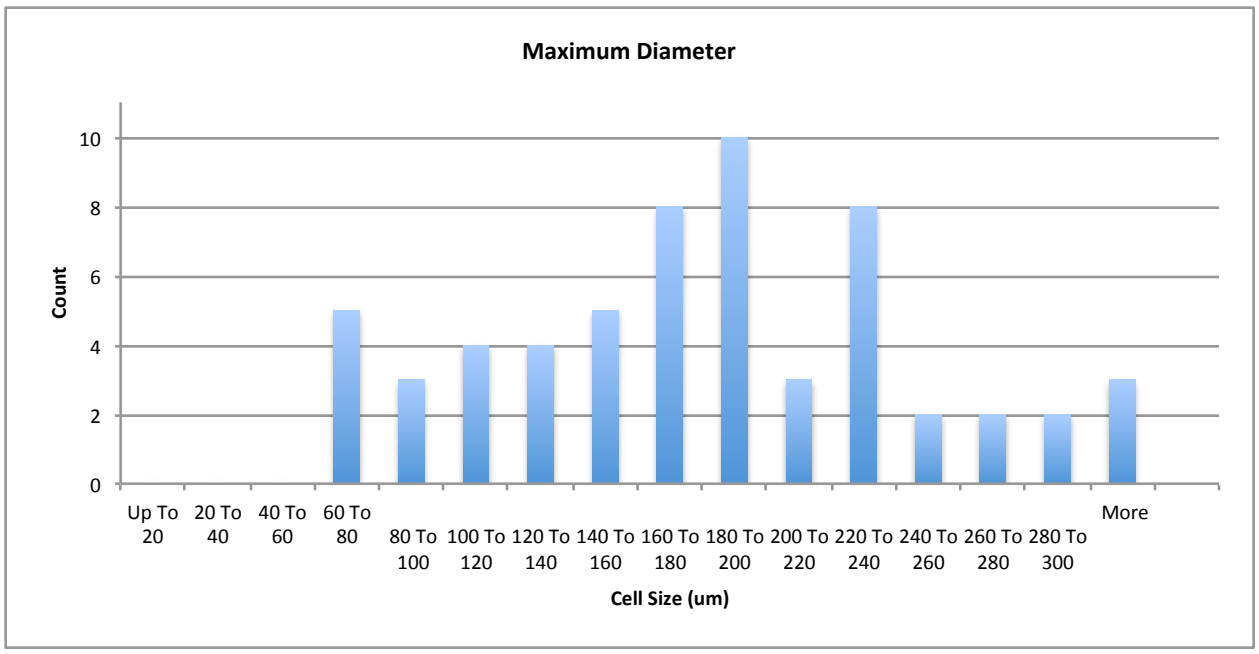

(a)

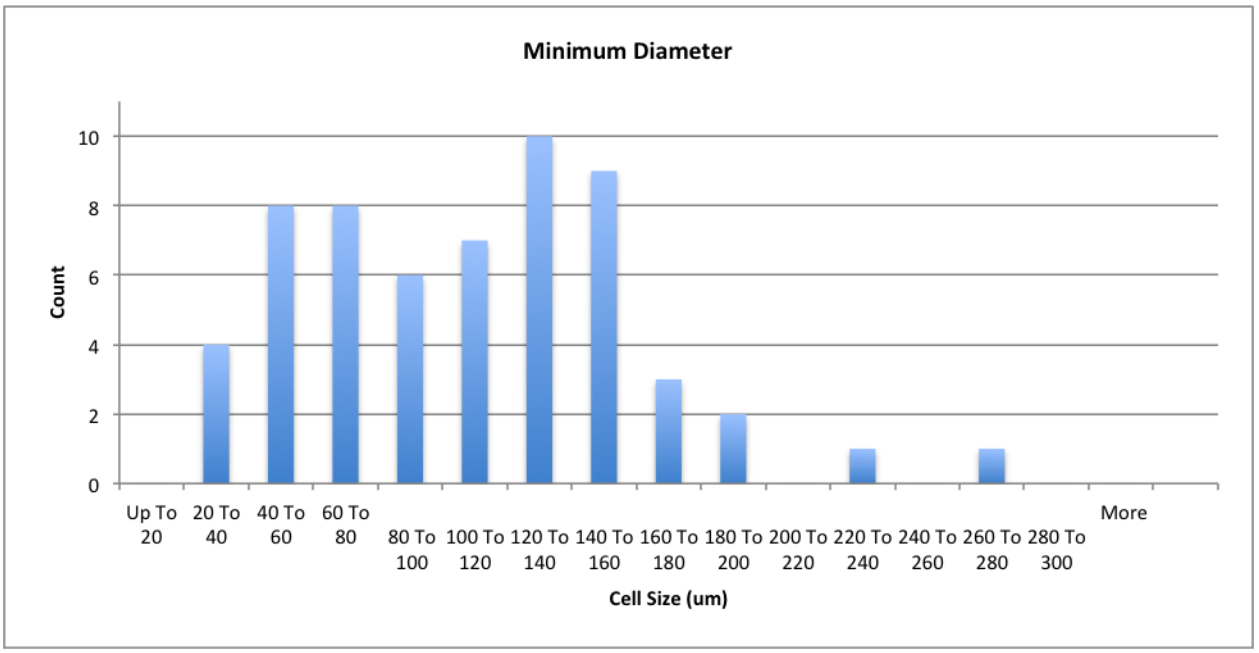

(b)

Figure 3.28: Max and min cell diameters of 60 cells in rigid PUR/PIR foam with 8 wt% TDI M GnP(750): (a) Histogram of maximum cell size (μm); (b) Histogram of minimum cell size (μm)

CHAPTER 4

MULTIFUNCTIONAL PERFORMANCE OF RIGID PUR/PIR FOAM

4.1 Introduction

As technology goes further into space there is a greater need for cost-effective materials with high-functionality. The necessity from the aerospace field as well as others has led to the development of multifunctional materials. The challenge is structuring these materials while maintaining certain properties that historically have been considered opposite, like high surface area and low weight, or they be both thin and strong. This has motivated a move beyond classic material classes to developing new ones. Such as the development of composite materials. With their commercial success and the discovery of nanomaterials there has been an uptick in the experimentation and implementation of nanocomposite materials. Research has already found that few weight% addition of high-functioning nanoparticles can greatly increase a materials performance, especially in polymers [8, 6].

Polymers are generally a low-cost material that come in a variety of properties. In addition, they are a multitude of ways to synthesize them and are readily formable. The various methods employed to make polymers suggest it could be relatively easy to add nanoparticles to the polymer matrix. Small weight% additions of nanoparticles have been found to improve their properties broadening their potential applications in everything from from robotics [14] to energy applications [10], to electromagnetic interference (EMI) shielding devices [69, 70, 71] to packaging [7] and more as uses are being researched all the time. In addition, gas can be added to the system to make light-weight cellular structures. Such nanocomposite foam materials have shown improved mechanical, dielectric and electrical performance [68, 16, 85, 86].

When it comes to determining what nanoparticles to put inside polymer nanocomposites

it mostly depends on the application. Carbon based nanoparticles are some of the more heavily utilized ones, which includes graphene, as due to carbon bonding structure this nanoparticle has multifunctional properties. Single layer graphene has been demonstrated to have a high Young's modulus of around 1 TPa[22], high thermal conductivity of about 3000 W/m K[21] and excellent carrier mobilities greater than 15,000 cm^2/Vs[19]. Current methods to synthesize single layer graphene are very particular. High purity graphene comes with a high cost and low yield by methods such as chemical vapor deposition [26, 27] or expitaxial growth [29], and low purity graphene has a low cost and high yield such as seen with reduced graphite oxide [33, 43]. Another popular method forcibly separate the graphene sheets from its naturally occurring parent, graphite [43]. This method offers high purity, high yield thin, robust particles consisting of multiple layers of graphene sheets making it a potential filler for bulk polymer nanocomposites.

4.2 Experimental Methods

4.2.1 Materials

The foam is a chemically blown polymer. This means that upon the mixture of two components the material polymerizes and evolves gas simultaneously. The polymer matrix is polyurethane/polyisocyanurate (PUR/PIR) mixed foam, a common commercial material. It has been around for decades with a well-understood process-structure-properties relationship. Urethane in this case is formed from the addition reaction of isocyante and hydroxyls [51]. Isocyanurate describes the trimers that form from the reaction of three isocyanate groups with the assistance of a catalyst. The addition of the cyclotrimerization reaction during the polymerization of the foam results in a more thermally stable material [51]. A chemically blown foam also contains a blowing catalyst and blowing agent. The blowing agent chosen for this experimentation was environmentally friendly water. Lastly, a surfactant is added to assist in cell formation, which in PUR foams is commonly a polysiloxane.

Huntsman generously supplied the polymeric methylenebisphenyl diisocyanate (pMDI) and the polyols. The pMDI (Rubinate M), a standard pMDI with a viscosity of 190 cP s a specific gravity at 25 °C of 1.23 and an isocyanate content of 31.1 %NCO [54]. The polyols are Jeffol FX31-240 and Jeffol G30-650 both difunctional. Jeffol FX31-240 is a low viscosity polyol at 250 cP-s compared to Jeffol G30-650, which has triple the viscosity at 880 cP-s[54]. Ethylene glycol reagent from CCI (#216500), which has a water-like viscosity, was also used as a hydroxyl component to lower the viscosity of the system [55]. The catalysts were supplied by AirProducts: Dabco BL-11 is a standard blowing catalyst and Dabco TMR-3 is a standard cyclotrimerization catalyst for water-blown foams [57]. The polysiloxane surfactant is also from AirProducts, Dabco DC193 [57]. Lastly, the blowing agent is distilled water. The ratios for these components are as listed in Tables 2.1 and 2.2 on page 18. The source of the 2,4'-toluene diisocyanate (TDI) that was used to functionalize the GnP was TCI Chemicals (#T0264) [58].

All the nanoparticles used in this research are sourced from XG Sciences. Different types of graphene nanoplatelets (GnP) are utilized as a cost-effective replacement for single-layer graphene and consists of multiple stacks of graphene sheets. Table 4.1 shows the different types of GnP used in this research and their physical characteristics. The GnP basal plane is not disrupted by any chemical groups. All chemical groups are focused on the edges, the majority of which are hydroxyls. All as-received GnP is first heat treated to 450 °C for 2 h prior to use.

Table 4.1: Properties of different types of as-received GnP used in nanocomposite foams.

Property	*GnP-25*	*GnP-5*	*GnP(750)*
Surface area (m^2/g)	120	120	750
Average Diameter (μm)	25	5	<1
Thickness (nm)	6-8	6-8	3-4

4.2.2 Synthesis of PUR/PIR Nanocomposite Rigid Foam

The PUR/PIR rigid foam was synthesized by first combining both difunctional polyols with ethylene glycol. This solution was then mixed with a paddle stirrer for 2 hin an environmental glove box kept at below 40% humidity. The surfactant, catalysts and blowing agent were then added and stirred for an additional h. If GnP was required then it was added to the polyol solution at either 6 wt% for GnP-5 and GnP(750) or 3 wt% for GnP-25. The remaining GnP was added to the pMDI. Each GnP blend was then individually high-speed shear-mixed at 1600 rpm for 2 min followed by 2400 rpm for 1 min. Followed by ultrasonication with a 2.54 cm probe at 100 W until well blended, which was typically between 5-10 min. Adequate dispersion in the polyol blend was checked using an optical microscope. After confirmation of the dispersion the polyol blend is poured into the pMDI component, and stirred with an immersion blender for 45 s, prior to pouring into a mold. The foam was then allowed to free-rise and cure overnight. The neat foam had an average density of 0.16 g/c^{3}m.

4.2.3 Edge-functionalization of GnP

To improve the interaction of GnP with the polymer matrix the particle edges were functionalized. As mentioned previously many of the edge groups of GnP are hydroxyls which as already mention react with isocyanates to form urethanes. The first set of experiments to functionalize the GnP simply added pMDI to the GnP and relied on heat to force a reaction to occur between the pMDI and hydroxyls forming polyurethanes.

1. Heat-treated GnP is added to beaker and heated to >100 °Con a hot plate to remove any adsorbed water molecules

2. Enough pMDI is poured over GnP to cover

3. Solution reacts at 140 °C for one hour

4. Solution is removed from heat and cooled

5. Material is washed with acetone and solids are collected by centrifuge and excess is decanted.

6. Process is repeated six times

7. GnP is dried to remove acetone at a slightly elevated temperature

The second set of experiments attempted to create a minimal (M) amount of reacted groups on the edges of the particles. This was done with both the polymeric MDI and the molecular TDI. The detail of their structures is in Figure 2.2 on page 16.

1. GnP is dispersed in acetone using a 2.54 cm ultrasonication probe at 100 W at a concentration of about 6 g of GnP per every L of acetone.

2. The solution is ultrasonicated for at least 1 h. The dispersion is observed with an optical microscope.

3. A small amount of pMDI or TDI is added to the solution at a ratio of 64 μL for every 6 g of GnP.

4. Ultrasonication with the same probe and power is done for an additional h.

5. The edge-functionalized GnP is then retained using the same washing-centrifuging-decant procedure from before

6. GnP is dried to remove acetone at a slightly elevated temperature

4.2.4 Testing Procedures

4.2.4.1 XPS

X-ray photoelectron spectroscopy (XPS) was used to characterize the amount and type of reacted groups on the GnP after treatment with pMDI and TDI. XPS is a surface characterization technique with a penetration depth up to 1 μm making it the best spectrometer to

measure the small amount of reacted groups on the GnP edges. In addition, the spectrometer can measure energy shifts in the atomic groups giving information about the molecular structure as well. GnP-5 and GnP-25 initially have no nitrogen and GnP(750) has only about 1 atomic percent (at%) so the focus was on the nitrogen spectra to identify the level of functionalization. First, a scan was done on a neat PUR/PIR sample that contained no GnP. The only peak that appeared on the nitrogen spectra was a broad peak at 400 eV, which means all the groups formed in the foam center around this peak. The nitrogen spectra of the edge-functionalized GnP shows three peaks resolved from the overall peak at 400 eV: the first is centered at around 399 eV and is commonly attributed to amine groups [64] including urea [64], the second is the highest peak centered over 400 eVfor urethanes and the third is centered at around 401.3 eV, likely due to pMDI. The pMDI could be from excess unreacted pMDI or simply to any unreacted segments of the polymer chain.

4.2.4.2 Mechanical and Electrical

The testing completed on the rigid PUR/PIR foam samples includes their mechanical performance, electrical performance and dielectric properties. For the mechanical properties four specimens were cut from the PUR/PIR foam samples to the size of 25.8 cm^2 by 2.54 cm thick. The specimens were compressed at a rate of 2.5 mm/min to a 3.8 mm deflection on a Universal Testing System (UTS). Compression testing is the common mechanical testing method for rigid foams, in addition compression tests are not as dependent on defects in the sample. Electrical resistivity was tested on three specimens with the dimensions: 40 mm long by 10 mm wide by 3 mmthick. Two probes were in contact with the surface by conductive silver paste and tested on the Gamry using AC at 1 Hz.

4.2.4.3 Dielectric and EMI SE

The dielectric performance was measured using the transmission line technique on a vector network analyzer (VNA) between 8.2 GHz to 12.0 GHz. Three specimens were cut to 10.05

mm wide by 22.4 mm long and a maximum thickness of 7.4 mm. The VNA supplies the electromagnetic (EM) wave to the sample and then measures how much of that is reflected (S_{11}) or transmitted (S_{21}) through the sample. The NRW algorithm developed by Nicolson and Ross [65] and Weir [66] is then applied to these values to determine the complex relative permittivity (ε_r) assuming an isotropic material. The equations describing the relative permittivity are complex numbers made up of real and imaginary parts, shown in Equation 2.5 on page 28. ε'_r describes the materials ability to store electronic energy when encountered by an electromagnetic field, $\varepsilon"_r$ is the factor that shows how much of that energy is lost instead. The real relative permittivity value is also known as the dielectric constant.

In addition, S_{21}, which is a measure of the ratio of power or voltage when a material is present (V_1) versus when it is not (V_2) is used to determine the electromagnetic interference (EMI) shielding effectiveness (SE) according to equation 2.13 on page 28. The SE of any material is the combination of three terms: the amount of wave that is reflected (SE_R), absorbed (SE_A) or reflected multiple times (SE_M). The fraction of applied field that is transmitted (T), reflected (R) and absorbed (A) is given by the scattering parameters as shown in the equations below [67]

$$T = |S_{12}|^2 \tag{4.1}$$

$$R = |S_{11}|^2 \tag{4.2}$$

$$A = 1 - R - T \tag{4.3}$$

4.2.4.4 Microscopy

As previously stated a reflectance optical microscope was used to observe the dispersion of the GnP in the acetone and polyol blend by drop-casting the solution onto a glass slide. A high resolution field emission secondary electron microscope (FESEM) was used in conjunction with a focused ion beam (FIB) to observe the dispersion of the GnP in the foam matrix. A FIB uses a beam of gallium ions to cut through a specimen while under vacuum in the SEM.

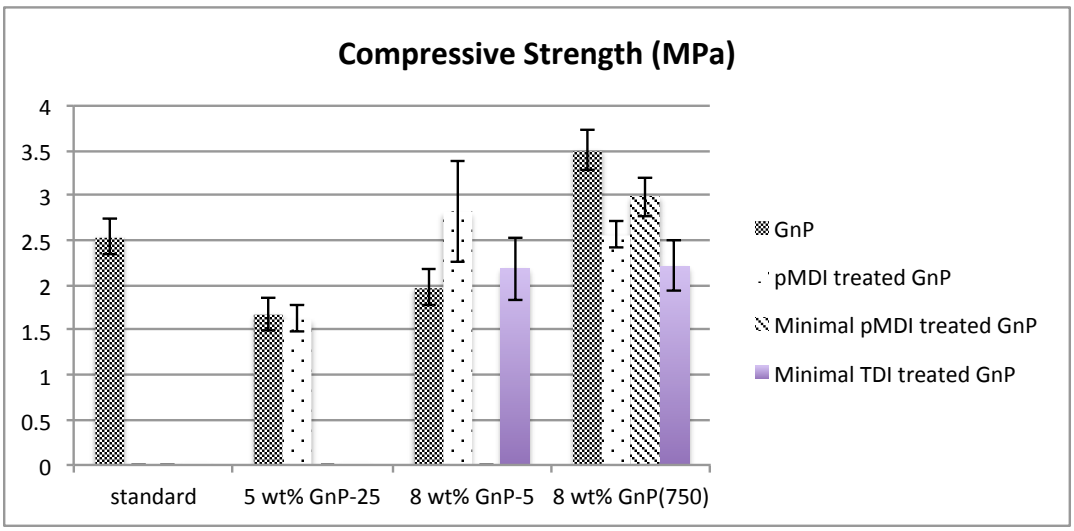

Figure 4.1: Compressive strength of foam with no GnP ("standard") compared to the nanocomposite foam with sample deviations at 10% deflection or maximum strength.

This is a good method for showing micrometer architectural features in a material as there is less of a chance of artifacts appearing on the sample due to the cutting and prepping methods commonly employed elsewhere. The surface was coated with 6 nm of gold and grounded to the stub with conductive carbon paste prior to imaging. All the FIB cuts are done through the struts of the foam, which is the term used to describe the point in the matrix between two gas cells as defined in Figure 3.1 on page 36.

4.3 Results

4.3.1 Mechanical Properties

The compressive mechanical properties of the standard foam compared to the nanocomposite foams with both neat and treated GnP are shown in Figures 4.1.- 4.2.

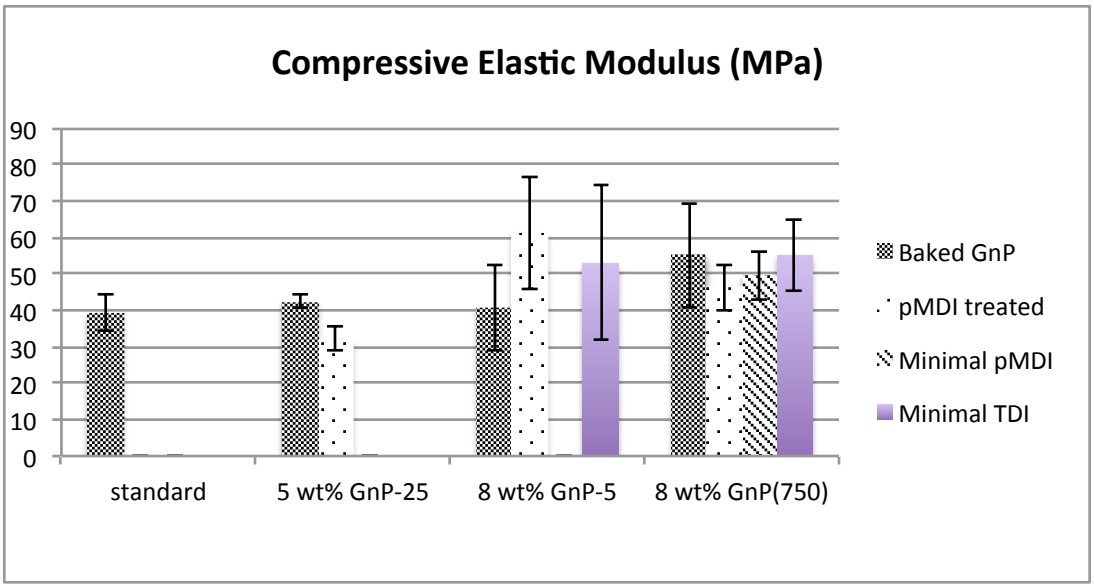

Figure 4.2: Compression elastic modulus of foam with no GnP ("standard") compared to the nanocomposite foam with sample deviation.

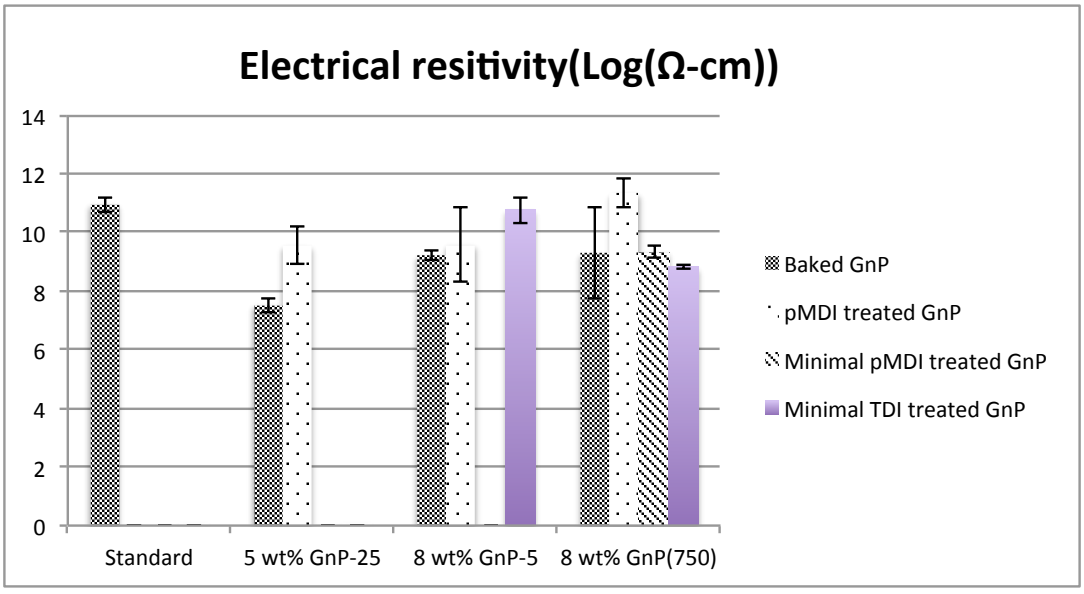

Figure 4.3: The resistivity of the foam specimens shown on a logarithmic scale comparing the standard with no GnP to the nanocomposite foam with sample deviation.

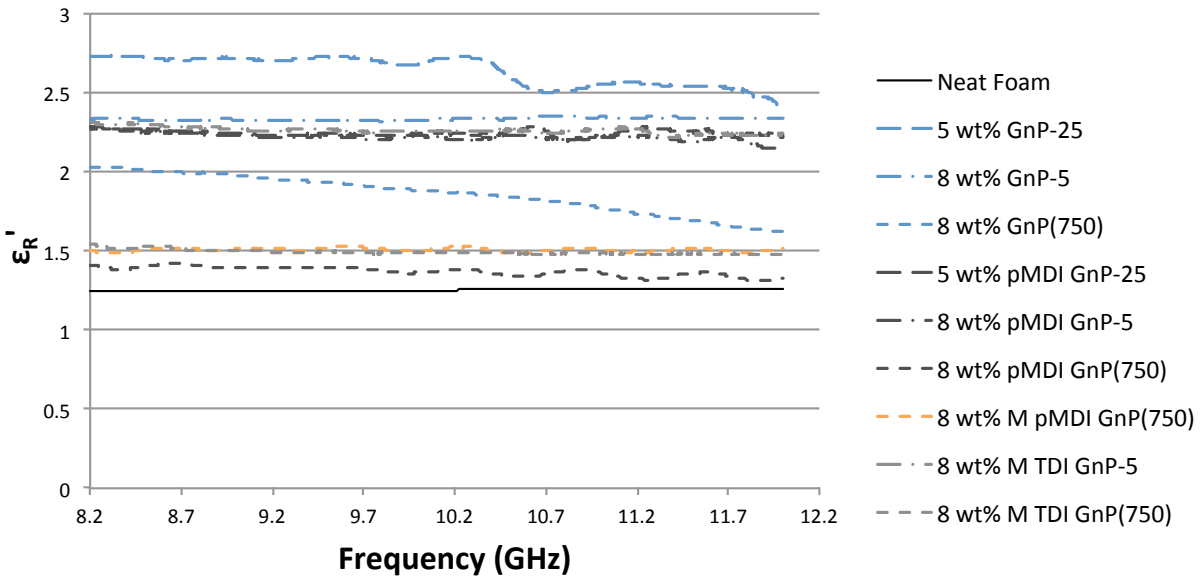

Figure 4.4: The ratio of the real permittivity of the foam samples relative to free space from 8.2 to 12.0 GHz.

4.3.2 Electrical Properties

Figure 4.3 show the results of the electrical resistivity for the PUR/PIR rigid foam samples with heat-treated and functionalized GnP compared to the standard that contains no GnP using a two-point probe method.

4.3.3 Electromagnetic Properties

Figures 4.4-4.8 are the electronic behavior of the neat and various nanocomposite foam samples when exposed to an electromagnetic (EM) wave. Real permittivity, also called the dielectric constant is shown Figure 4.4. The fraction of the wave that is transmitted and the approximate amount of that wave that is reflected and absorbed by the samples are plotted in Figures 4.5-4.7 over the frequency. The total EMI shielding effectiveness is given in Figure 4.8.

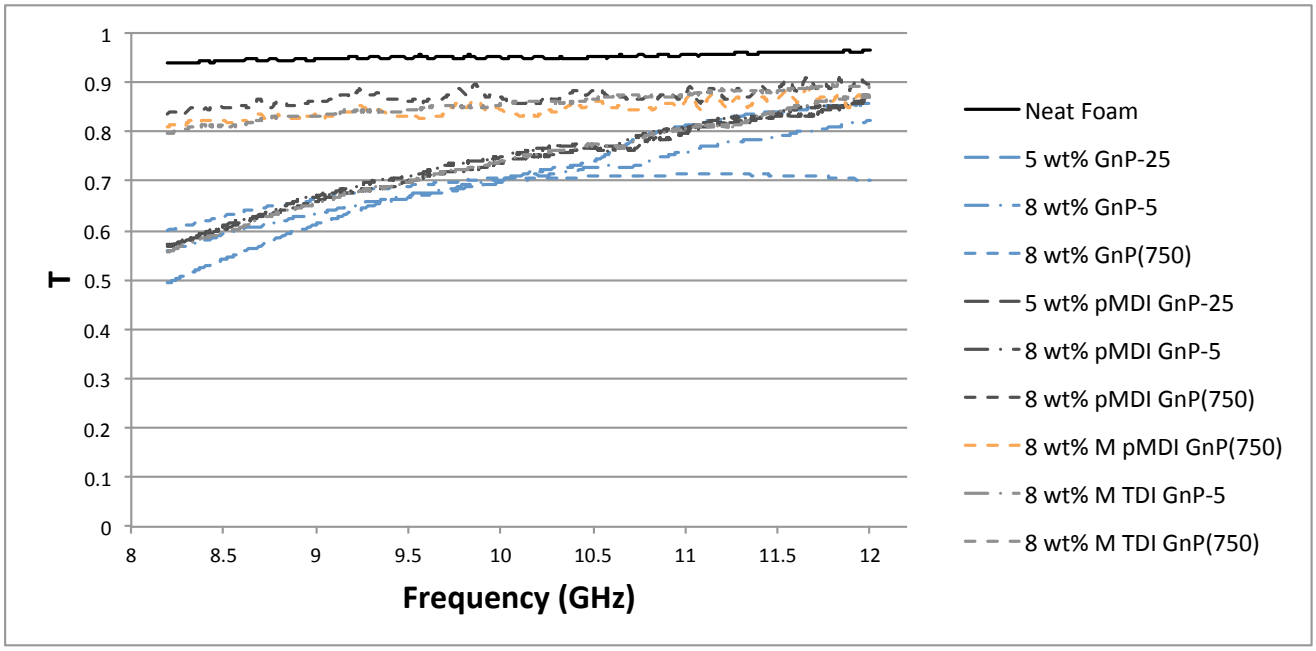

Figure 4.5: The fraction of the total EM wave that is transmitted through the different foam samples from 8.2 to 12.0 GHz.

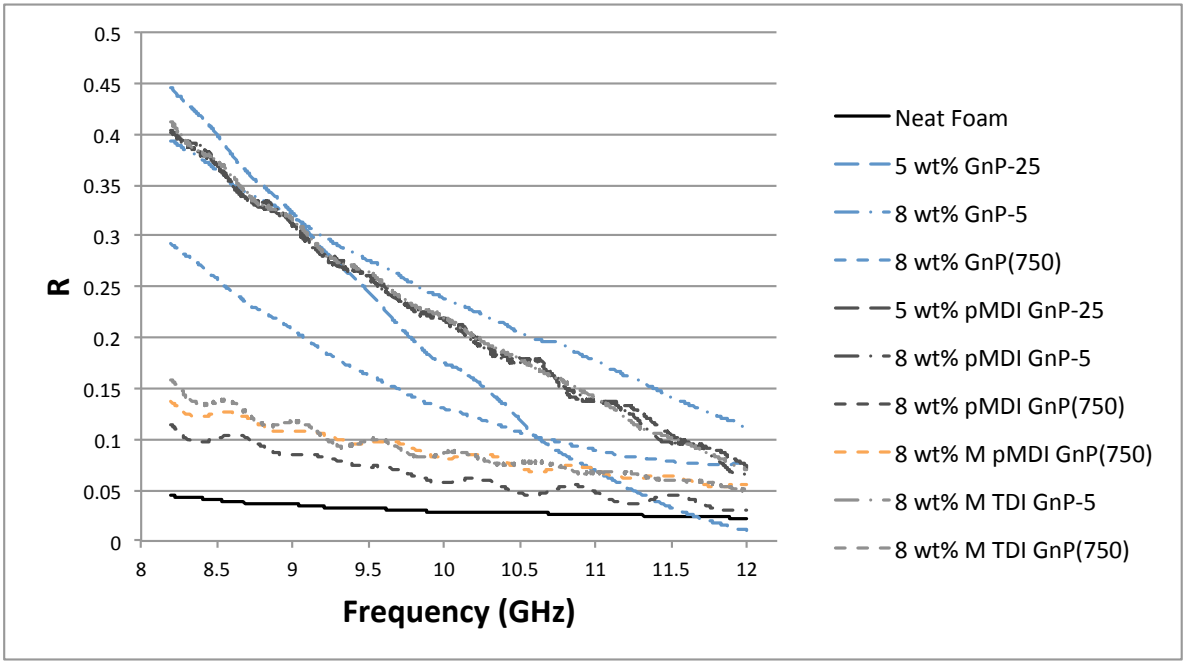

Figure 4.6: The fraction of the total EM wave that is reflected back from the different foam samples from 8.2 to 12.0 GHz.

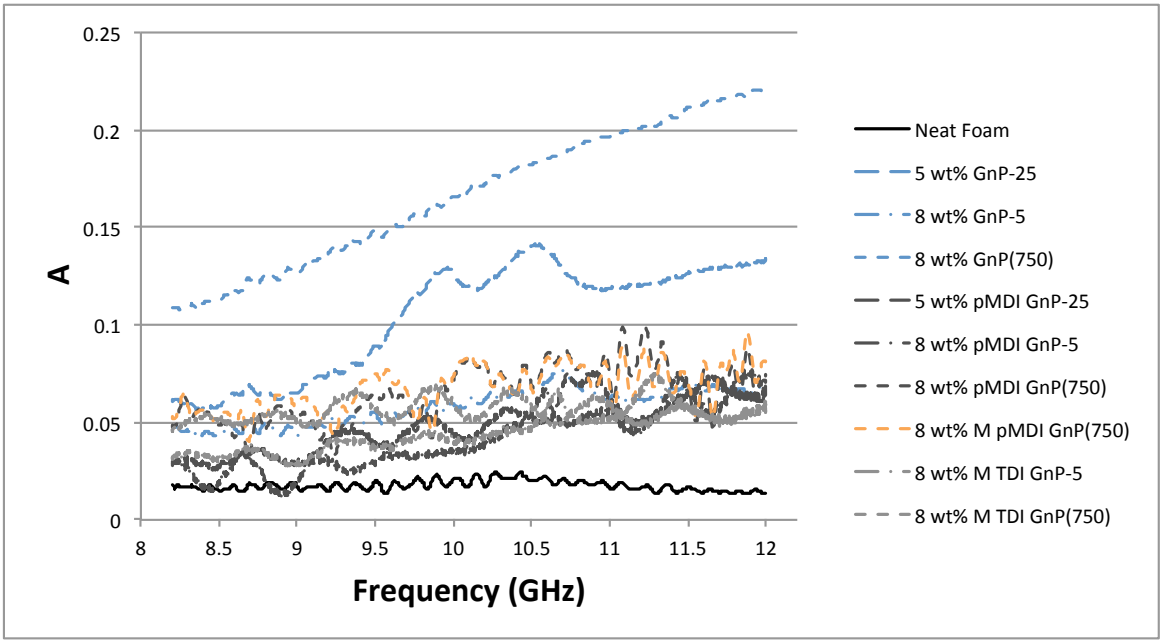

Figure 4.7: The fraction of the total EM wave that is absorbed by the different foam samples from 8.2 to 12.0 GHz.

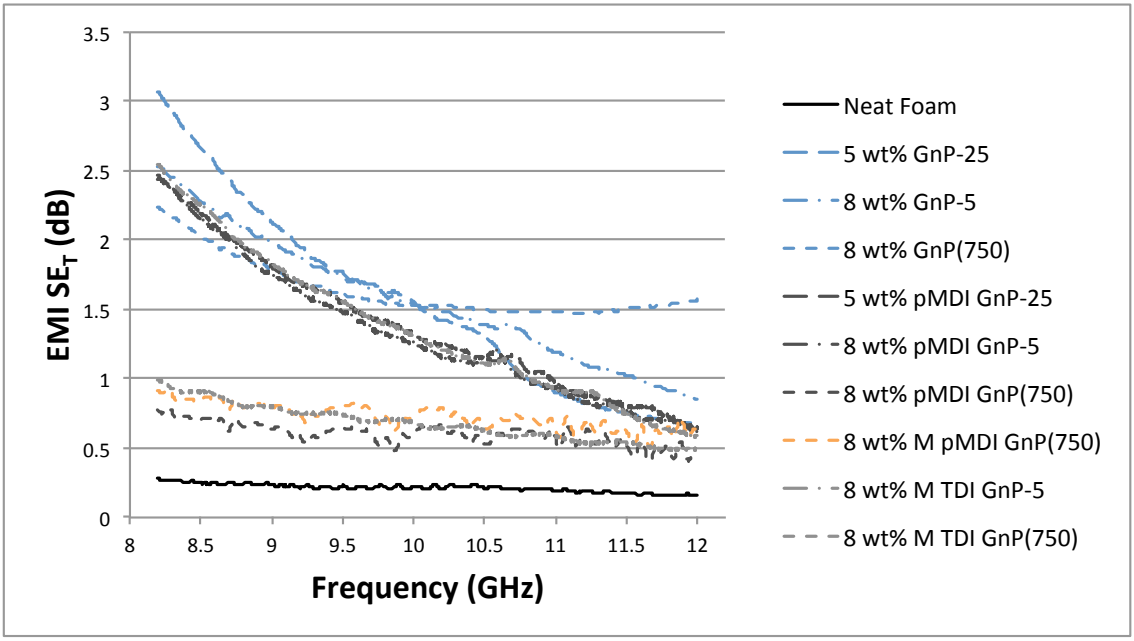

Figure 4.8: The total EMI SE of the standard rigid PUR/PIR foam as compared to the nanocomposite foam from 8.2 to 12.0 GHz.

4.4 Discussion

Adding nanoparticles to a polymer seems pretty simplistic in theory, but the reality turns out to be far more complicated. As discussed in the previous chapter the addition of the nanoparticles is not an inert process and there is a molecular interaction that takes place not only between the polymer and the particles, but also between the particles themselves that has a profound impact on the local molecular properties that in turn affects the macroscopic ones.

4.4.0.1 Mechanical Properties of Nancomposite Rigid PUR/PIR foam

The mechanical properties of any foam is partly dependent on the solid properties of the matrix and partly on the structure, including the degree of open- to closed-cells. When a foam has a high degree of closed-cell the compressive strength includes an added restoring force from compressing the entrapped liquid along with the mechanical contribution from the cell walls as they are stretched during compression to increase stiffness [87]. For open-cell foams only the struts contribute to the mechanical performance. Figure 4.9 shows that while this is a closed-cell foam the cell walls are consists of very thin membranes. Such thin cell membranes do not contribute to the mechanical stiffness and in fact easily bend and rupture releasing the entrapped gas.

Such thin cell walls would certainly benefit from the reinforcing effect of GnP, but during the expansion process the PUR surface tension causes the liquid to form at the edges [87] pulling the majority of GnP into the struts although some amounts can still be seen even in the thin membranes in Figure 4.9. The optical images of the cell structure make it hard to distinguish how thick the cell walls are and to determine if any have the stiffness required to actually contribute to the mechanical performance. The images do show, however, that GnP displays a kind of clumping behavior in the foam which would be difficult to accommodate in the very thin cell walls. In general, cell walls are probably not the main contributors to

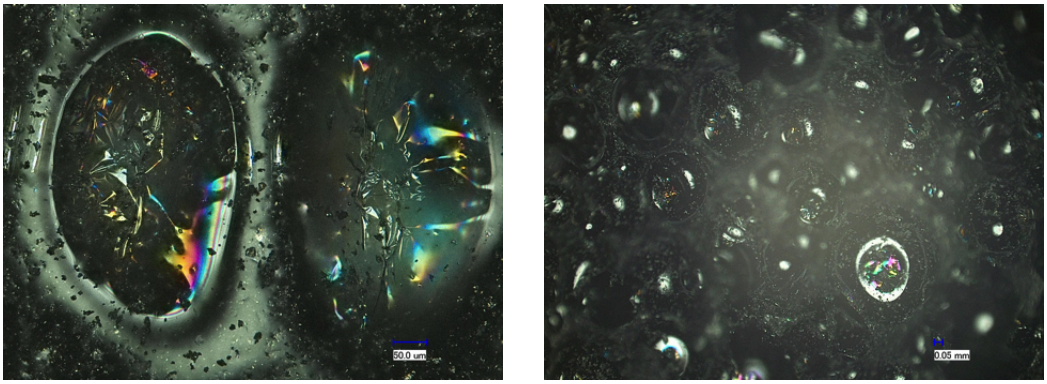

(a) (b)

Figure 4.9: Optical reflectance images of cell walls in rigid PUR/PIR nancomposite foam: (a) Cell walls are so thin they are wrinkled from gas expansion; (b) Easy to identify thin cell walls, but the small amount could be do to a higher number of thicker cell walls

mechanical stiffness, but a more in-depth analysis of each type of GnP will follow.

When talking about foams the compressive stress-strain curves can also give insight into its properties. There exist three types of compressive curves for foams that describe an elastomeric foam, an elasto-plastic foam and lastly, a brittle foam. PUR foam is not a brittle foam in compression and, in fact, follows the stress-strain behavior of either the elastomeric foam or an elasto-plastic foam, both types are shown in Figure 4.10.

The mechanical data reported in this research focuses on the elastic region of the foams, which shows two different behaviors in compression. Linear elasticity is controlled by the bending of the struts and possibly the stretching of the cell walls along with internal fluid pressure, which continues until either elastic buckling or the formation of plastic hinges, a non-recoverable process giving the peak seen in the stress-strain curve of the elasto-plastic foam. The neat foam and the foam loaded with 8 wt% GnP(750) demonstrate purely elastic behavior in the elastic region, but some of the nanocomposite foam samples show the formation of a maximum plastic stress. It is inconsistent within each sample, except the sample with minimal treated TDI treated GnP-5 that displays only elasto-plastic response, suggesting that for that for the all the other nanocomposite foams the addition of the nanoplatelets

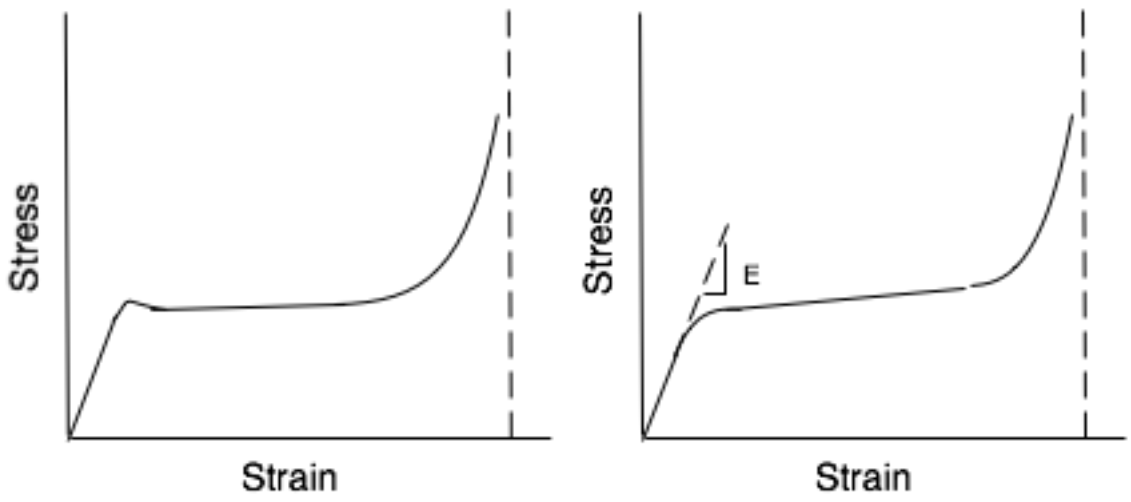

Figure 4.10: Standard stress-strain curves of elasto-plastic (left) and elastomeric (right) foams.

creates variations in the local response throughout the foam. The raw data of some samples demonstrating the different behavior in the elastic region is given in the appendix. This could lead back to the changes in microphase that the addition of the nanoplatelets are likely causing shown in the thermal degradation profile and in the low T_g. As discussed in chapter 3, PUR foam has been found to be a phase-segmented structure as it consists of hard segments, commonly attributed to polyurea in water-blown foams and soft segments of polyurethane chains. Analysis of the thermal degradation profiles in chapter 3 suggests that one of the modes for compensating the addition of the nanoplatelets include an increase in polyurea and possibly thereby an increase in size of hard segments or separation. These hard segments could form plastic hinges within the foam causing the foam to display an elasto-plastic response in compression at the macroscopic level.

As seen with the thermal properties the addition of GnP does not always result in a positive outcome. GnP has high mechanical properties that the expectation was that adding them to the polymer foam would result in an increase in mechanical performance in the elastic region, but as seen in Figure 4.1 the addition of neat GnP-5 and GnP-25

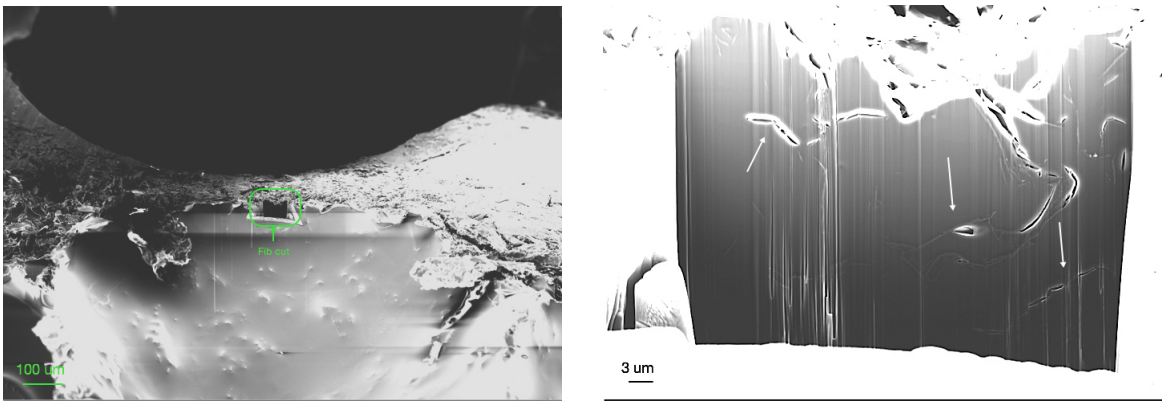

(a) (b)

Figure 4.11: FESEM image of FIB cut in rigid PUR/PIR foam with 5 wt% GnP-25: (a) FIB cut of strut; (b) Dispersion of GnP-25 in strut

is actually detrimental to the compressive strength, only the high surface area GnP(750) causes an increase. The elastic modulus, however, appears unaffected as there is statistically insignificant changes in the Young's modulus (see Figure 4.2) for the various loadings of GnP. The nanocomposite foam with 8 wt% GnP(750) is also the only neat sample to maintain the same glass temperature and have a cell size similar to the neat sample. The improvement in mechanical properties is due to a lack of aggregates and possibly from having a size on a similar scale to the microphase structure so the microstructure is maintained. In order to see a significant change in the mechanical properties for the larger particles they would have to overcome their own attraction by improvement in the interfacial contact between the foam and the particles. Images of the dispersion of the particles show that the large particles tend to agglomerate preferentially bonding to each other rather than the foam as seen in Figure 4.11. The basal plane is dominating the nanoparticle behavior and the only way that can be minimized is by either shrinking the particle as with the GnP(750) or functionalizing the basal in way that it is preferential to the matrix but that does not disrupt the electronic character.

Otherwise, these aggregates will act as stress concentrators reducing the mechanical

performance of the nanocomposite foam. In addition, high concentrations of the particles in one part of the foam mean that other areas have a low concentration, for example, in thin cell walls and struts. This appears to be the case as even the smaller GnP-5 particles show thin polymer areas like in Figure 4.12 that contain no GnP at all. The difference between Figure 4.11 and 4.12 is the size of the strut. The strut that contains GnP-25 is on the order of 100 μms, whereas the one with no GnP-5 has a size of around 6 μm. GnP(750) has platelets sizes under 1 μm, so the expectation was that these particles could disperse in these thin areas, which is confirmed in Figure 4.13. However, notice that even these small particles do not orient along the thinning direction; an effect that would be necessary for the larger GnP to stay in these regions. In order for reorientation to occur a sufficient shear stress must be applied or there must be a strong bond with the matrix. The lack or reorientation suggests that interfacial adhesion is weak since the particles do not reorient in the thinning direction. Another effect to investigate is where these particles orient within the microphase structure. If they are dispersed in the hard segment to that tends to form spherelites [82], there would be no way to align these segments in the thinning direction. Even though the particles do not reorient their better dispersion still results in an increase in mechanical strength. These images combined with the mechanical results confirm that changes in the local microscopic concentration has a resulting effect on the overall macroscopic mechanics in composites and the weak links dominate performance.

Because there seemed to be such poor interfacial properties between the GnP and the polymer, edge-functionalization was employed to try and improve the interaction. Functionalization was restricted to the edges as a way to prevent disruption of the basal plane. The particles were reacted with pMDI and TDI to form urethane-type groups on the edges as the particles are known to have hydroxyl edge groups. Table 3.2 on page 38 shows the amount and type of molecular groups on the particles after reaction. Once again, the peak at 399 eV is amine groups including urea, the peak at 400 eV is urethane type groups and the peak at 401.5 eV is unreacted pMDI. A couple of things to note, the first is that

Figure 4.12: FESEM image of FIB cut of strut in rigid PUR/PIR foam with 8 wt% GnP-5.

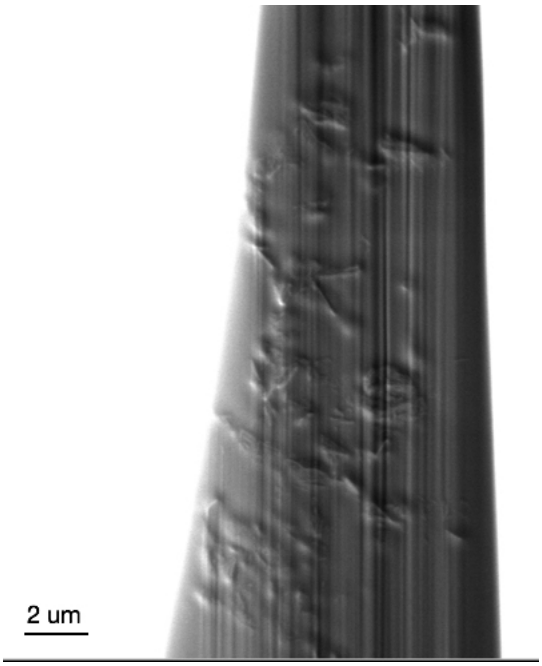

Figure 4.13: FESEM image of FIB cut strut in PUR/PIR rigid foam with 8 wt% GnP(750).

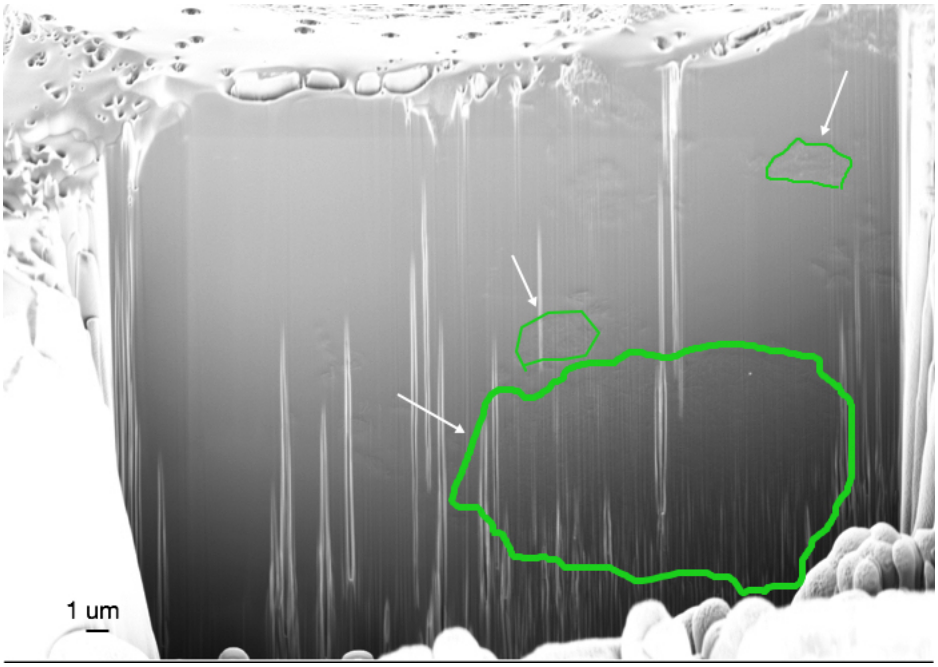

Figure 4.14: FESEM image of strut cut with FIB in PUR/PIR rigid foam with 8 wt% pMDI treated GnP(750). The pMDI treated GnP(750) agglomerates are highlighted.

the minimal treatment did result in a reduction of functionalization. Secondly since the functionalization is limited to the edges as the edge density increases there should be an a resulting increase in the concentration of total reacted groups. This is true for GnP-5 and GnP-25, but GnP(750) shows a similar concentration to GnP-5. As-received GnP(750) comes as sub-micron aggregates, if the aggregates are not broken up prior the pMDI just coats the surface of aggregates unable to penetrate the internal edges. And as was seen with the sample with GnP-25 these aggregates act as stress concentrators reducing the mechanical strength which is the case for nancompostie foam pMDI treated GnP(750) (see Figure 4.1). This also means that ultrasonication done on the pMDI treated GnP(750) after addition to the pMDI or polyol blend is unable to break apart the particles and this is confirmed by images in the SEM. Figures 4.14 - 4.18 clearly shows large sub-micron aggregates

The minimal treatment method breaks apart the particles prior to functionalization resulting in decrease of concentrated groups on the edges. However, this method now follows the expected pattern in concentration where the amount of reacted groups on TDI treated

Figure 4.15: FESEM image of GnP dispersion in rigid PUR/PIR foam with 8 wt% pMDI treated GnP(750). Strut was prepared with the FIB and aggregates are outlined in black.

GnP(750) is greater than that on the TDI treated GnP-5 according to Table 3.1 on page 36. This improvement is also confirmed by the mechanical strength that shows that the minimal pMDI treated GnP(750) has a higher compressive strength than the regular treated pMDI GnP(750) and shows improvement over the standard. The images of the GnP dispersion support this as well, where many particles in the polymer appear like the GnP shown in Figure 4.16 (b) demonstrating a morphology more similar to platelets. This is in contrast to Figure 4.16(a), which shows a much larger aggregate particle coated in polymer. And the particles in the foam continue to show this trend comparing Figures 4.17 and 4.18 to Figure 4.13 the particle microstructure in the polymer now resembles that of the neat GnP(750) in the polymer.

Figures 4.1 and 4.2 show that edge-functionalization degrades the mechanical performance of the samples that contain pMDI treated GnP-25 and GnP(750). GnP-25 does not have a sufficient edge density as already discussed due to the Van-der-Waal attraction between graphene layers causing them to re-stack. The dominant factor is the particle diameter

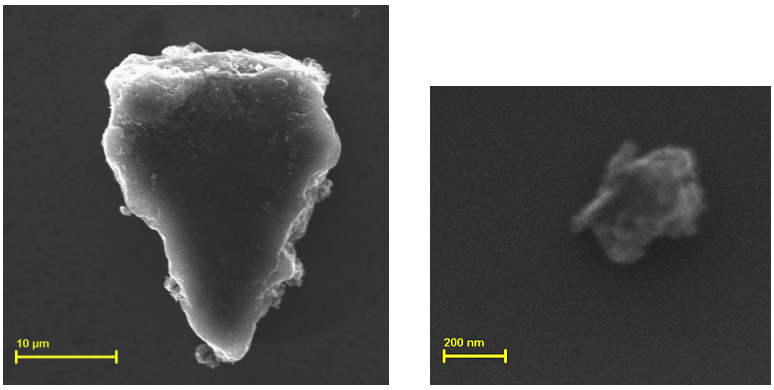

(a) (b)

Figure 4.16: SEM image of GnP(750) reacted with pMDI by both methods (a) GnP(750) treated by excess method; (b) GnP(750) treated by minimal method

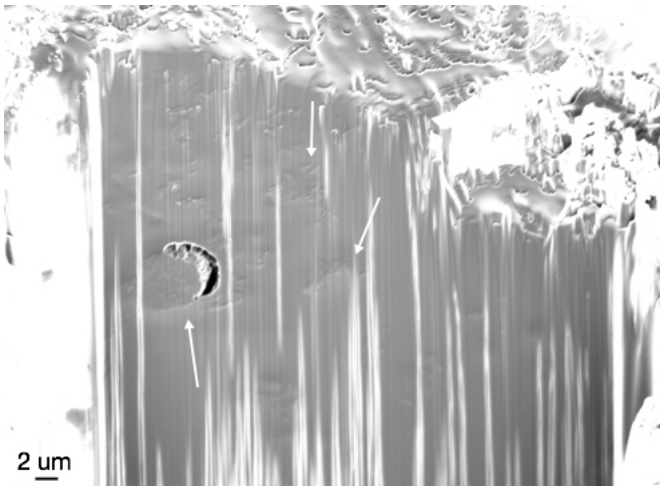

Figure 4.17: FESEM image of strut cut with FIB in PUR/PIR rigid foam with 8 wt% pMDI treated GnP(750) by minimal method. Some GnP is highlighted with arrows.

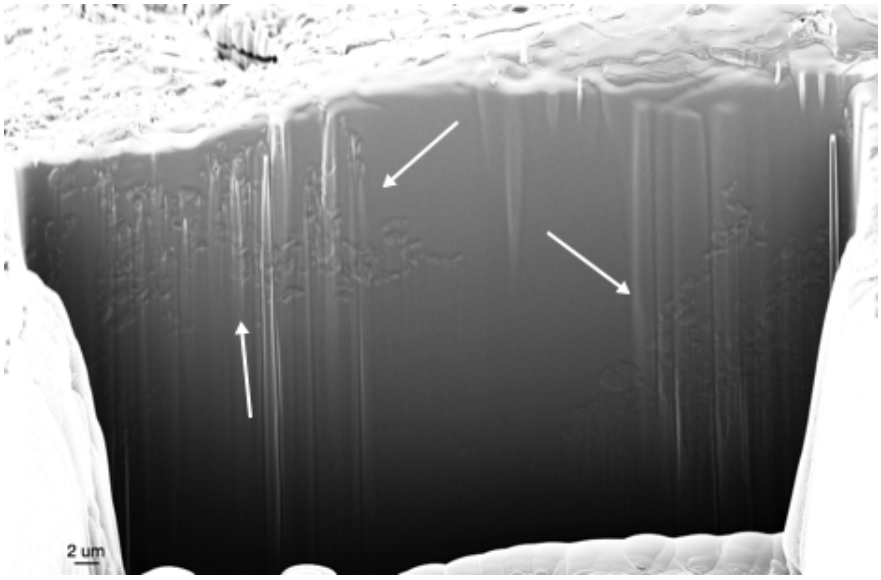

Figure 4.18: FESEM image of strut cut with FIB in PUR/PIR rigid foam with 8 wt% pMDI treated GnP(750) by minimal method. Some GnP is highlighted with arrows.

and is why the mechanical performance does not change from neat. The problems with pMDI treated GnP(750) is a special case as discussed in the previous paragraph. The pMDI treated GnP-5, however, shows marginal improvement in the mechanical strength. This suggests that the smaller particles with the higher edge density are able to be affected by the edge-functionalization treatment and confirmed by the significant changes in the mechanical properties of the treated GnP(750) over that of the neat. GnP-5 does appear to small enough, however, along with GnP(750) although, the pMDI treated GnP-5 specimens suggest the particle dispersion is still not uniform due to agglomerations causing the large sample deviation, but could still be able to increase the interfacial strength. Also the long polymer chains on the edges appear to improve the interaction with the matrix better than the short molecular groups as both the minimal TDI treatment of the GnP-5 and GnP(750) cause do not result in a statistically significant change in the mechanical strength over the standard. In addition the mechanical strength between the two is almost the same. Figure 4.19 show a dispersion that is not as good as the neat GnP(750) or even the minimal treated pMDI GnP(750) causing a decrease in mechanical response. It raises the question of whether the T_g

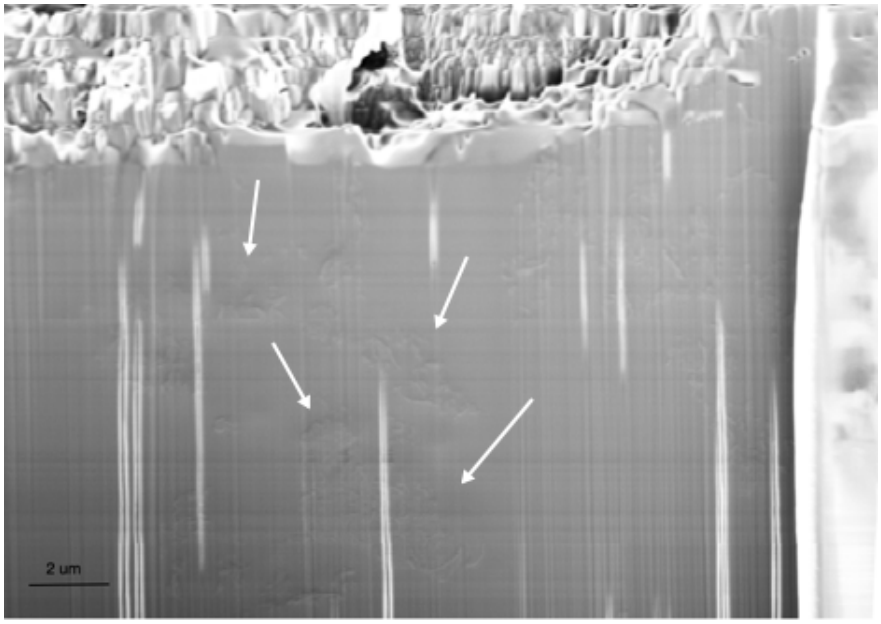

Figure 4.19: FESEM of FIB cut of strut in rigid PUR/PIR foam with 8 wt% minimal treated TDI GnP(750). Some GnP is highlighted with arrows.

would match between the two if the dispersion was similar with no agglomerations or if there is another factor. Another interesting features is that there is similarity in pattern between the compressive strength behavior and T_g from chapter 3. As the T_g lowers the mechanical strength also lowers in comparison to the standard though not by the same margin. Also all the nanocomposite foam with treated GnP(750) and TDI treated GnP-5 show significantly larger median cell sizes as compared to the standard (see Chapter 3) and it is commonly accepted that smaller cell sizes are better for mechanical properties. Both the mechanical properties and cell size, suggest another factor, namely the microphase structure.

4.4.0.2 Electrical resistivity of Nancomposite PUR/PIR Rigid Foam

With foams, resistivity is found to increase as the relative density to the solid decreases [88, 87]. Gibson and Ashby proposed that this is due to the tortuous path a cellular structure forces the electrons to follow. As density increases circular cells with significant amount of polymer surrounding them, get thinner as the cells appear as many sided convex polygons. This is

an addition to the low conductivity the polymer already has, the whole of the conductivity then rests completely on the ability of the conductive fillers to form a conductive network. This means that the charge can transfer easily from particle to particle, that is physically possible when the particles themselves are touching or close enough to allow for tunneling. When this path is formed through the polymer there will be a sharp change in the electrical resistance called the percolation threshold. Percolation is a mathematics concept that defines the phenomenon where a "simple probabilistic model...exhibits a phase transition," [89], or in this case, electrical phase transition where the macroscopic nanocomposite foam no longer acts as an insulator but exhibits the electrical behavior of a semiconductor or conductor. Having particles with a large aspect ratio are ideal for this purpose as they have less points of contact resistance and are able to achieve percolation at lower loadings. The limiting concentration model [90] takes this into account for rod-like particles with strong interaction and describes the electrical phase transition occurring when the critical concentration, f_c is reached:

$$f_c \approx \frac{3d^2}{2L^2}$$

Where d and L are the diameter and length of the particles. The effect of aspect ratio as a key factor appears to hold true for the GnP-5 and GnP-25, as the electrical resistivity scales with aspect ratio in Figure 4.3. The aspect ratio for each nanoplatelet is listed in Table 4.2. Aspect ratio is important because it reduces the number of times an electron must transfer to another particle, the move times this happens the higher the total contact resistance. The electrical response of the much smaller GnP(750), which should have a significantly higher total contact resistance, is about the same as the neat GnP-5. However, the large sample deviation suggests that certain areas of the foam are experiencing a higher concentration of particles without agglomerating, meaning a reduction in particle distance, improving particle transfer. The effect of aspect ratio does scale with the pMDI treated GnP, although the coating on the edges electrically isolates the particles as PUR and its related polymers have low electrical conductance.

Table 4.2: Aspect ratio for GnP according to the product sheets for largest thickness.

GnP	**Aspect Ratio**
GnP-25	3125:1
GnP-5	625:1
GnP(750)	$<$ 250:1

Because having particles that are close to each other is necessary for electron transfer agglomerations are no longer a concern as long as a path can form. Figure 4.3 shows the high resistivity of the neat foam and with 5 wt% GnP-25 which forms heavy agglomerations in the foam, the result is a decrease of about 5 orders of magnitude. Percolation theory only requires there to be at least one path of long range connectivity, that allows for some of those points on the path to be larger than others due to agglomerations. As previously mentioned, density is also a defining factor, but for different physical reasons for the filler. Lower density causes particles to pull apart as the amount of polymer per unit volume simultaneously decreases. Yan, et al. studied how foam density affects percolation with MWNTs in polyurethane foam that showed a increasing electrical conductivity with increasing density and concluded a critical density at about 0.16 g/cm^3 for electrical contact. Since electrical conductivity was always a goal for this polymeric foam this density was chosen for observation. In addition to particles being pulled apart they can also be radially compressed creating aggregated points that are also being further separated from each other. Aggregates are more likely to form with the larger particles, decreasing the local concentration in especially the thin areas where they would be most needed for connectivity. So, there is the potential that the larger platelets could be even more affected by the changing microstructure due to their morphology.

For these reasons the pattern of improvement in electrical properties does not match that of the mechanical properties. However, there two outliers for the electrical performance. The sample with 8 wt% minimal pMDI treated GnP(750) has the same resistivity as that of the neat GnP-5. Possibly because the foam with 8 wt% neat GnP-5 tends to agglomerate,

therefore, the resistivity could be more an effect of the dispersion, as the compressive strength for the minimal pMDI treated GnP(750) demonstrates a likely slight increase in the mechanical performance over that of the standard foam suggesting less agglomeration. In addition, because the GnP-5 particles are so much smaller than the GnP-25 they could be more affected by aggregation decreasing the local concentration and disrupting the conductive path especially as Figure 4.12 has shown that because of the lack of reorientation they tend not to go into areas of really small volume. Another outlier exists between the minimal TDI treated GnP-5 and GnP(750), where the particles with the smallest aspect ratio significantly outperform the larger ones. Because the electrical resistivity of the TDI treated GnP(750) is so low the much shorter molecules on the edges are not isolating the particles like the polymer coating did. The similarities in compressive strength suggest a similar dispersion. But there is a change in one key value and that is the cell size. The TDI treated GnP-5 has a much larger cell structure a difference of about 70 μms between the two. To accommodate larger cells there are thinner struts reducing the concentration of particles. The size of the GnP-5 could be in between two physical phenomenons, they are small enough to be more affected by agglomerations, but not small enough to locate within thin areas of the foam because even the aggregates of the TDI treated GnP(750) are smaller. Also the change in molecular and likely phase structure that causes the 10 °C difference in T_g could also be responsible possibly affecting how the particles and smaller aggregates organize in the structure.

4.4.0.3 Dielectric Performance

When it comes to polymeric foams the majority have a low dielectric constant (real relative permittivity) and a low dissipation factor (loss). This relates to how much energy is stored in the material when exposed to an external alternating electric field and how much of that energy is lost. The low dielectric constant is due to the non-polar nature of the polymer which is the true for PUR/PIR. Only the polymer contributes to the dielectric properties of the foam, as carbon dioxide has a very low real permittivity [91, 92]. As less space is filled or

the density decreases the permittivity experiences a linear decrease [87]. This is the reasoning behind adding conductive nanoparticles to the polymer as conductivity is another avenue for dielectric response beyond polarization caused when an external electromagnetic (EM) wave is applied. Important factors for electrical conductivity have already been discussed and as such all the nanocomposite foam samples have an increased dielectric constant over the standard. To better understand this it is necessary to go into a more in-depth discussion of permittivity.

Permittivity is slightly different than conductivity as it an be affected by the small scale response of bound charges to an applied electric field, in addition to mobile charges. Each bound charge can be thought of as being surrounded by an electric dipole, either natural or induced, by an external field. As the dipoles align and stretch this represents stored energy in the material (real), but energy can also be lost represented by the imaginary part. To go into more detail there are different modes of dielectric response that are more prominent at certain frequencies. The electronic/atomic response which focuses on the electron cloud surrounding the nucleus of atoms is a minimal contribution in this frequency range (8.2-12.0 GHz) and also constant and so it can be ignored. The main contributors to the dielectric character in the tested range are the ionic and polarization modes. Since there no ionic bonding in the system this mode can also be ignored.

Polarization can either be induced or permanent and the low real permittivity of the standard suggests any dipoles are probably induced, but mostly PUR/PIR is nonpolar. GnP has an interesting polar effect due to its bonding. The core is made up of the sp^2 carbon atoms which leaves an extra π electron per carbon atom creating a π-cloud over the platelet, which is responsible for the electronic properties. This π-cloud is then readily available to orient itself when an electric field is applied separating and creating an interface between the mobile electrons and the positive core giving a better dielectric response; a phenomenon commonly referred to as the interface/space charge dielectric mode. Adding the particles should then increase the dielectric response due to the ability of the GnP' to polarize. Figure 4.4 confirms

the improvement in energy storage of the material. Unlike the electrical resistivity, however, the dielectric response seems to scale for aspect ratio for all neat and treated GnP instead of following the pattern seen with electrical resistivity. The treatment of the GnP seems to decrease this response, but unlike for the electrical performance minimal treated GnP(750) has a lower real relative permittivity than the neat and TDI treated GnP-5. In fact, the energy storage seems to be even more sensitive to aspect ratio as the individual plots GnP tend to clump together according to size except for nanocomposite foam with neat GnP(750). Now it is not unusual for the dielectric response of a material to change over a frequency range what is significant is that it is only observed in the sample with neat GnP(750). However, the dielectric response deals with both conducting charges and bound charges and the previous chapter demonstrated that the addition of GnP changes the microstructure. It could be that this result is due the effect that GnP(750) is having either on molecular structure and/or phase separation. The same could be true for why the minimal treated GnP(750), which had a similar electrical response to the neat, shows a significantly less real permittivity.

Electromagnetic interference (EMI) shielding effectiveness (SE) is of great importance when trying to maintain optimal performance of so many electronics that are in close proximity to each other. The EMI shielding character is not only about being able to prevent EM waves, but also focuses on how this is done. Currently many EMI shielding devices are high electrically conducting metals, but these materials tend to reflect the EM waves back which could still disrupt the internal electronics [93]. Finding materials that absorb instead of reflect, then, is also important. Figures 4.5-4.7 show what happens to the wave when encountered by the rigid PUR/PIR foam. The neat sample with no GnP offers limited shielding so any shielding in the material is due the GnP, due either to the conducting nature GnP itself or possibly from changes in the microstructure of the polymer. It appears that like with the electrical properties the best performance is with the neat GnP, which changes with frequency and because frequency is such an important factor, the transmittance does not scale with aspect ratio. At the lower end of the range the large particles are more

effective at lowering transmittance and at the higher frequency the nanocomposite foam with GnP(750) is a significant outlier. The sample with GnP(750) is the same sample that showed strong frequency dependence for the real permittivity in this range (see Figure 4.5. For this nanocomposite foam it appears that electrical conductivity is not the only method responsible for the EMI response. The reflectance (Figure 4.6) and absorbance (Figure 4.7) plots give more of an insight into this. The reflectance is decreasing with increasing frequency for all nanocomposite foam samples although the sample with GnP-25 is doing so at a faster rate compared to the treated GnP(750) at a much slower rate. The increase in transmittance for the foam with GnP-25 is a combination effect from the fast decrease in reflectance that is only partially compensated for by a slower increase in absorbance. The decrease in transmittance for the neat GnP(750) is due to the corresponding increase in absorbance that is significantly better than the foam with GnP-25. The small particles appear to be more effective at absorbance, but considering the outlier that the foam with neat GnP(750) is across not only the dielectric plots, but also in the mechanical and electrical properties this effective absorbance is likely due to the better dispersion that traps the EM waves and possibly changes in polymer microstructure that could be more effective at absorbance. The ideal nanocomposite foam would be one where the nanoparticles instead prevented the waves from transmitting and then the polymer absorbed them, but the low absorbance of the standard shows that microstructure of the PUR/PIR matrix is not the polymer to do this as the chart in Figure 4.7 confirms. But it is possible that changes in the microstructure including the microphase could offer corresponding improvements in the shielding properties.

Treatment of the edges of the GnP seems to offer little benefit and in general decreases the SE. The only exception is the edge-functionalized GnP-5 that shows little effect over the neat GnP-5. Figure 4.8 also shows that the edge-treated GnP(750) is not only ineffective at stopping the EM waves it appears to be only minimally affected by the frequency which is completely different than all the other nanocomposite samples. While it is not surprising that the small particles with the higher edge density are more affected by the edge treatment,

they have nearly the same EMI SE and it appears that all that matters for the small particles whether they are treated or untreated. This also says that edge character can be an important for SE, when it is significant an effective that has been seen in all the properties. The GnP-5 which demonstrated that changes in the edge character could affect the macroscopic mechanical and electrical properties showed little change in the SE except the neat GnP-5 had a slower slope loss in reflected SE. The changes in all the SE plot suggest that the nanocomposite foam might also be more effective in another range which is not uncommon as many different types of shielding materials have optimal frequency ranges.

4.5 Conclusions

There are many challenges that need to be overcome when trying to create a multifunctional material. In general there is a decrease in many polymeric properties that scale with density, so working with a cellular material has additional challenges. Nanoparticle addition offer a unique way to overcome those challenges, but can also create new ones. For example, the interaction between the particles and the matrix can have a significant effect on the level of success. More specifically for polymer foams it is important that particles match well with the matrix so a good interface is created between the filler and the matrix for mechanical properties and dispersion otherwise aggregates form. A significant problem with the largest GnP as seen in the decrease in mechanical performance of about 40% and that was confirmed with the SEM images. These aggregates then act as stress concentrators decreasing the mechanical strength. Aggregation does not prevent the formation of a percolated network but may affect the critical concentration. At 5 wt% GnP-25 there was decrease in electrical resistivity of over 5 magnitudes. A much higher loading of the GnP-5 and GnP(750) that had a difference in aspect ratio of about 2.5 times showed similar electrical resistivity and images of the dispersion show that the agglomeration of the GnP-5 likely increases the critical concentration for percolation. While these aggregations may not affect the electrical properties there still have to be enough of them to form a percolated network, this becomes

a bigger concern as the particles get smaller.

Care must be taken when trying to improve the interaction between the particles and the matrix. Edge-treatment is only sufficient to reduce agglomeration when the edges dominate otherwise the basal plane character does as demonstrated by the no change in the mechanical performance for the neat and edge-treated GnP-25. It is not just about the creating a good adhesion between the two, but also being careful in regards to the molecular structure formed in these regions. Treating the GnP with chemical groups to improve interaction between the particles and the polymer resulted in the particles being electrically isolated due to the coating of polymer that was formed on the edges and offered minimal improvement int the mechanical strength. The electrical resistivity increased about three orders of magnitude with the treated GnP-25 over the neat. In general a key factor was the aspect ratio,as electrical resistivity with the treated GnP was similar to the neat for all other samples, but the mechanical performance did not change from the foam with non-treated GnP or the edge treatment resulted in a decrease of anywhere from 16 to 35% that was observed with the different treatments of the GnP(750). The only exception was the sample with 8 wt% GnP-5 that showed average improvement of about 30%. Although the sample deviation was also the largest out of any of the samples and images showed the particles were still agglomerated.

The dielectric properties improved by a factor of 2.2, 1.8, 0.7 for the nanocomposite foam with neat GnP-25, GnP-5 and GnP(750), respectively. The real permittivity improved with electrical conductance, but not at the same degree because permittivity is a response of mobile and bound charges and the stronger response of the larger particles to the applied electric field is a significant factor a response that did not change by more than 20% when edge-treated. The large particles good for electrical contact were effective at reflecting the EM waves as the reflectance about 8-9 times higher over the standard foam for GnP-25 and GnP-5 at 8.2 GHzand the GnP(750) was only about 6 times higher. But the smaller particles were good for absorbing them as at the same frequency the GnP(750) was about 5.5 times higher for absorbance compared to the neat GnP-5 and GnP(750) that only demonstrated

triple the absorbance over the standard foam. The EMI SE improved for all samples with both neat and treated GnP. The edge-treated GnP(750) about tripled the SE, GnP-5 and GnP(750) improved the SE by about 10 and 9 times, respectively and GnP-25 increased the SE about 12 times at 8.2 GHz, amounts that decreased by about 20% when the edges of the larger GnP were treated. Also this improvement tended to decrease at higher frequencies with GnP(750) out performing all of them due to the more significant frequency dependence demonstrated by the foam samples with neat and treated GnP-25 and GnP-5. It could be that the EMI SE would improve if the samples were tested at other frequencies.

Unique solutions must be found to improve the nanocomposite as simply overloading the foam with more fillers is not as solution as one of the goals is to keep the weight as low as possible, which would also help to keep costs down, an important factor for any commercial application. The key then is smarter particle loading. Keeping in mind to choose reinforcing material that matches the matrix and identify which groups create the ideal local molecular structure so that the local properties stay consistent throughout the foam and allows electron transfer to occur easily throughout the material. The larger the particles the more effect the basal plane of the platelet morphology becomes and it's important to identify a way to functionalize the basal plane that does not include chemical bonds that would destroy its character if electrical conductance is important as even edge-treatment which does not effect the basal plane still increased the electrical resistivity. The changes are also reflected in the microstructure and could be affecting the resultant properties. To gain a better understanding of the physical interaction of GnP with a polymer a study of the microphase needs to be done. Depending on where the GnP is preferentially locating in the phase structure could affect the ability to form a percolated network especially as the particle size decreases. It could also be that changing the microphase of the polymer with GnP could improve the EMI SE or more specifically its absorbance. In conclusion the development of these multifunctional hybrid materials relies in engineering the structure from the molecular level on up.

Appendix

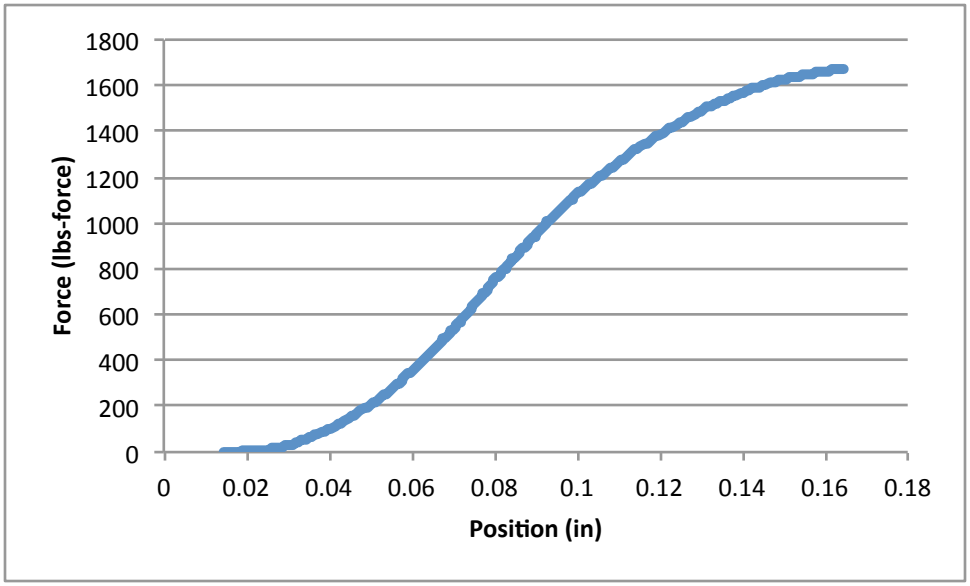

Figure 4.20: Raw data of neat rigid PUR/PIR foam specimen's mechanical performance during compression

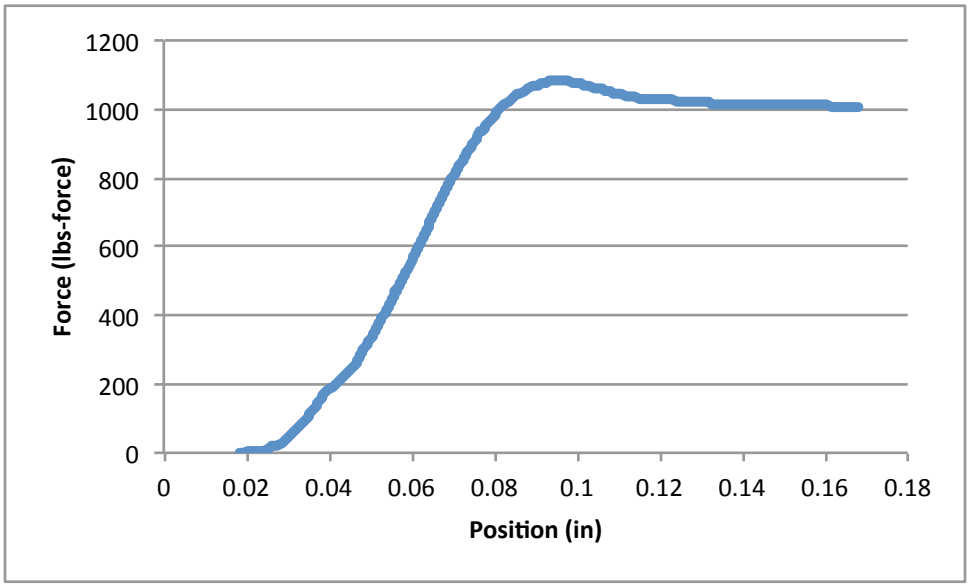

Figure 4.21: Raw data of rigid PUR/PIR foam with 5 wt% GnP-25 specimen's mechanical performance during compression

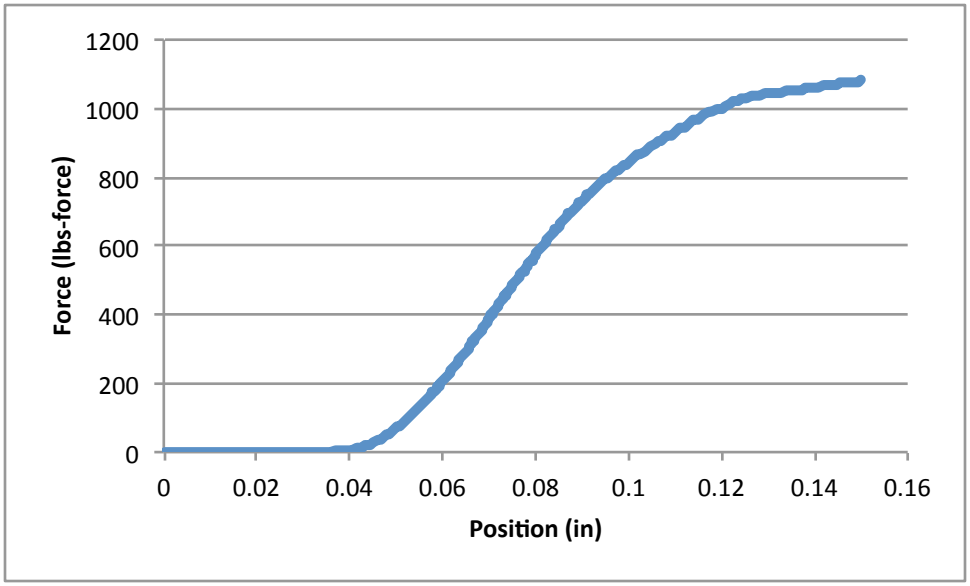

Figure 4.22: Raw data of rigid PUR/PIR foam with 5 wt% pMDI treated GnP-25 specimen's mechanical performance during compression

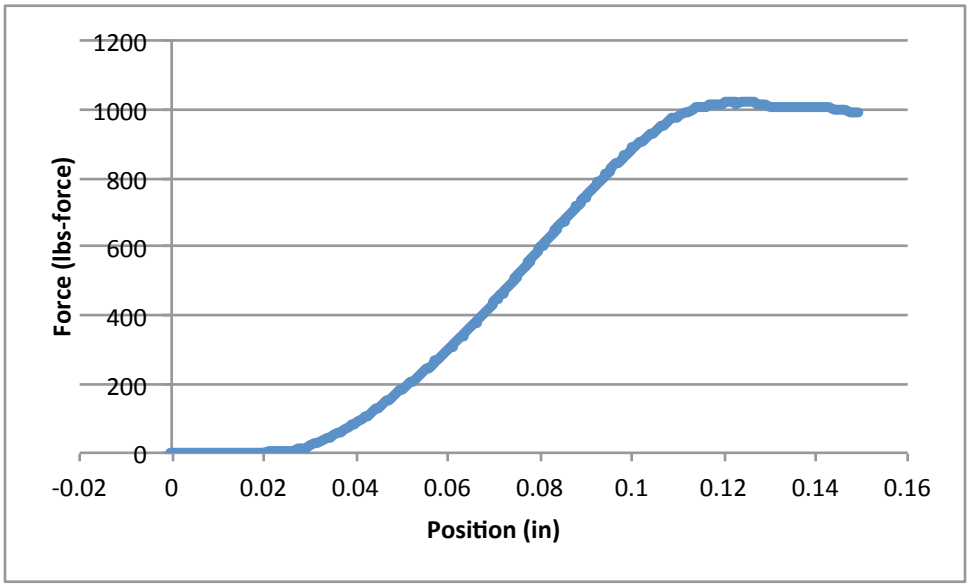

Figure 4.23: Raw data of another rigid PUR/PIR foam with 5 wt% pMDI treated GnP-25 specimen's mechanical performance during compression

CHAPTER 5

DIELECTRIC AND EMI SHIELDING PROPERTIES OF PDMS AND PDMS SYNTACTIC FOAM NANOCOMPOSITES

5.1 Introduction

A multifunctional material is a relatively new concept that requires the development of a new material usually through nanostructuring to make a composite. Nanocomposites are promising because low weight percent additions of nanoparticles can result in improved properties of the matrix and even new functionalities that do not exist in the neat matrix. Polymers are one type of matrix material that has been shown to greatly benefit from the addition of nanoparticles. These materials especially show promise in aerospace applications due to their lower weight and processing variability and cost. Carbon based nanoparticles are common fillers in polymeric systems [8, 94, 95] and graphene specifically has been used in a variety of polymers as well as polymer foams [96, 97, 98, 7, 71], regardless of the challenges working with the material presents.

Graphene is such a promising material due its unique bonding structure that gives it a diverse array of desirable properties. It is a single layer of sp^2 bonded carbon atoms that stack together to make up graphite. This covalent bonding results in a material that is very stiff with a high tensile modulus greater than 1 TPa that leaves an extra electron/atom creating a π cloud that gives the material mobilities greater than 15,000 cm^2/Vs [45, 19]. The multifunctional nature of graphene makes it very promising for aerospace applications as using one filler at low concentrations could make light-weight composite systems.

There are both top-up and bottom-down approaches to making graphene. Some result in high-purity single to few-layer graphene sheets [26, 27, 29, 30], but are very expensive to synthesize. Some top-down inexpensive methods start with graphitic structures then separate the sheets to make the graphene. Reduced graphite oxide produces very thin sheets but the

oxidation step causes more damage to the graphitic structure resulting in poorer properties [38, 39]. Exfoliated graphite relies on intercalated groups to separate the layers and produces multilayer sheets with comparable properties to single layer graphene in a more robust form [43, 44, 38, 33].

Silicone is a flexible high performance polymer that could greatly benefit from the addition of graphene. It is used in aerospace applications due to their flexibility at low temperatures and environmental resistance due to their unique inorganic-organic structure, but like many polymers has low electrical properties. There are many different types of silicone materials, but the elastomers are commonly polydimethylsiloxane, an optically clear polymer, but can also appear white from the addition of silicon-dioxide fillers. It is an insulator with a low dielectric constant, but if the properties could be improved it shows promises as a multifunctional seal and gasket for aerospace applications. In addition, utilizing a PDMS foam would also weight savings an important factor in space crafts.

There are many different routes to make foams including either chemical [71, 16, 99] or physical [100, 85] blowing agents. Another method is to create a syntactic foam where the cells are replaced with some type of spherical particle such as a hollow glass sphere [101]. Syntactic foams offer the benefit over other methods in that the cell size is relatively consistent and glass sphere can potentially improve the mechanical properties of the overall composite [102, 103]. In this chapter a nancomposite PDMS syntactic foam is investigated to see the effect that the glass bubbles and a graphene filler have on the effect on the electromagnetic properties of the foam.

5.2 Materials/Synthesis

5.2.1 Materials

5.2.1.1 PDMS

RTV615 from Momentive Performance Inc was used as the matrix [59]. It is a PDMS elastomer with no fillers from Momentive and comes in a 2-part kit where part 1 is a vinyl-terminated PDMS and part 2 contains the curing agent. The material has a relatively low viscosity of 4 Pas and a specific gravity of 1.02.

5.2.1.2 GnP

The graphene material was donated by XG Sciences. The graphene nanoplatelets (GnP) contain multiple layers of graphene for a more robust particle. Three different grades were selected. The first are xGnP-M-25 and xGnP-M-5, both grade M with surface areas between 120 - 150 m^2/g and between 6-8 layers of graphene thick [63]. GnP-25 will designate xGnP-M-25 which has an average particle diameter of 25 μm and GnP-5 designates xGnP-M-5 which has average lateral dimensions of 5 μm[63]. The last grade is xGnP-C-750, the C-grade is a high surface area material and in this case has a surface area of 750 m^2/g[63]. It contains platelets less than 2 μm in diameter and thicknesses of only a few nm that are generally aggregated into sub-micron particles [63]. To distinguish these high surface area particles from the low surface area platelets xGnP-C-750 will be labeled GnP(750).

5.2.1.3 Hollow Glass Spheres

The hollow glass spheres (HGS), iM16K, were donated by 3M™ (#98021327964) [60]. The white powder contains soda lime borosilicate glass spheres with an average diameter of 20 μmand contain less than 3% of a synthetic amorphous silica that is necessary to ensure the glass spheres flow. The glass bubbles with the amorphous silica granules can be seen in Figure

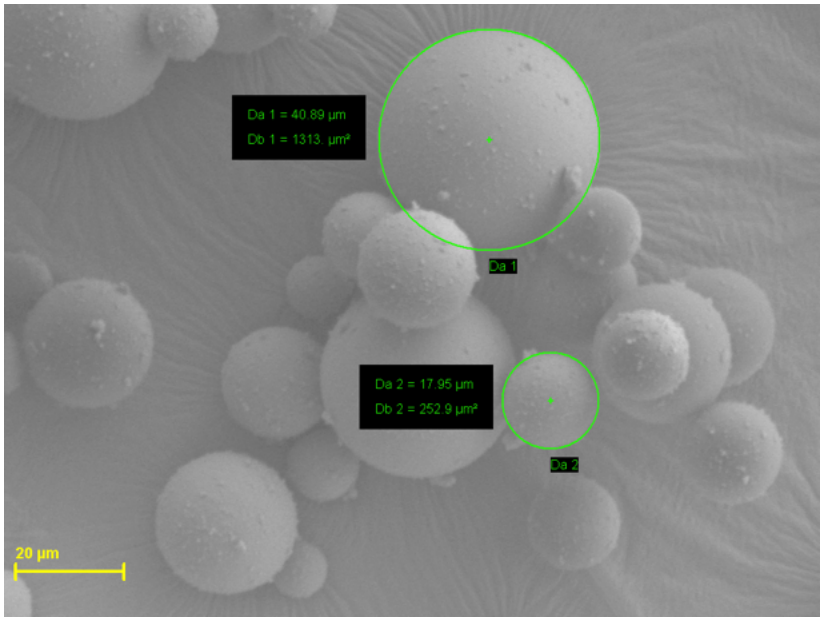

Figure 5.1: SEM image of 3M™ iM16K glass bubbles sprinkled with amorphous silica on surface and measured diameters

5.1. The 3M™ iM16K glass bubbles were chosen for their high crush strength of greater than 110 MPa that makes them able to withstand the large thermal expansion coefficient of the PDMS. Lastly, due to their relatively small diameter the hollow glass spheres have a density of 0.46 g/cm^2. A silane coupling agent was used to adhere the GnP to the glass bubbles. The binder is a trimethoxysilylpropyl modified PEI silane (tPEI) from Gelest (#SSP-060) [61].

5.2.2 Experimental Procedure

5.2.2.1 GnP/PDMS

The neat PDMS elastomer is made by pouring part A then part B into a mixing vessel at a ratio of 10:1 by weight. The material is then hand mixed for 30sfollowed by high speed shear mixing at 3000 rpm for 2 min. After mixing it is poured into a secondary container for degassing then cast into molds. The cast specimens are then baked at 100 °Cfor 1 h. For the samples that contain GnP, it is added after the hand mixing of part A and B and prior to the high speed shear mixing. The weight additions are determined relative to the neat

sample. The GnP/PDMS is then high speed shear mixed at 3000 rpm for 2 minfollowed by an additional minute after the material cools down to prevent the material from heating up and kickstarting the cure.

5.2.2.2 Coating Glass Bubbles

The glass bubbles are coated with GnP-5 and GnP(750) prior to adding to the PDMS elastomer. The total weight percent (Wt%) of GnP needed to coat the spheres with 5 layers is given by equation 2.4 on page 23. In this equation, t is the thickness, ρ_{GnP} and ρ_{HGS} is the relative gravity of the GnP and hollow glass spheres, respectively, and D_{iM16K} is the average diameter of the glass bubbles. The total amount is multiplied by 5 because 5 layers should be enough to ensure a conductive coating. The resulting amount of GnP-5 and GnP(750) was divided by two since both types of GnP were simultaneously coated on the surface. The procedure is as follows:

1. GnP(750) is added to reverse osmosis (RO) water at a ratio of about 90 mg to 500 ml.
2. The solution is ultrasonicated with a 2.54 cm probe at 100 W for 1 h.
3. The GnP-5 is then added followed by additional ultrasonication for 1 h with the same parameters.
4. Add the tPEI binder to the solution at a ratio of 1:1 wt% to GnP.
5. Ultrasonicate for 4 minwith a 2.54 cm probe at 50 W.
6. Slowly add the HGS while stirring
7. Continue stirring overnight
8. The GnP coated HGS are then collected by filtration before drying.
9. After drying the GnP coated iM16K is high speed shear mixed at 1200 rpm for 30 s to break up the clumps.

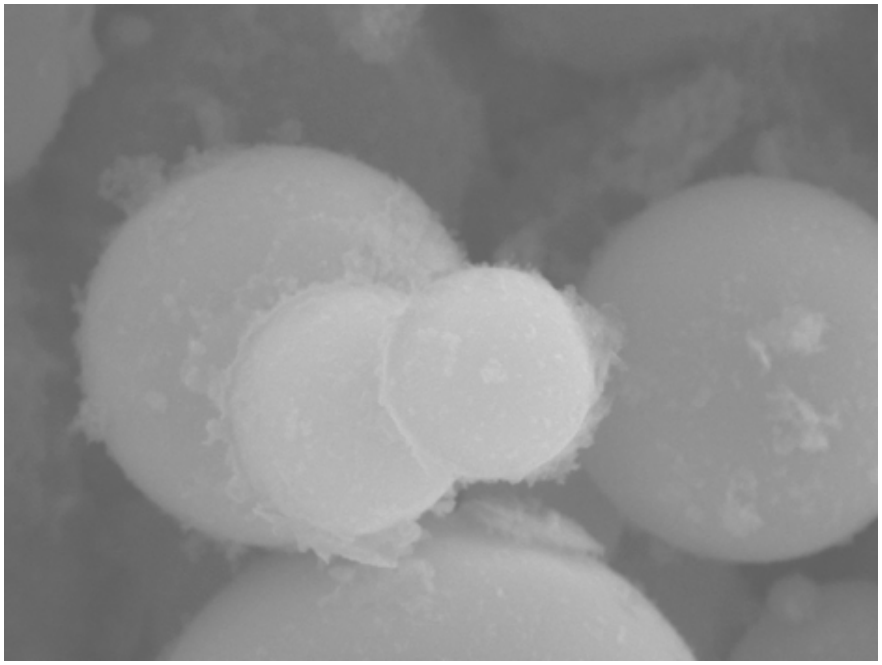

Figure 5.2: SEM image of HGS coated with GnP-5 and GnP(750) after drying. The sample was not coated prior to imaging.

The resulting glass bubbles are shown in Figure 5.2. Comparing the neat and GnP coated iM16K there is more fluffy platelet like appearance on the surface due to the GnP. Because the GnP on the surface is very thin and small it appears that the GnP(750) is more effective at coating the spherical surface.

5.2.2.3 PDMS syntactic foam

The initial steps are the same for the neat PDMS sample where the two parts of the elastomer are combined by hand mixing for 30 s. The hollow glass spheres are added by volume percent to the PDMS elastomer prior to being high speed shear mixed at 3000 rpm for 2 min. The GnP coated glass bubbles are mixed for an additional min at 3000 rpm after cool down to ensure adequate mixing and to ensure cure does not start prematurely. The material is then poured into a secondary container for degassing, followed by casting into molds. The material is then heated at 100 °C for 1 h.

5.2.3 Testing

5.2.3.1 Vector Network Analyzer

The dielectric properties were determined using a transmission line system which includes a vector network analyzer (VNA) connected to a waveguide. The averaging factor was set at 64, an IF bandwidth of 5 kHz was selected and the impedance was set to 1 Ω. The waveguide dimensions were as follows: 10.5 mm by 22.9 mm by 7.4 mm thick for X-band testing. Four specimens were cast to these dimensions and 3 were tested. The NRW (Nicholson and Ross [65] and Weir [66]) algorithm was used to determine the relative permittivity and permeability as a ratio to vacuum according to the relationships given in Section 2.3.5. In addition, S_{12} in this set-up is a measure of the respective voltages when a material is present and when it is not present, and is used in the definition of the shielding effectiveness according to equation 2.13, shown again here. All testing was done at room temperature.

$$SE_T = 20 \log \frac{V_1}{V_2} = 20 \log |S_{12}| \text{ (dB)}$$

The total shielding effectiveness is the sum of the losses from reflection SE_R, absorption SE_A and multiple reflections SE_M as the wave propagates through the sample. The transmittance (T), reflectance (R), and absorbance (A) with respect to the incident wave shown in chapter 2 is also given again here,

$$T = |S_{12}|^2 \tag{5.1}$$

$$R = |S_{11}|^2 \tag{5.2}$$

$$A = 1 - R - T \tag{5.3}$$

5.2.3.2 Microscopy

All images were taken on a variable pressure scanning electron microscope (SEM). The sample surface for imaging was prepared by tearing the specimens after a slight cut to begin the separation. The specimens were adhered to the sample holder using conductive carbon paste

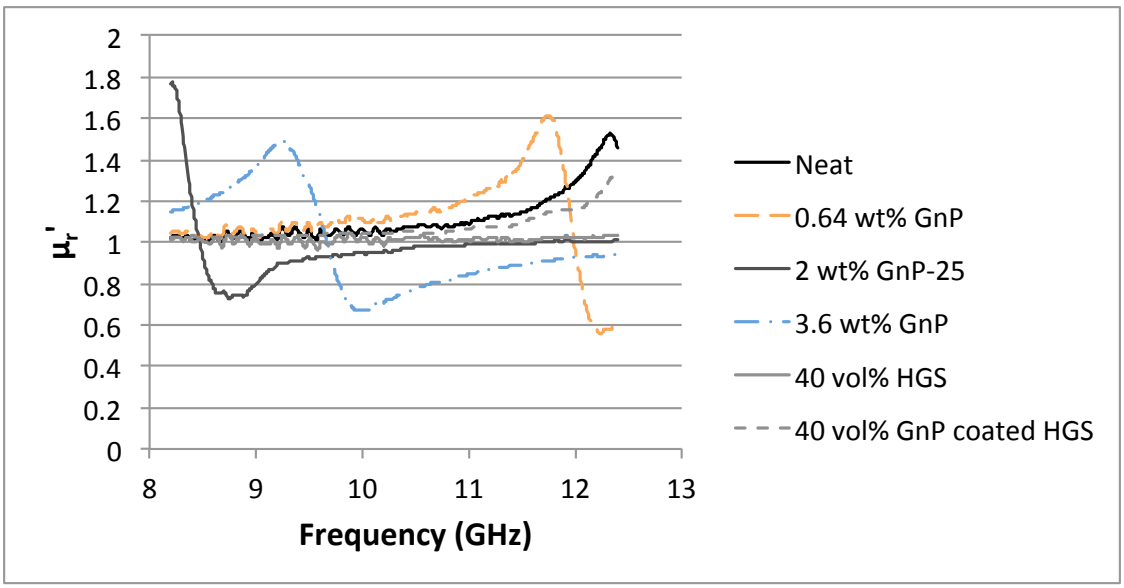

Figure 5.3: Real permeability as a ratio to the permeability of free space for nanocomposite PDMS samples from 8.2 to 12.4 GHz, compared to the neat PDMS elastomer.

and all the cured PDMS samples were coated with about 3 nm of tungsten prior to imaging. The glass bubbles were not coated, but adhered to the stub with the same conductive carbon paste before going into the SEM chamber under variable pressure mode for imaging.

5.3 Results

The following charts show the real permeability and permittivity of the samples relative to the permeability and permittivity of free space as well as the alternating electric loss tangent and lastly the different EM shielding characteristics calculated from the S_11 and S_12 scattering parameters.

5.4 Discussion

PDMS is a non-magnetic polymer, which is confirmed by the low relative permeability given in Figure 5.3. Graphene along with graphite has also been found to be low paramagnetic materials [104]. The permeability results substantiate this claim as the magnetic capabilities of

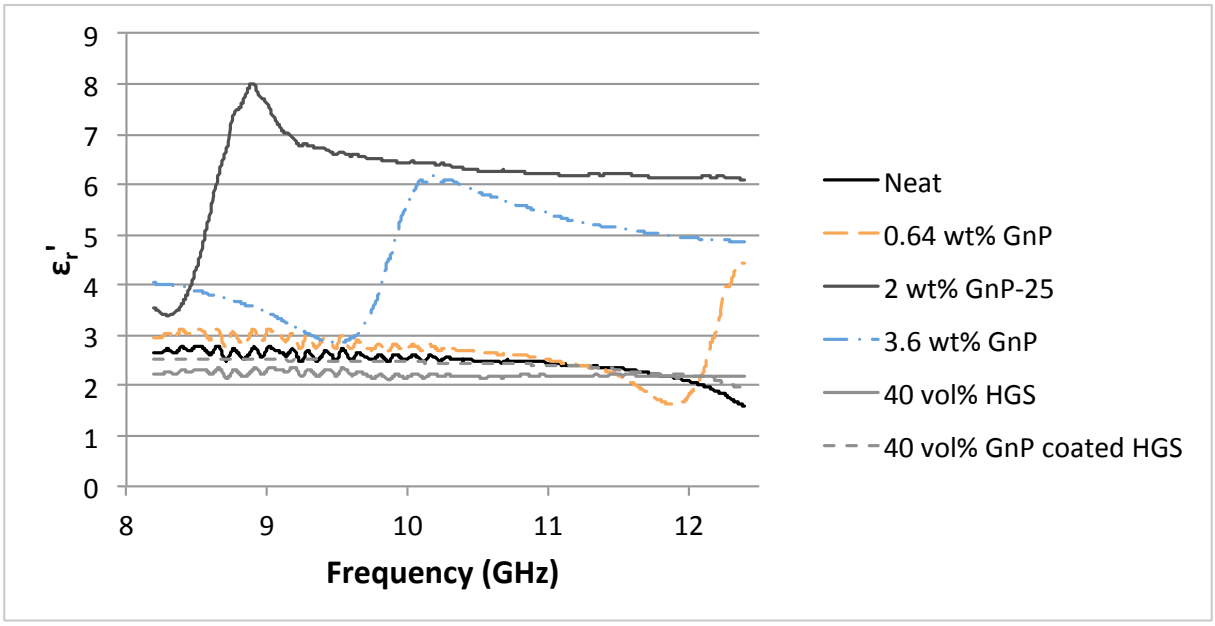

Figure 5.4: Real permittivity as a ratio to the permittivity of free space for nanocomposite PDMS samples from 8.2 to 12.4 GHz, compared to the neat PDMS elastomer.

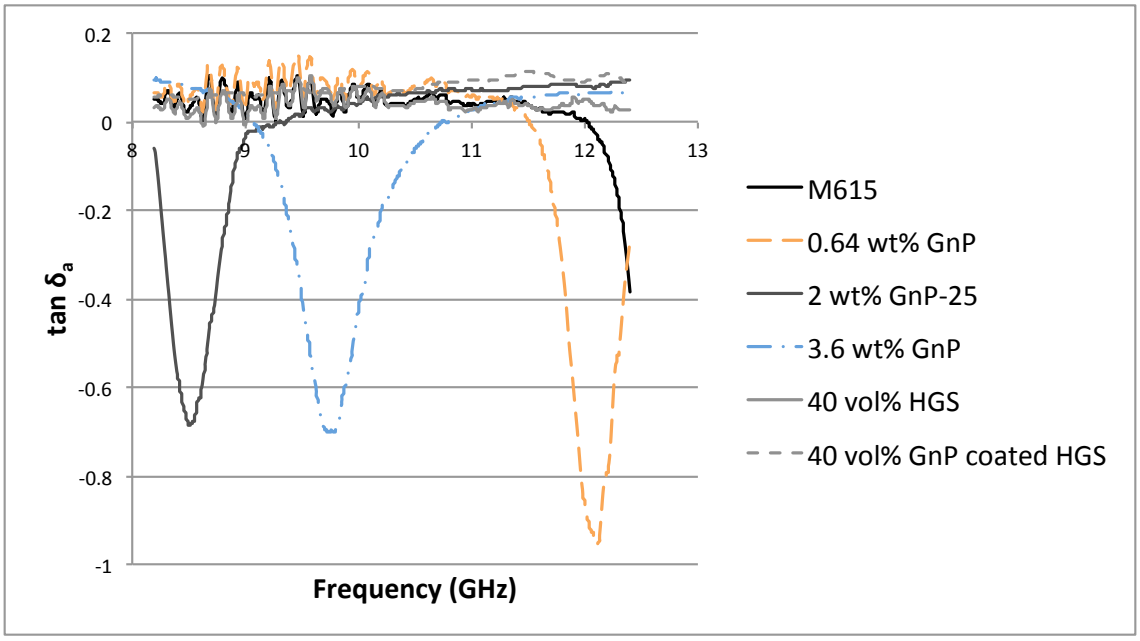

Figure 5.5: Alternating electric loss tangent ($\tan \delta_a = \varepsilon"/\varepsilon'$) of nanocomposite PDMS samples from 8.2 to 12.4 GHz.

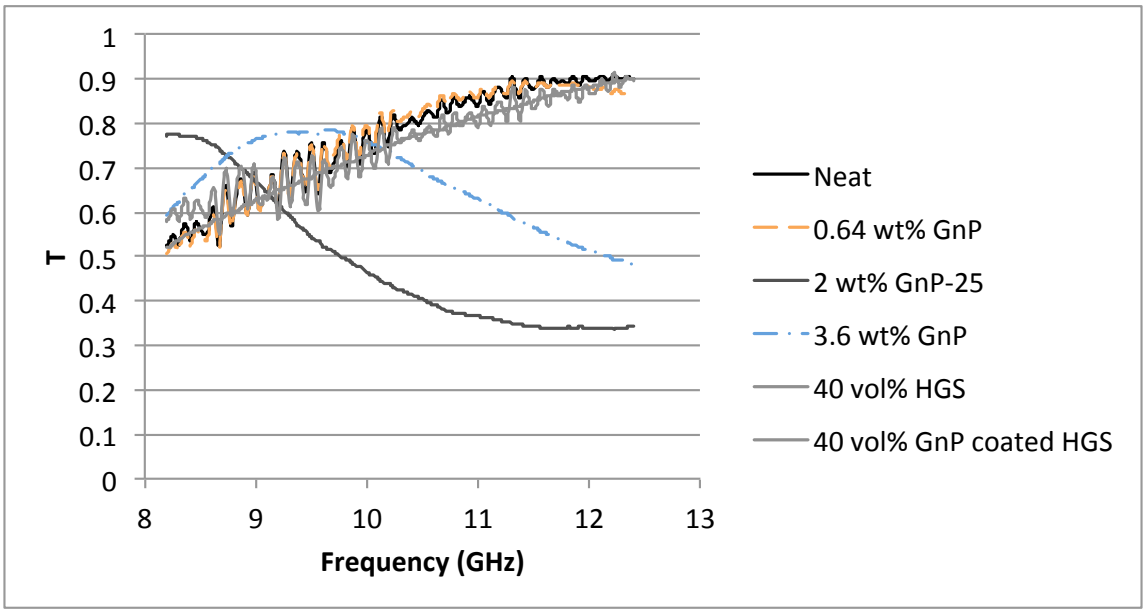

Figure 5.6: Fraction of applied electric field that transmits through the nanocomposite PDMS samples from 8.2 to 12.4 GHz.

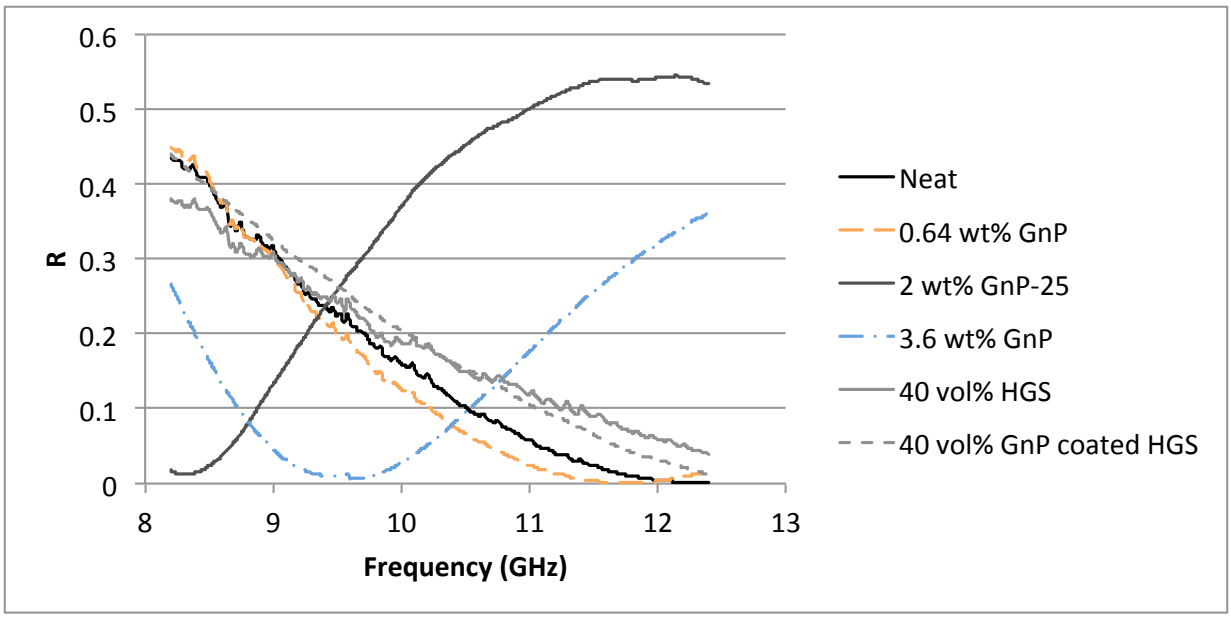

Figure 5.7: Fraction of applied electric field that reflects of nanocomposite PDMS samples from 8.2 to 12.4 GHz.

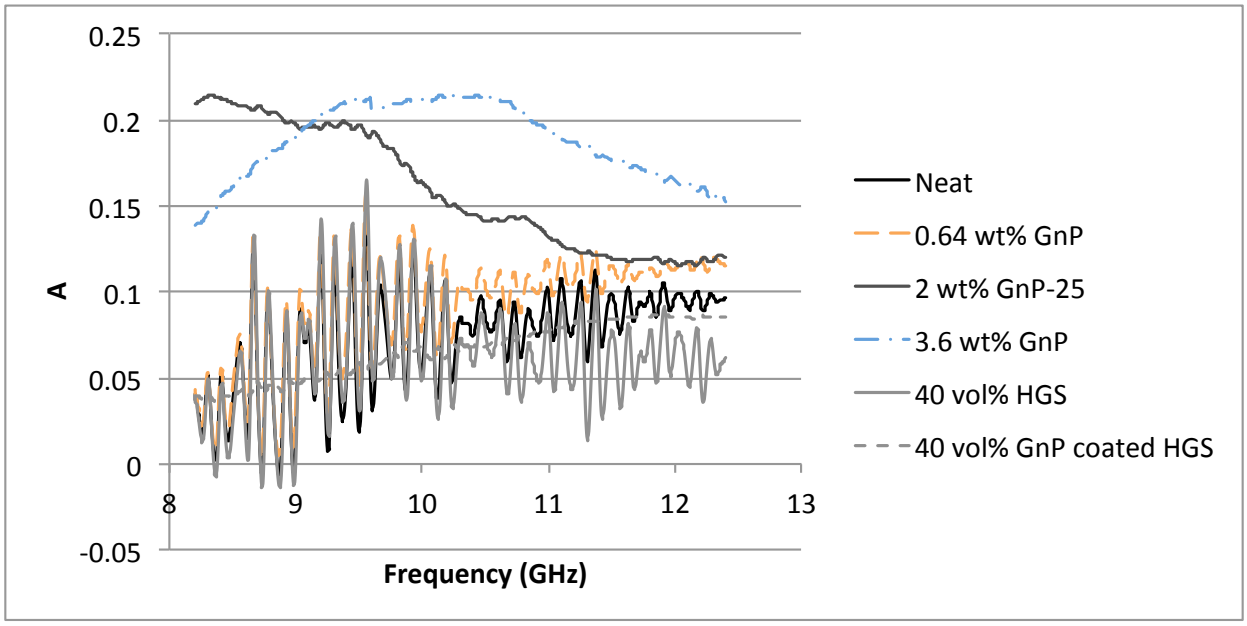

Figure 5.8: Fraction of applied electric field that is absorbed by the nanocomposite PDMS samples from 8.2 to 12.4 GHz.

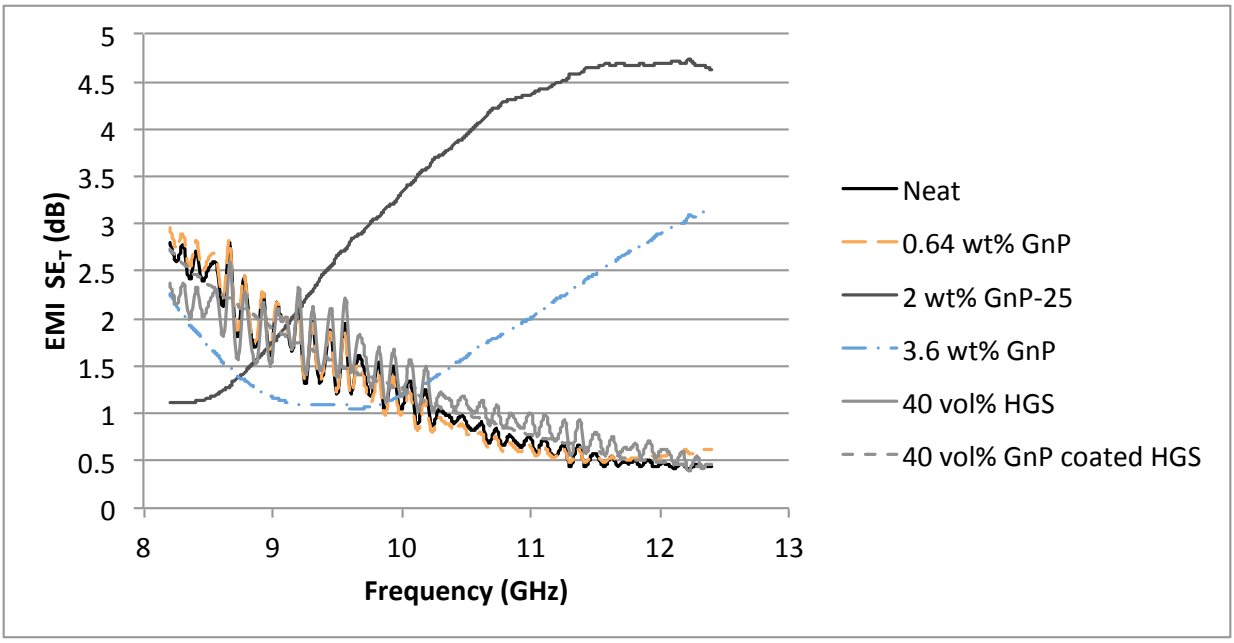

Figure 5.9: Total EMI shielding effectiveness of nanocomposite PDMS samples from 8.2 to 12.4 GHz.

the nanocomposite PDMS is minimal as all the graphs of the samples show real permeabilities of around 1 H/m. Both the neat and nanocomposite samples are considered to be non-magnetic so the rest of the discussion will focus on the electric properties.

5.4.1 Modes of Dielectric Response

When an electromagnetic field is applied to any material there will be a dielectric response. The strength of the response will depend on the degree and ease of alignment in the local areas of the material. ln any material there are what could be called electric dipoles, the areas of positive and negative charges. This is commonly associated with atoms, but there can also be positive and negative areas in a material on a larger scale. This means that when an electric field is applied these positive and negative parts in local areas that will align according to an applied field as the electric field is a vector field that has a force and direction. The more powerful the applied field the greater resulting separation between these charges. For any material the majority of the electric dipoles are bound charges where their function is not conduction, but they can shift when exposed to an electric field. Usually these dipoles are oriented randomly in a material; the dielectric response then of any material describes the ability of these dipoles to align according to an external electric field. If the fields align easily there is more energy stored in the system, the more difficult the more energy that is lost in the system. There are four different areas in a material that are affected by an applied electric field.

If ionic atoms are present they can be affected by the electric field as each pair of ions is basically an electric dipole. Because ions are relatively large these particles are only affected up to certain frequencies before the rate of the alternating field is too fast of a motion for the ions to keep up with. Another mode that operates only at those same frequencies is the dielectric response the orientational or polar effect. These polarities are due to either be permanent dipoles or if the local area is non–polar, those induced by the applied field that causes a shifting of the centers of the positive and negative parts so they are no longer

concentric. To induce dipoles where there are none requires a force strong enough to overcome the attraction of the positive and negative charges. Once again the response of these dipoles is limited to lower frequencies due the ability of these larger dipoles to keep up with the frequency. Another low frequency dielectric mechanism is the interface/space charge response where the focus in now on materials that have metallic-like conduction, where the conducting electrons in the material have no band gap and could easily align and separate in the material when a field is applied creating an interface between the electrons and the now positive core. For higher frequencies the dielectric response is dominated by the electronic and atomic responses of the dielectric. At low frequencies these factors are constant and small relative to the other contributions, but at frequencies greater than about 10^{12} Hz these mechanisms start to dominate as the others no longer function. Both modes have to due with the induced electric dipole that an atom forms when exposed to an external field, but because these measurements are taken in the X-band frequency they are not contributing modes to the dielectric response.

5.4.2 Probable modes of dielectric response in nanocomposite PDMS

Since the nanocomposite PDMS is being tested in the X-band frequency from 8.4-12.2 GHz the electronic and atomic contributions to the dielectric response are both constant and small so they will be ignored for the remainder of the discussion. PDMS is a unique polymer due to its flexible properties at low temperatures from its unconventional inorganic-organic structure that consists of a silicon-oxygen backbone with organic methyl side groups. As with any foam the dielectric properties are dependent only on the polymer and changes with density [87]. The lower the density the lower the real permittivity as the addition of gas in the hollow glass sphere contributes minimal dielectric response [92]. PDMS is both non-ionic and non-polar so there will be a limited number of weak permanent dipoles any others will have to be induced. This is an insulating material so any free electrons that appear on the surface screening the interior from the effect of an external alternating field [87]. Free electrons are also beneficial

for reflecting electromagnetic (EM) waves for electromagnetic interference (EMI) shielding, of which insulators have a small amount. The behavior as an insulator is confirmed by the low real permittivity and shows significant loss for a material according to Figures 5.4 and 5.5. A general guide is to consider a lossy dielectric one that has an alternating loss tangent, $\delta_a > 0.1$ and a low-loss has a $\delta_a < 0.01$, the PDMS is showing an alternating loss tangent right between these two cut-offs.

Compare the matrix to the soda lime borosilicate glass spheres. The structure of any glass is amorphous and in this glass is made up of different ceramic oxide molecules that have local order to form silicon dioxide, calcium oxide ("lime"), boron trioxide (B_2O_3) and sodium oxide ("soda"-Na_2O) in decreasing order of concentration. This structure has ionic bonding and thereby can be susceptible to an electric field, but theses spheres are hollow not solid and have a dielectric constant of 1.2 to 1.7 F/m @100 MHz according to the 3M™ product sheet. This value is not within the X-band frequency but results from replacing some of the PDMS material with the hollow glass spheres does result in a decrease in the real relative permittivity but not the loss (see Figure 5.4). This could simply be due the fact there is simply less material to be affected by the applied field as the PDMS syntactic foam has a 20% less as compared to the neat. The last factor to take into account is the contribution of the GnP to the nanocomposite. As stated previously the sp^2 bonding creates a π cloud made up of the extra π electrons that are available for conduction. When an electric field is applied it is easy to imagine these π electrons aligning to the field separating from the positive honeycomb lattice core creating an interface/space charge region similar to metals. All the other modes of dielectric response would be minimal contributors compared to the effect of having the conducting charges. So then adding these particles to PDMS results in an increase in dielectric response even at low loadings as seen from the Figure 5.4 where there is positive increase on the real relative permittivity due to the addition of the nanoplatelets.

5.4.3 Effect of conductivity on permittivity

Figure 5.4 is a plot of the real relative permittivity of all synthesized PDMS specimens with GnP and with hollow glass spheres relative to the neat PDMS sample. Some of the samples show a sharp increase in the dielectric response at certain frequencies. This due to the resonance frequency of the sample, which only occurs in this frequency range for the samples with GnP. In all materials at all times atoms are not static, but constantly vibrating at temperatures above absolute zero. In an alternating electric field these bound atoms are oscillating much like any damping harmonic oscillator between the positive and negative ionic or electronic parts. Resonance describes the phenomenon when the frequency of the applied field matches the frequency of the ionic or electronic polarization mechanism. This can result in improvement in the dielectric performance when there is an increase in the dielectric response from the increase in amplitude of oscillations resulting in a larger polarization or separation between the oppositely charged parts creating a larger dipole. Because this only occurs in the samples with addition of GnP only, this dipole describes the interface between electron the cloud and positive core of the platelets. All dipoles have a dipole moment, which is related to the magnitude of the charge. P is the dipole moment per unit volume, which is linearly related to the electric susceptibility, χ, a dimensionless quantity that describes how easily a material polarizes due is to an applied electric field which in turn relates to the relative permittivity according to equations 5.4 and 5.5.

$$\mathbf{P} = \chi_e \varepsilon_0 \mathbf{E} \tag{5.4}$$

$$\varepsilon_r = 1 + \chi_e \tag{5.5}$$

Where this resonance wavelength occurs is dependent on the dielectric properties of the material. While PDMS seems to be a relatively lossy dielectric it also contains good conducting particles. A plane wave propagating in a good conductor $\lambda = 2\pi\delta$ is different from how it would propagate in free space $\lambda_0 = c/f$. The factor δ is the penetration/skin depth and is the point at which the wave energy decreases to $1/\exp$. It is related to the

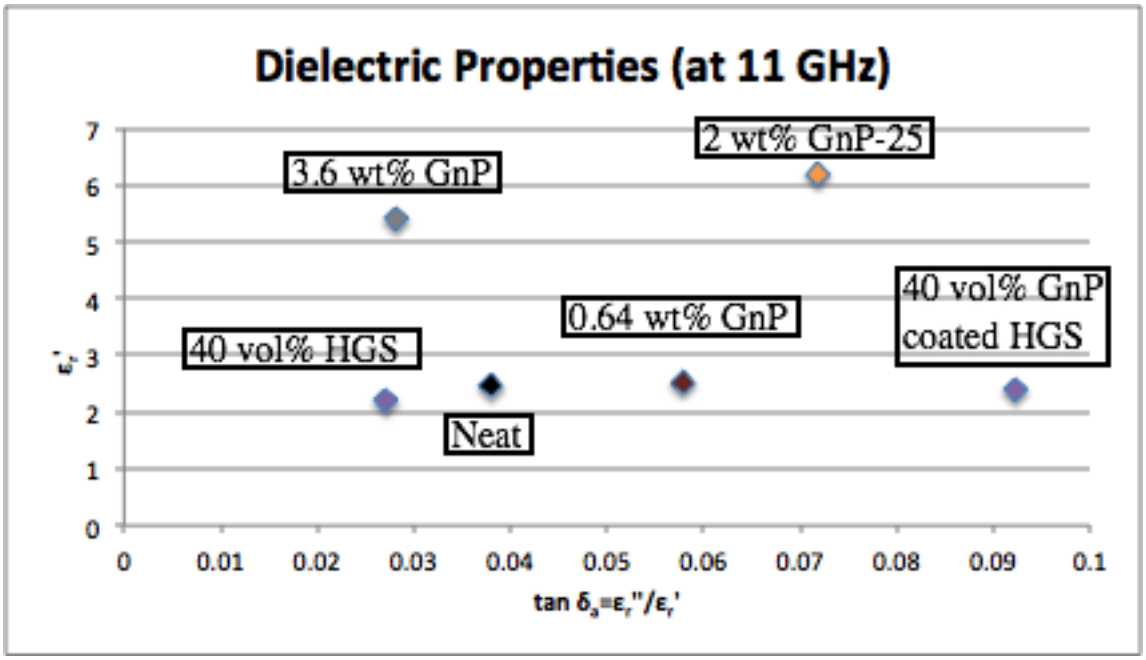

Figure 5.10: Real relative permittivity (ε_r') versus alternating loss tangent ($\tan\delta_a$) of nanocomposite PDMS samples and neat elastomer at 11 GHz.

conductivity, σ, or conversely the resistivity, ρ, according to equation 5.6 [105].

$$\delta = \frac{1}{\sqrt{f\pi\mu\sigma}} = \sqrt{\frac{\rho}{\pi f\mu}} \tag{5.6}$$

Since the material is non-magnetic μ can be taken as 1 and f is the frequency, for this material the skin depth, $\delta \propto \sigma^{-1/2}$. As the conductivity increases, the penetration depth decreases and causing the wavelength through the material to be shorter than if the wave were propagating through free space. For the same resonance wavelength the frequency at which this wavelength is reached will be different due to the effect the material. The fact that the resonant wavelength is changing suggests the material now has some characteristics of a good conductor which can only be due to the addition of the GnP. It suggests than the GnP has at least percolated through the sample creating a conductive pathway.

The effect of whether the material has percolated or not seems to be having an effect on the behavior on the material which is shown clearly in the performance between the samples. This effect is highlighted in Figure 5.10 where all the samples basically plot out

in two horizontal lines when comparing the real relative permittivity to the alternating loss tangent. It shows the significant improvement in real permittivity between the samples with the highest loading of GnP as compared to the others. This marked improvement once again suggests that material is behaving like a conductor at these frequencies which is true when the percolation threshold is reached which seems to be the case for the samples with 2 wt% GnP-25 and 3.6 wt% GnP (2.15 wt% GnP-5, 1.45 wt% GnP(750)). The sample with 2 wt% GnP-25 shows the best permittivity at lower loading because of the much larger aspect ratio of the particle which is known to be a contributing factor to the percolation threshold [52].

5.4.4 Modes of loss in dielectrics

Conductivity can have both positive and negative effects on the dielectric response of material when exposed to an electromagnetic wave. It can also contribute to the loss if It produces collisions between the many free electrons in the material. That is however not the only mode of loss in a dielectric. Another factor relates directly to the loss of energy of the applied electric field due to heat either from friction and/or the difficulty in acceleration/deacceleration of the dipoles [106]. The first condition is described by the static loss tangent and the latter by the alternating electric loss tangent. For many materials one of these terms dominates more than the other, but since the nanocomposite PDMS contains conductive particles in an insulating matrix both terms contribute to the total loss.

$$\tan\delta_e = \tan\delta_s + \tan\delta_a \tag{5.7}$$

$$\text{where, } \tan\delta_s = \frac{\sigma}{\omega\varepsilon'} \text{ and } \tan\delta_a = \frac{\varepsilon''}{\varepsilon'} \tag{5.8}$$

For most of the samples the contributing loss will be the alternating loss tangent, but for the samples with significant loadings of GnP the static loss tangent will become more significant. Overall the material loss does not change a significant amount through all the samples so for the most part the matrix properties still seem to be dominating factor in determining the permittivity losses.

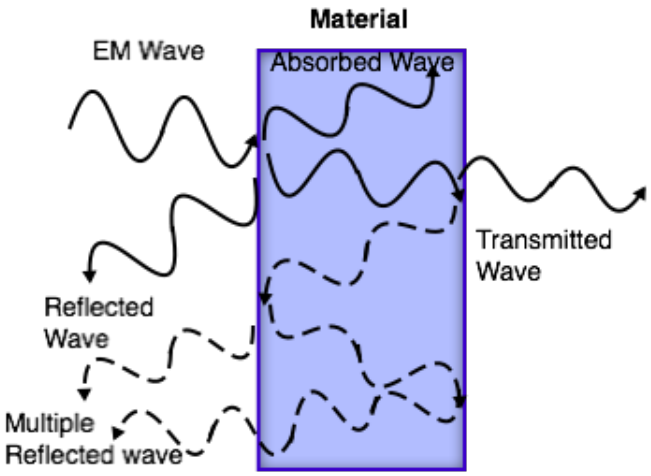

Figure 5.11: A graphic illustrating the three ways an electromagnetic plane wave can be affected when confronted with a material.

5.4.5 EMI Shielding

Electromagnetic interference (EMI) shielding effectiveness (SE) quantifies how effective a material is at preventing electromagnetic power from transferring through it. For transmission line experiments this factor is related to the scattering parameter S_{21} by the equation: $SE_{total} = 20 \log S_{21}$, where the scattering parameter is a relation between voltages when the material is present versus when it is not. There are three ways in which an electromagnetic wave interacts with a material, it can be reflected, absorbed and/or experience multiple reflections, the total SE is the sum of all these factors. The three modes are shown in Figure 5.11 and demonstrate what happens to a plane wave when it encounters a material. Out of all of these modes the most desired is absorbance as reflection is only able to reflect outside electronics, but allows the electromagnetic waves to be reflected back in causing disruption in the internal system and is the current drawback with traditional metallic shielding materials.

Figure 5.7 gives further evidence that PDMS with 2 wt% GnP-25 and 3.6 wt% GnP has mobile charge carriers demonstrated by the increase in reflectance. They are also the only two samples that show improvement in absorbance, it is difficult to distinguish in the rest of them. The only exception to this is the samples with the glass bubbles while the

absorbance is still low the noisiness of the plots has significantly decreased. Absorbance depends on thickness that becomes more prominent when the thickness is greater than the skin depth, which correspondingly is when multiple reflections can also be ignored. According to equation 5.6 skin depth decreases as the conductivity or permeability increases. Since this material is essentially non-magnetic changes the increase in absorbance are due to the increase in conductance. Conductivity is of course also an important factor in improving the reflectance of the samples and the same nanocomposite samples show overall a much better transmittance and reflectance. For the nanocomposite PDMS the reflectance and transmittance seem to be inversely related for the most part, as one decreases the other increases proportionally this can be seen in the charts that show the fraction of each mode the incident electromagnetic wave is affected by. The changes in transmittance, reflectance and absorbance can be solely explained by the addition of the GnP as the addition of the hollow glass spheres simply reduces the amount of solid and glass is an insulator. The strong frequency dependence of all the samples though suggest a material is still behaving more like an insulator than a conducting medium as conductors like copper and polyaniline show a much more constant SE over varying frequencies [67].

5.4.6 Improvements

The nanocomposite PDMS samples with 2 wt% GnP-25 and 3.6 wt% GnP showed improved connectivity regardless of the poor distribution of the GnP throughout the sample. Figures 5.12 and 5.13 clearly show multiple agglomerations that appear in the images as really thick stacked particles or, in the case of GnP(750), as amorphous particles. High-speed shear mixing does not seem to be a vigorous enough method to break down the larger GnP(750) sub-micron agglomerates or separate the larger GnP-25 particles. The arrows in Figures 5.12 (b) and (d) points to GnP that appears to not be agglomerated, but all these particles are also of a smaller diameter. This is not surprising since the agglomeration of the GnP is due to the attraction between the basal planes of the particles; smaller particles do not have as

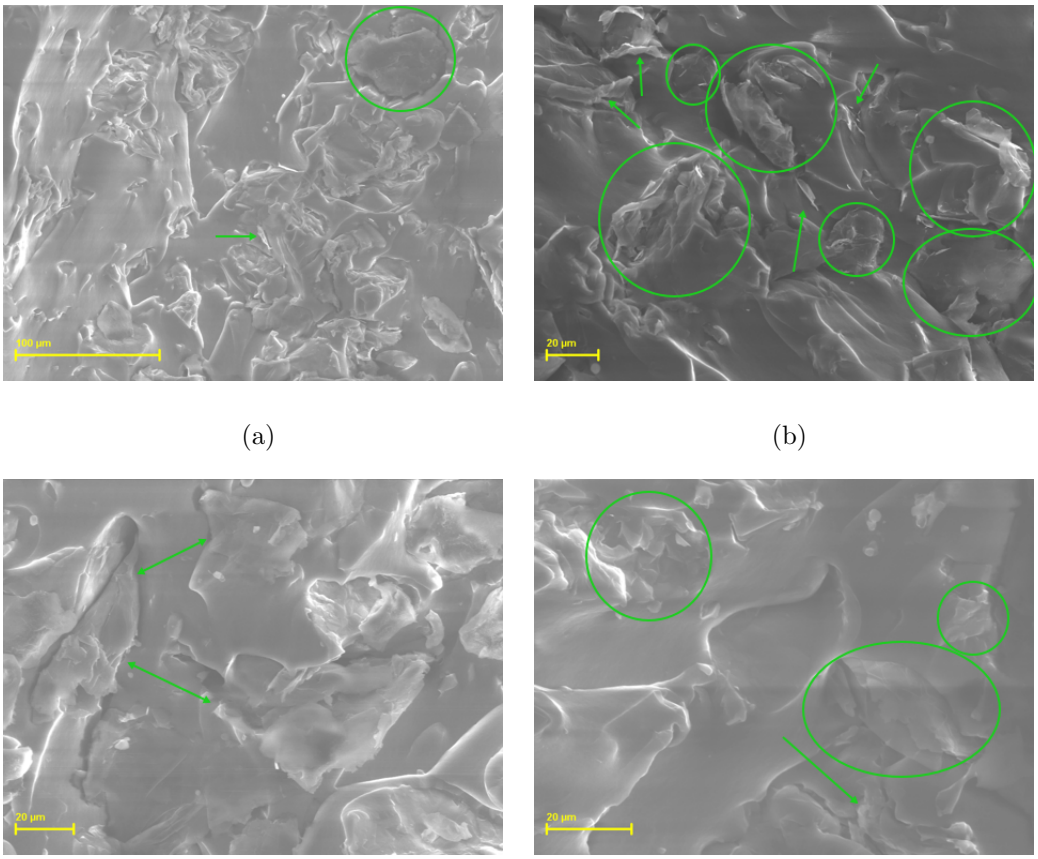

(a) (b)

(c) (d)

Figure 5.12: SEM images of 2 wt% GnP-25 in PDMS elastomer. Arrows and circles are to highlight the location of some of the distinguishable GnP: (a) Large agglomerate of GnP-25 in top right corner and arrow points to a thin platelet; (b) Agglomerates and thin GnP are relatively close together; (c) Distance between some GnP agglomerates; and, (d) GnP agglomerates can be very close or decently far from each other.

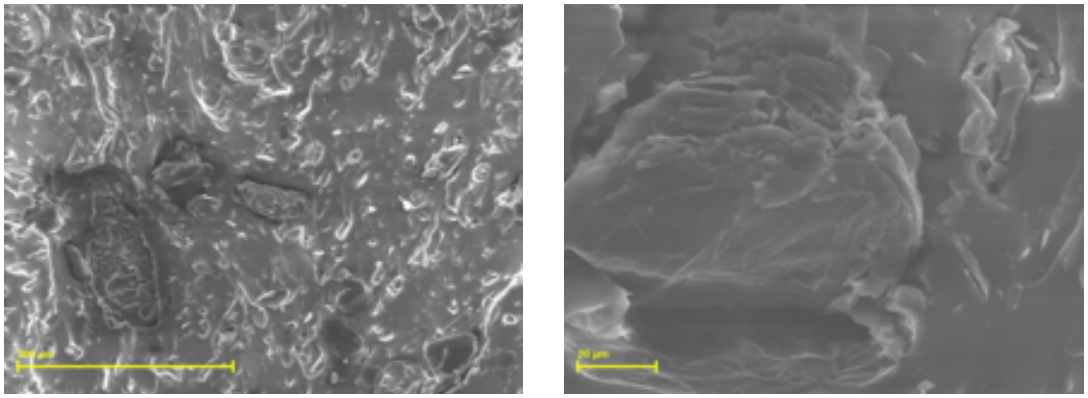

(a) (b)

Figure 5.13: SEM images of PDMS with 2.15 wt% GnP-5 and 1.45 wt% GnP(750): (a) Dark large particles are agglomerates of GnP(750); (b) Stack of GnP-5.

large of basal plane making them easier to separate. The difference with the GnP(750) is that the particles are not simply stacked, but overlapped many different directions containing a much larger amount of platelets that need to be separated. Agglomeration is generally to be avoided as it increases the loading necessary to achieve percolation, in addition, they act as stress concentrators reducing the mechanical properties. However, the stacked particles allow for easier local conduction resulting in a larger local dielectric response potentially contributing to a higher polarization/unit volume. If the particles are separated and oriented in many different directions that could reduce the local polarization and even though there would be more areas of smaller local polarization that could still be less than the polarization that amounts when GnP stacked together in the same direction.

Figure 5.14 demonstrates how the microstructure varies from the neat elastomer to that with 40 vol% loading of HGS that are responsible for the loss in the real permittivity with the addition of the empty "cells" in the syntactic foam. Compare the images of the nanocomposite PDMS to the nancomposite PDMS syntactic foam where it appears that there is no GnP in the syntactic foam, but the improvement in dielectric performance in the syntactic foam with GnP over that without suggesting that the GnP can combat the loss of density. This also

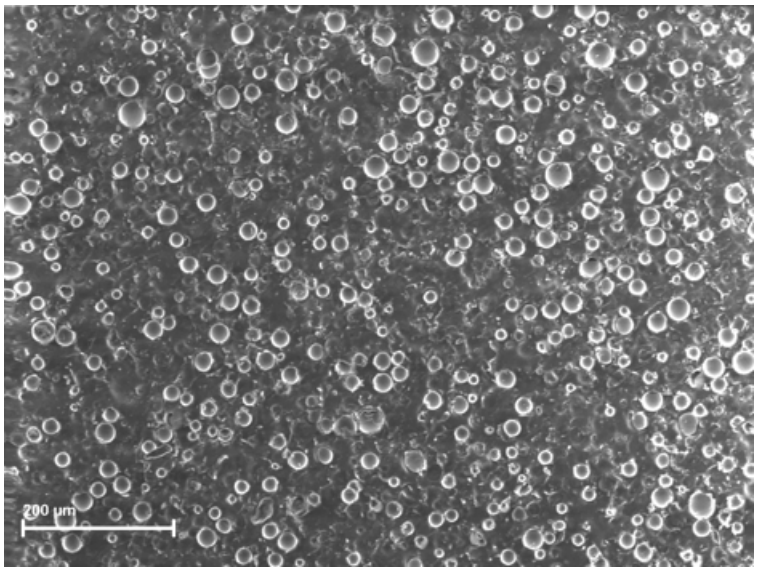

Figure 5.14: SEM image of dispersion of 40 vol% HGS in PDMS elastomer

confirms that there is GnP although it is difficult to distinguish in Figure 5.15 (a). What is also missing are the large agglomerates of GnP that appeared in the nanocomposite GnP samples. It appears that the addition of ultrasonication and then adhering the particles to the HGS seems to do a relatively good job of breaking down and maintaining the separation of the GnP and especially the GnP(750), which is difficult to see at these magnifications due to their small diameter (< 2 µm). However, the agitation of the lower speed of the high speed shear mixer was apparently not able to break down all the clumps of GnP coated HGS as now the agglomerates in the system are of GnP coated HGS that appear to have been minimally coated with the polymer as shown in Figure 5.15 (b). For the dielectric performance, however, the hollow glass spheres seem promising as generally borosilicate glass is a low loss material and out of all the specimens in Figure 5.10 the one with 40 vol% has the lowest alternating loss tangent at 11 GHz. Coating the spheres in GnP improves the real permittivity relative the sample with non-coated HGS and offers comparable shielding performance to the neat sample demonstrating comparable absorbance while being 20% lighter.

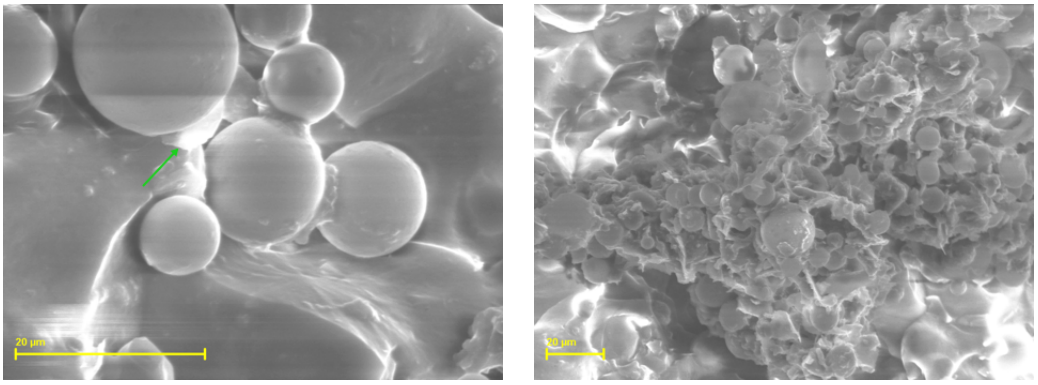

(a) (b)

Figure 5.15: SEM images of 40 vol% GnP coated HGS in PDMS elastomer. The amount of GnP relative to the spheres is 2.15 wt% GnP-5 and 1.45 wt% GnP(750): (a) Able to distinguish only 1 GnP on HGS in PDMS; (b) Clump of GnP coated HGS in PDMS.

5.5 Conclusion

Foams are rather promising materials due to their low density making them ideal materials for applications in which weight is a concern. However, both permittivity and EMI SE decrease with foam density, GnP was added as a way to overcome that by the GnP forming a percolated network. GnP is a multifunctional nanoparticle that includes high electrical conductivity as well as a positive central core surrounded by a π-cloud of electrons properties that is beneficial for improving both the dielectric and EMI shielding properties. Adding GnP to PDMS resulted in improvement of the dielectric properties and shielding effectiveness of the samples including increasing the ability of the polymer to absorb electromagnetic waves likely by decreasing the skin depth. All of these improvements can be solely explained by the addition of the conducting particles.

The greatest improvement was seen in the samples that had the highest loading of GnP in the solid. A large aspect ratio has been found to be an important property for achieving electrical percolation at lower loadings. The PDMS with 2 wt% GnP-25 increased the real permittivity about 2.5 times over the neat material and improved the SE effectiveness about 9

times at its highest while increasing the absorbance and reflectance. Compared to the PDMS sample with 1.6% more GnP that is mixture of two sizes of significantly smaller aspect ratio were only able to double the dielectric constant and was able to improve the EMI SE, but is unclear by how much due to the strong dependence on frequency. However, the earlier shift of the resonance frequency by about 1 GHz suggests that the sample with 2 wt% GnP-25 is more conductive. Whether a percolated network formed in the system is unclear as the strong frequency dependence suggests a material that is still not behaving as a metallic conductor. If the GnP dispersion were more uniform and less aggregated that could result in a corresponding improvement in electrical performance by creating much more connected paths. The challenge with increasing the diameter on the GnP creates a stronger attraction due the Van der Waals forces on the basal plane that preferentially aggregate GnP rather than interact with the polymer and any future methods employed to improve the interaction between the GnP and the matrix must do so without disrupting the basal plane character responsible for its strong electrical performance.

PDMS already has applications in aerospace due to their flexibility at low temperatures and adding GnP seems to show promise as a multifunctional nanofiller for this material. Coating the HGS prior to dispersing in the polymer improved the behavior of the nanocomposite syntactic foam. It had the same real permittivity as the neat PDMS and improved the real permittivity by about 12% at only 0.64 wt% GnP. It demonstrated the same EMI SE as the neat and PDMS with 0.64 wt% GnP while still being 20% lighter. However, the resultant images of the foam made it unclear whether the GnP managed to stay adhered to the spheres during processing. Also the occasional clumps of coated spheres reduces the connectivity producing areas of high and low local conductance, the coated HGS could benefit from a more vigorous mixing prior to adding to the polymer to break up the clumps, but carefully so that the GnP stays adhered.

The materials and methods employed in this research are relatively low-cost, which makes nanostructuring a promising method to improve the properties of polymers. If the interaction

between the GnP and the matrix were improved in such a way that the conductivity of the basal plane was not disrupted the percolation could be done at even lower loadings. A synergistic approach also shows promise such as adding a small concentration of large GnP that would act as a bridge between the conductive contact points that are the GnP coated HGS. The versatility of this nanoparticle is what makes it so promising in nanocomposite applications.

CHAPTER 6

SUMMARY AND FUTURE WORK

For many decades now the aerospace industry has been a leader in developing new technologies. This is partially due to the extreme and in many ways unfamiliar environment that the technology must operate in. This industry is unique in that its focus is not only the short term, but tries to anticipate and meet challenges several decades or even a century in advance. But to make such technology possible requires that the materials already be in place. One such promising material is a nanocomposite which allows for nanostructuring, a new way of combining polymers with multifunctional materials that could do multiple jobs thus replacing many individual components. The less components that have to be made could translate to less weight and a lower cost, important factors for viable aerospace technologies.

There are many areas in technology that could benefit from the nanostructuring of materials, everything from energy applications to sensors to biological applications to space flight. Polymers are a promising material matrix due to their ease of formability and processing, relatively low density as well as their relatively low synthesizing costs. Extensive work has already been done on forming polymer nanocomposites, but it became clear early on that with this new material comes new challenges. While there are many benefits to adding nanoparticles, the extent of these benefits depends on how the nanofiller interacts with the material matrix on molecular and microscopic level, which then affects the macroscopic properties. The results of this investigation highlight some of the challenges that must be dealt with and overcome to make a beneficial polymer nanocomposite using low-cost materials and methods, and highlights some methods employed to overcome them. In addition, this dissertation exposes some unique obstacles that come from working with a microcellular structure and the effect that can have on the overall properties of the nanocomposite material.

6.1 Rigid PUR/PIR nanocomposite foam

The addition of a nanomaterial to a chemically blown foam appears to disrupt the polymeric system on a physical and chemical level changing the resultant polymer's molecular and microscopic properties. The gas expansion process alone causes changes in the thermal degradation behavior, but not in the crosslink density, as the expanded structure results in a larger surface area, but similar glass temperature (T_g). Suggesting that the removal of decomposed products, which is a diffusion controlled process, is affected by the change in microstructure between the solid and the foam. A large surface area is commonly more beneficial when diffusion is a factor. A cellular structure allows for more volume at or near the surface, which is confirmed by the much higher rates of degradation experienced by the foam. This structure can also be disadvantageous as it seems to prevent the removal of the decomposed products of the internal structure owing to the tortuosity and resulting in all the foam samples having a higher rate retention than the monolithic polymer at 750 °C. In general the rate of decomposition is much broader for the monolithic polymer structure due to the diffusion limitations in the solid polymer.

The addition of the GnP to the foam results in an increase in thermal stability owing to the high specific heat capacity of the nanoparticle. However, this was not observed in the solid with the addition of neat GnP. In fact, the thermal degradation onsets overlap for rigid PUR/PIR nanocomposites with some exceptions for the pMDI treated GnP. As to why the GnP is not helping to mitigate the heat, it could be the result of the weight loss with increasing temperature being dependent on diffusion so that any benefit of the GnP is mitigated by the fact that the rate of removal of the decomposed products is controlled by the barrier structure making it difficult to determine any improvements between the neat and naonocomposite samples. The neat GnP-25 in both the solid and the foam showed the same cross-link density suggesting that the large platelets interact the same way in both which none of the others samples demonstrated. This is largely due to the agglomerated nature of the particles that limits its interaction with the matrix. Although, the addition of

the neat GnP-25 in the foam also resulted in the cells being almost 40 μm smaller than the standard so the larger particles helped to stabilize the bubbles and prevent coalesce. The GnP-5 helps in this regard, but not as significantly as the cells are only about 20 μm smaller. The smallest particles (GnP(750)) do nothing for the cell structure resulting in the median cells being 12.7 μm larger than the standard. The larger cell size could be due to a change in the microphase that allows for bubble coalesce for which the microstructure of the standard is more effective at limiting. It does appear, however, that the foam is better able to adapt its molecular structure as the T_g of the neat GnP-5 is on average about 3 °C higher than when in the solid, but both show large variation in T_g likely brought on my the non-uniform dispersion. In addition it appears that the smaller particles do better at maintaining the cross-link structure as the Tg of the foam with neat GnP(750) matches that of the standards. There is also minimal aggregation so the local concentration is uniform throughout the foam. This match in cross-link density could be because the small size of the particles is on the scale of the microphase structure. Polyurethane consists of hard and soft segments either of which can be cross-linked and on the scale tens to hundreds of nm in length and GnP(750) have particle sizes on the scale of hundreds of nm.

Treatment of the edges with isocyanate was conducted to promote the formation of urethane-type groups that would bond better with the foam. In general, the effect was negative or offered no improvement. The exception is for the GnP(750), which demonstrated changes in microstructure as well as macroscopic properties due to the higher edge density of these small particles. The monolithic polymer with treated GnP showed early onset for the separation of polyurethane into its monomers and pMDI treated GnP-25 showed early degradation of the urethane. The Tg shows that there are vast changes in the microstructure. The increase in T_g of 3 °C for pMDI treated GnP-25 over the neat GnP-25 is probably due to local changes around the aggregates as the T_g for the foam and solid still match. The changes in T_g of caused by the addition of the pMDI treated GnP-5 demonstrated that the higher concentration of the moderately sized particles disrupts the network in both the monolith and

the foam although large variation in sample deviation results from a non-uniform dispersion. In addition, the foam samples with treated GnP(750) have a similar T_g to the standard. The only exception is the pMDI treated GnP(750), and images show they have large micron aggregates and could be reason it shows a similar T_g as the pMDI treated GnP-25. Edge-treatment of the smallest particles resulted in a similar cross-link density and were most affected by the edge treatment due to their higher edge density and did not interfere with the ability of the GnP to absorb heat, although the degradation profiles so that the shifts in onset temperature are about 50% less. These same profiles suggest that the addition of GnP tends to prevent the formation of isocyanurate, which the polymer compensates for by increasing the concentration of polyurea to maintain the cross-link density.

When it comes to cellular materials many properties decrease as the density and nanoparticle addition offer a unique way to overcome that effect, but can also create new challenges. The poor interaction of the GnP with the matrix resulted in the largest GnP showing a decrease in mechanical strength of about 40% over the standard due to the agglomerations confirmed by imaging. These aggregates act as stress concentrators decreasing the mechanical strength. Aggregation does not prevent the formation of a percolated network but may affect the critical concentration. At 5 wt% GnP-25 there was decrease in electrical resistivity of over 5 magnitudes. A much higher loading of the GnP-5 and GnP(750) that had a difference in aspect ratio of about 2.5 times showed similar electrical resistivity at the same concentration and images of the dispersion show that the agglomeration of the GnP-5 likely increases the critical concentration for percolation. While these aggregations may not affect the electrical properties there still have to be enough of them to form a percolated network, this becomes a bigger concern as the particles get smaller.

Edge-treatment was found only to be sufficient to reduce agglomeration when the edge density is high otherwise the basal plane character does, as demonstrated by the no change in the mechanical performance for the neat and edge-treated GnP-25. It is not just about the creating a good adhesion between the two, but also being careful in regards to the

molecular structure formed in these regions. Treating the GnP with chemical groups to improve interaction between the particles and the polymer resulted in the particles being electrically isolated due to the coating of polymer that was formed on the edges and offered minimal improvement int the mechanical strength. The electrical resistivity increased about three orders of magnitude with the treated GnP-25 over the neat. Using a minimal amount of edge-functionalization improved the electrical resistivity over the pMDI treated GnP(750) by about 3 magnitudes, however, in general the biggest factor was still the aspect ratio for GnP-5 and GnP(750) as the neat and treated GnP show similar electrical contact. The mechanical performance either did not change from the foam with non-treated GnP or the edge treatment resulted in a decrease of anywhere from 16 to 35% that was observed with the different treatments of the GnP(750). The only exception was the sample with 8 wt% pMDI GnP-5 that showed an average improvement of about 30% over the foam with 8 wt% GnP-5, although, the sample deviation was also the largest out of any of the samples and images showed the particles were still agglomerated.

GnP is a multifunctional nanoparticle that includes high electrical conductivity as well as a positive central core surrounded by a π-cloud of electrons properties that is beneficial for improving both the dielectric and EMI shielding properties. The dielectric properties improved by a factor of 2.2, 1.8, and 0.7 for the nanocomposite foam with neat GnP-25, GnP-5 and GnP(750), respectively. The real permittivity improved with electrical conductance, but not at the same degree because permittivity is a response of mobile and bound charges and larger particles seemed to demonstrate a stronger response; a significant factor that did not change by more than 20% when edge-treated. The large particles good for electrical contact were effective at reflecting the EM waves as the reflectance was about 8-9 times higher over the standard foam for GnP-25 and GnP-5 at 8.2 GHzand the GnP(750) was only about 6 times higher. But the smaller particles were good for absorbing them as at the same frequency the GnP(750) was about 5.5 times higher for absorbance compared to the neat GnP-5 and GnP-25 that only demonstrated triple the absorbance over the standard foam.

The EMI SE improved for all samples with both neat and treated GnP. The edge-treated GnP(750) about tripled the SE, GnP-5 and GnP(750) improved the SE by about 10 and 9 times, respectively and GnP-25 increased the SE about 12 times at 8.2 GHz, amounts that decreased by about 20% when the edges of the larger GnP were treated. This improvement tended to decrease at higher frequencies with GnP(750) out performing all of them due to the more significant frequency dependence demonstrated by the foam samples with neat and treated GnP-25 and GnP-5. It could be that the EMI SE would show improvement if the samples were tested at other frequencies.

6.2 Flexible Nancomposite PDMS Syntactic Foam

Adding GnP to PDMS resulted in improvement of the dielectric properties and shielding effectiveness of the samples including increasing the ability of the polymer to absorb electromagnetic waves likely by decreasing the skin depth. All of these improvements can be solely explained by the addition of the conducting particles. The greatest improvement was seen in the samples that had the highest loading of GnP in the solid. A large aspect ratio has been found to be an important property for achieving electrical percolation at lower loadings. The PDMS with 2 wt% GnP-25 increased the real permittivity about 2.5 times over the neat material and improved the SE effectiveness about 9 times at its highest while increasing the absorbance and reflectance. Compared to the PDMS sample with 1.6% more GnP that is mixture of two sizes of significantly smaller aspect ratio that were only able to double the dielectric constant. As for EMI SE there appears to be improvement, but is unclear by how much due to the strong dependence on frequency. However, the earlier shift of the resonance frequency by about 1 GHz suggests that the sample with 2 wt% GnP-25 is more conductive. Whether a percolated network formed in the system is unclear as the strong frequency dependence in the EMI shielding suggests a material that is still not behaving as a metallic conductor. If the GnP dispersion were more uniform and less aggregated that could result in a corresponding improvement in electrical performance by creating many more

connected paths. The challenge with increasing the diameter on the GnP creates a stronger attraction due the Van der Waals forces on the basal plane that preferentially aggregate rather than interact with the polymer.

PDMS already has applications in aerospace due to their flexibility at low temperatures and adding GnP seems to show promise as a multifunctional nanofiller for this material. Coating the HGS prior to dispersing in the polymer improved the behavior of the nanocomposite syntactic foam. It had the same real permittivity as the neat PDMS and improved the real permittivity by about 12% at only 0.64 wt% GnP. It demonstrated the same EMI SE as the neat and PDMS with 0.64 wt% GnP while still being 20% lighter. However, the resultant images of the foam are unclear on whether the GnP managed to stay adhered to the spheres during processing. Also the occasional clumps of coated spheres reduces the connectivity producing areas of high and low local conductance, the coated HGS could benefit from a more vigorous mixing prior to adding to the polymer to break up the clumps, but carefully so that the GnP stays adhered.

6.3 Future work for making nanocomposites with GnP

It appears that the key to improving the performance of nanocomposites is about smarter particle loading. Keeping in mind to choose reinforcing material that matches the matrix in terms of molecular groups and identify which groups create the ideal local molecular structure so that the local properties stay consistent throughout the foam and allows electron transfer to occur easily throughout the material. For particles with a platelet morphology such as GnP, choosing binders or surfactants that interact with the basal plane with naphthalene or pyrene compounds that would be functionalized to interact with the polymer could be done as a way to improve the the interaction. The larger particles produced a greater effect of the basal plane of the platelet and it is important to identify a way to functionalize the basal plane that does not include chemical bonds that would destroy its character. Since electrical conductance is important, edge-treatment, which does not effect the basal plane,

still increased the electrical resistivity. For PUR foam that has a microphase structure a more in depth investigation on how GnP affects size and distance between the hard and soft segments needs to be done to gain a better understanding of the physical interaction of GnP especially with size when the particles are well dispersed. Depending on where the GnP is preferentially located in the phase structure, it could affect the ability to form a percolated network especially as the particle size decreases. It could also be that changing the microphase of the polymer with GnP could improve the EMI SE or more specifically its absorbance capabilities. In addition some of these challenges could be met by using a combination of particle sizes to create a synergistic effect. This concept could offer significant improvement in the PDMS with 40 vol% GnP coated HGS by creating bridges between the conductive spheres. It could also help reduce the agglomerations in the foam, by allowing for lower loadings of the large GnP decreasing the amount or size of the aggregates that form.

REFERENCES

REFERENCES

[1] John Fuegi and Jo Francis. Lovelace and babbage and the creation of the 1843 'notes'. *IEEE Annals of the History of Computing*, pages 16–26, 2003.

[2] Sumio Iijima. Helical microtubules of graphitic carbon. *Nature*, 354(1):56–58, 1991.

[3] Petronela Pascariu, Anton Airinei, Mircea Grigoras, Loredana Vacareanu, and Felicia Iacomi. Applied Surface Science Metal – polymer nanocomposites based on Ni nanoparticles and polythiophene obtained by electrochemical method. *Applied Surface Science*, 352:95–102, 2015.

[4] Norazriena Yusoff, Alagarsamy Pandikumar, and Ramasamy Ramaraj. Gold nanoparticle based optical and electrochemical sensing of dopamine. *Microchim Acta*, 182:2091–2114, 2015.

[5] Deesy Pinto, Luís Bernardo, Ana Amaro, and Sérgio Lopes. Mechanical properties of epoxy nanocomposites using titanium dioxide as reinforcement – A review. *Construction and Building Materials*, 95:506–524, 2015.

[6] S. H. Yang, T. P. Nguyen, P. Le Rendu, and C. S. Hsu. Optical and electrical properties of PPV/SiO2 and PPV/TiO 2 composite materials. *Composites Part A: Applied Science and Manufacturing*, 36:509–513, 2005.

[7] Kyriaki Kalaitzidou, Hiroyuki Fukushima, and Lawrence T. Drzal. Multifunctional polypropylene composites produced by incorporation of exfoliated graphite nanoplatelets. *Carbon*, 45(7):1446–1452, 2007.

[8] Nadeem Iqbal, Mohammad Bilal Khan, Sadia Sagar, and Asghari Maqsood. Fabrication and characterization of multiwalled carbon nanotubes/silicone rubber composites. *Journal of Applied Polymer Science*, 128(4):2439–2446, may 2013.

[9] Hang Zhao, Yu-Juan Xia, Zhi-Min Dang, Jun-Wei Zha, and Guo-Hua Hu. Composition dependence of dielectric properties, elastic modulus, and electroactivity in (carbon black-BaTiO 3)/silicone rubber nanocomposites. *Journal of Applied Polymer Science*, 127(6):4440–4445, mar 2013.

[10] Yiqing Sun and Gaoquan Shi. Graphene/polymer composites for energy applications. *Journal of Polymer Science Part B: Polymer Physics*, 51(4):231–253, feb 2013.

[11] S. K. Samal, S. K. Nayak, and S. Mohanty. Polypropylene nano-composites: Effect of organo-modified layered silicates on mechanical, thermal and morphological performance. *Journal of Thermoplastic Composite Materials*, 21(3):243–263, 2008.

[12] Hyunwoo Kim, Ahmed a. Abdala, and Christopher W. MacOsko. Graphene/polymer nanocomposites. *Macromolecules*, 43(16):6515–6530, 2010.

[13] M. K. Corbierre, N. S. Cameron, M. Sutton, S. G J Mochrie, L. B. Lurio, A. Rühm, and R. B. Lennox. Polymer-stabilized gold nanoparticles and their incorporation into polymer matrices. *Journal of the American Chemical Society*, 123(42):10411–10412, 2001.

[14] N. Elango and a. a. M. Faudzi. A review article: investigations on soft materials for soft robot manipulations. *The International Journal of Advanced Manufacturing Technology*, 80:1027–1037, 2015.

[15] Jinglei Xiang and Lawrence T. Drzal. Templated growth of polyaniline on exfoliated graphene nanoplatelets (GNP) and its thermoelectric properties. *Polymer (United Kingdom)*, 53(19):4202–4210, 2012.

[16] L Lee, C Zeng, X Cao, X Han, J Shen, and G Xu. Polymer nanocomposite foams. *Composites Science and Technology*, 65(15-16):2344–2363, dec 2005.

[17] Mao Peng, Mingxing Zhou, Zhijiang Jin, Weiwei Kong, Zhongbin Xu, and Damien Vadillo. Effect of surface modifications of carbon black (CB) on the properties of CB/polyurethane foams. *Journal of Materials Science*, 45(4):1065–1073, dec 2009.

[18] Xiang-Bin Xu, Zhong-Ming Li, Lei Shi, Xiang-Cheng Bian, and Zhi-Dong Xiang. Ultralight conductive carbon-nanotube-polymer composite. *Small (Weinheim an der Bergstrasse, Germany)*, 3(3):408–11, mar 2007.

[19] a K Geim and K S Novoselov. The rise of graphene. *Nature materials*, 6(3):183–91, mar 2007.

[20] K S Novoselov, a K Geim, S V Morozov, D Jiang, Y Zhang, S V Dubonos, I V Grigorieva, and a a Firsov. Electric field effect in atomically thin carbon films. *Science (New York, N.Y.)*, 306(5696):666–9, oct 2004.

[21] Shanshan Chen, Qingzhi Wu, Columbia Mishra, Junyong Kang, Hengji Zhang, Kyeongjae Cho, Weiwei Cai, Alexander a. Balandin, and Rodney S. Ruoff. Thermal conductivity of isotopically modified graphene. *Nature Materials*, 11(3):203–207, 2012.

[22] Changgu Lee, Xiaoding Wei, Jeffrey W Kysar, and James Hone. Measurement of the Elastic Properties and Instrinsic Strength of Monolayer Graphene. *Science*, 321(July):385–388, 2008.

[23] R R Nair, P Blake, a N Grigorenko, K S Novoselov, T J Booth, T Stauber, N M R Peres, and a K Geim. Fine structure constant defines visual transparency of graphene. *Science (New York, N.Y.)*, 320(5881):1308, 2008.

[24] Jishan Wu, Wojciech Pisula, and Klaus Müllen. Graphenes as potential material for electronics. *Chemical reviews*, 107(3):718–47, mar 2007.

[25] Dongxing Yang, Aruna Velamakanni, Gülay Bozoklu, Sungjin Park, Meryl Stoller, Richard D. Piner, Sasha Stankovich, Inhwa Jung, Daniel a. Field, Carl a. Ventrice, and Rodney S. Ruoff. Chemical analysis of graphene oxide films after heat and chemical

treatments by X-ray photoelectron and Micro-Raman spectroscopy. *Carbon*, 47(1):145–152, jan 2009.

[26] Peter W Sutter, Jan-Ingo Flege, and Eli a Sutter. Epitaxial graphene on ruthenium. *Nature materials*, 7(5):406–11, may 2008.

[27] Alfonso Reina, Xiaoting Jia, John Ho, Daniel Nezich, Hyungbin Son, Vladimir Bulovic, Mildred S Dresselhaus, and Jing Kong. Large area, few-layer graphene films on arbitrary substrates by chemical vapor deposition. *Nano letters*, 9(1):30–5, jan 2009.

[28] a.J. Van Bommel, J.E. Crombeen, and a. Van Tooren. LEED and Auger electron observations of the SiC(0001) surface. *Surface Science*, 48(2):463–472, 1975.

[29] Walt a. de Heer, Claire Berger, Xiaosong Wu, Phillip N. First, Edward H. Conrad, Xuebin Li, Tianbo Li, Michael Sprinkle, Joanna Hass, Marcin L. Sadowski, Marek Potemski, and Gérard Martinez. Epitaxial graphene. *Solid State Communications*, 143(1-2):92–100, jul 2007.

[30] Claire Berger, Zhimin Song, Xuebin Li, Xiaosong Wu, Nate Brown, Cécile Naud, Didier Mayou, Tianbo Li, Joanna Hass, Alexei N Marchenkov, Edward H Conrad, Phillip N First, and Walt a de Heer. Electronic confinement and coherence in patterned epitaxial graphene. *Science (New York, N.Y.)*, 312(5777):1191–6, may 2006.

[31] Christopher D. Simpson, J. Diedrich Brand, Alexander J. Berresheim, Laurence Przybilla, Hans Joachim Räder, and Klaus Müllen. Synthesis of a giant 222 carbon graphite sheet. *Chemistry - A European Journal*, 8(6):1424–1429, 2002.

[32] Xiaoyin Yang, Xi Dou, Ali Rouhanipour, Linjie Zhi, Hans Joachim Räder, and Klaus Müllen. Two-dimensional graphene nanoribbons. *Journal of the American Chemical Society*, 130(13):4216–7, apr 2008.

[33] Héctor a. Becerril, Jie Mao, Zunfeng Liu, Randall M. Stoltenberg, Zhenan Bao, and Yongsheng Chen. Evaluation of solution-processed reduced graphene oxide films as transparent conductors. *ACS Nano*, 2(3):463–470, 2008.

[34] William S. Hummers and Richard E. Offeman. Preparation of Graphitic Oxide. *Journal of the American Chemical Society American Chemical Society*, 80:1339, 1957.

[35] B. C. Brodie. On the atomic weight of graphite. *Philisophical Transactions of the Royal Society of London*, 149:249–259, 1859.

[36] Tamás Szabó, Ottó Berkesi, Péter Forgó, Katalin Josepovits, Yiannis Sanakis, Dimitris Petridis, and Imre Dékány. Evolution of surface functional groups in a series of progressively oxidized graphite oxides. *Chemistry of Materials*, 18(11):2740–2749, 2006.

[37] Anton Lerf, Heyong He, Michael Forster, and Jacek Klinowski. Structure of Graphite Oxide Revisited. *Journal of Physical Chemistry B*, 102(23):4477–4482, 1998.

[38] Hannes C Schniepp, Je-luen Li, Michael J Mcallister, Hiroaki Sai, Margarita Herrera-alonso, Douglas H Adamson, Robert K Prud, Roberto Car, Dudley a Saville, and Ilhan a Aksay. Functionalized Single Graphene Sheets Derived from Splitting Graphite Oxide. *J of Physical Chemistry B Letters*, 2:8535–8539, 2006.

[39] Inhwa Jung, Dmitriy a Dikin, Richard D Piner, and Rodney S Ruoff. Tunable electrical conductivity of individual graphene oxide sheets reduced at "low" temperatures. *Nano letters*, 8(12):4283–7, dec 2008.

[40] Michael J Mcallister, Je-luen Li, Douglas H Adamson, Hannes C Schniepp, Ahmed a Abdala, Jun Liu, O Margarita Herrera-alonso, David L Milius, Roberto Car, Robert K Prud, and Ilhan a Aksay. Expansion of Graphite. *Society*, 19(4):4396–4404, 2007.

[41] Owen C Compton, Dmitriy a Dikin, Karl W Putz, L Catherine Brinson, and Sonbinh T Nguyen. Electrically conductive "alkylated" graphene paper via chemical reduction of amine-functionalized graphene oxide paper. *Advanced materials (Deerfield Beach, Fla.)*, 22(8):892–6, feb 2010.

[42] Sasha Stankovich, Dmitriy a. Dikin, Richard D. Piner, Kevin a. Kohlhaas, Alfred Kleinhammes, Yuanyuan Jia, Yue Wu, SonBinh T. Nguyen, and Rodney S. Ruoff. Synthesis of graphene-based nanosheets via chemical reduction of exfoliated graphite oxide. *Carbon*, 45(7):1558–1565, jun 2007.

[43] Matthew J Allen, Vincent C Tung, and Richard B Kaner. Honeycomb carbon: a review of graphene. *Chemical reviews*, 110(1):132–45, jan 2010.

[44] Huang Wu and Lawrence T. Drzal. Graphene nanoplatelet paper as a light-weight composite with excellent electrical and thermal conductivity and good gas barrier properties. *Carbon*, 50(3):1135–1145, 2012.

[45] Sasha Stankovich, Dmitriy a Dikin, Geoffrey H B Dommett, Kevin M Kohlhaas, Eric J Zimney, Eric a Stach, Richard D Piner, SonBinh T Nguyen, and Rodney S Ruoff. Graphene-based composite materials. *Nature*, 442(7100):282–6, jul 2006.

[46] Weili Wei and Xiaogang Qu. Extraordinary physical properties of functionalized graphene. *Small (Weinheim an der Bergstrasse, Germany)*, 8(14):2138–51, jul 2012.

[47] Dorsa Parviz, Sriya Das, H S Tanvir Ahmed, Fahmida Irin, Sanjoy Bhattacharia, and Micah J Green. Dispersions of non-covalently functionalized graphene with minimal stabilizer. *ACS nano*, 6(10):8857–67, oct 2012.

[48] Jingquan Liu, Wenrong Yang, L E I Tao, D A N Li, Cyrille Boyer, and Thomas P Davis. Thermosensitive Graphene Nanocomposites Formed Using Pyrene- Terminal Polymers Made by RAFT Polymerization. *Journal of Polymer Science: Part A: Polymer Chemistry*, 48:425–433, 2010.

[49] NASA. Nasa space technology research fellowships (nstrf). `https://www.nasa.gov/directorates/spacetech/strg/archives_nstrf.html#.VxmYoRIrK34`.

[50] 2015 NASA Technology Roadmaps.

[51] Kaneyoshi Ashida. *Polyurethane and Related Foams: Chemistry and Technology*. Taylor and Francis Group, LLC, 2007.

[52] Sheng-Hong Yao, Zhi-Min Dang, Mei-Juan Jiang, Hai-Ping Xu, and Jinbo Bai. Influence of aspect ratio of carbon nanotube on percolation threshold in ferroelectric polymer nanocomposite. *Applied Physics Letters*, 91(21):212901, 2007.

[53] J.P. Cohen-Addad, C Roby, and M Sauviat. Characterization of chain binding to filler in silicone-silica systems. *Polymer*, 26:1231–1233, 1985.

[54] Huntsman. Polyurethanes Product Line. `www.huntsman.com/Internet/html_includes/polyurethanes/ace/2010_ACE_Product_Line_Brochure.pdf`, 2013.

[55] Columbus Chemicals Industries. `www.columbuschemical.com/products/solvents/`.

[56] Manfred Kapps and Siegfried Buschkamp. The production of rigid polyurethane foam. Technical report, Bayer MaterlScience, 2004.

[57] Air Products. `www.airproducts.com/products/overview.aspx`.

[58] TCI America. `www.tcichemicals.com/eshop/en/us/commodity/T0264/`.

[59] Momentive. Rtv615: Technical data sheet. `www.momentive.com/Categories/Adhesives-and-Sealants/RTV615.aspx`, 2014.

[60] 3M™. Glass bubbles im16k: Product information. `www.3M.com\engineeredadditives`, 2013.

[61] Inc) (Gelest. Silane coupling agents: Connecting Across Boundaries. Technical Report 2, Gelest, Inc., Morrisville, PA, 2006.

[62] Jian-Hao Chen, Chaun Jang, Shudong Xiao, Masa Ishigami, and Michael S Fuhrer. Intrinsic and extrinsic performance limits of graphene devices on SiO2. *Nature nanotechnology*, 3(4):206–209, 2008.

[63] XG Sciences. `xgsciences.com/products/graphene-nanoplatelets/`, 2013.

[64] John F. Moulder, William F. Stickle, Peter E. Sobol, and Kenneth D. Bomben. *Handbook of X-ray Photoelectron Spectroscopy: A Reference Book of Standard Spectra for Identification and Intrepretation of XPS Data*. Perkin-Elmer Corpporation, Physical Electronics Division, Eden Prairie, 1992.

[65] A. M. Nicolson and G. F. Ross. Measurement of the Intrinsic Properties of Materials by Time-Domain Techniques. *IEEE Transactions on Instrumentation and Measurement*, 19(4):377–382, 1970.

[66] William B Weir. Automatic Measurement of Complex Dielectric Constant and Permeability. In *Proceedings of the IEEE*, volume 62, pages 33–36, 1974.

[67] Y. K. Hong, C. Y. Lee, C. K. Jeong, D. E. Lee, K. Kim, and J. Joo. Method and apparatus to measure electromagnetic interference shielding efficiency and its shielding characteristics in broadband frequency ranges. *Review of Scientific Instruments*, 74(2):1098–1102, 2003.

[68] Hao-Bin Zhang, Qing Yan, Wen-Ge Zheng, Zhixian He, and Zhong-Zhen Yu. Tough graphene-polymer microcellular foams for electromagnetic interference shielding. *ACS applied materials and interfaces*, 3(3):918–24, mar 2011.

[69] Yonglai Yang, Mool C Gupta, Kenneth L Dudley, and Roland W Lawrence. Novel carbon nanotube-polystyrene foam composites for electromagnetic interference shielding. *Nano letters*, 5(11):2131–4, nov 2005.

[70] Jean-Michel Thomassin, Isabelle Huynen, Robert Jerome, and Christophe Detrembleur. Functionalized polypropylenes as efficient dispersing agents for carbon nanotubes in a polypropylene matrix; application to electromagnetic interference (EMI) absorber materials. *Polymer*, 51(1):115–121, jan 2010.

[71] Varrla Eswaraiah, Venkataraman Sankaranarayanan, and Sundara Ramaprabhu. Functionalized Graphene-PVDF Foam Composites for EMI Shielding. *Macromolecular Materials and Engineering*, 296(10):894–898, oct 2011.

[72] Shoichiro Ozaki and Tsutomu Nagoya. On the Thermal Dissociation of Organic Compounds. XII. The Effects of the Substituents on the Thermal Dissociation of Substituted Phenylureas. *Bulletin of the Chemical Society of Japan*, 30(5):444–449, 1957.

[73] Norman Grassie and Gilberto A.Perdomo Mendoza. Thermal degradation of polyether-urethanes: Part 4—Effect of ammonium polyphosphate on the thermal degradation of polyether-urethanes prepared from methylene bis(4-phenylisocyanate) and low molecular weight poly(ethylene glycols). *Polymer Degradation and Stability*, 11(2):145–166, 1985.

[74] Vincent Gajewski. Chemical degradation of polyurethane. *Rubber World*, pages 15–18, 1990.

[75] Luigi Stradella and Massimo Argentero. A study of the thermal decomposition of urea, of related compounds and thiourea using DSC and TG-EGA. *Thermochimica Acta*, 219:315–323, may 1993.

[76] Xiaobin Li, Hongbin Cao, and Yi Zhang. Structures and physical properties of rigid polyurethane foams with water as the sole blowing agent. *Science in China Series B: Chemistry*, 49(4):363–370, aug 2006.

[77] Jozef Rychlý, Agnes Lattuati-Derieux, Bertrand Lavédrine, Lyda Matisová-Rychlá, Marta Malíková, Katarína Csomorová, and Ivica Janigová. Assessing the progress of degradation in polyurethanes by chemiluminescence and thermal analysis. II. Flexible polyether- and polyester-type polyurethane foams. *Polymer Degradation and Stability*, 96(4):462–469, apr 2011.

[78] John Chambers, Josef Jiricny, and Colin B Reese. The Thermal Decomposition of Polyurethanes and Polyisocyanurates. *Fire and Materials*, 5(4):133–141, 1981.

[79] Peter M. Schaber, James Colson, Steven Higgins, Daniel Thielen, Bill Anspach, and Jonathan Brauer. Thermal decomposition (pyrolysis) of urea in an open reaction vessel. *Thermochimica Acta*, 424(1-2):131–142, dec 2004.

[80] C. Dick, E. Dominguez-Rosado, B. Eling, J.J. Liggat, C.I. Lindsay, S.C. Martin, M.H. Mohammed, G. Seeley, and C.E. Snape. The flammability of urethane-modified polyisocyanurates and its relationship to thermal degradation chemistry. *Polymer*, 42:913–923, 2001.

[81] Marius Reinecker, Viktor Soprunyuk, Martin Fally, Antoni Sánchez-Ferrer, and Wilfried Schranz. Two glass transitions of polyurea networks: effect of the segmental molecular weight. *Soft matter*, 10(31):5729–38, 2014.

[82] M. Mar Bernal, Isabel Molenberg, Sergio Estravis, Miguel Angel Rodriguez-Perez, Isabelle Huynen, Miguel Angel Lopez-Manchado, and Raquel Verdejo. Comparing the effect of carbon-based nanofillers on the physical properties of flexible polyurethane foams. *Journal of Materials Science*, 47(15):5673–5679, mar 2012.

[83] E Pop, V Varshney, and Ak Roy. Thermal properties of graphene: Fundamentals and applications. *Mrs Bulletin*, 1273:1–28, 2012.

[84] Jin Ho Bang and Kenneth S Suslick. Applications of ultrasound to the synthesis of nanostructured materials. *Advanced materials (Deerfield Beach, Fla.)*, 22(10):1039–59, mar 2010.

[85] Marcelo Antunes, Miguel Mudarra, and José Ignacio Velasco. Broad-band electrical conductivity of carbon nanofibre-reinforced polypropylene foams. *Carbon*, 49(2):708–717, feb 2011.

[86] Joanna C H Wong, Elena Tervoort, Stephan Busato, Paolo Ermanni, and Ludwig J Gauckler. Engineering macroporous composite materials using competitive adsorption in particle-stabilized foams. *Journal of colloid and interface science*, 383(1):1–12, oct 2012.

[87] Lorna J Gibson and Michael F Ashby. *Cellular Solids: Structures and Properties*. Cambridge University Press, Cambridge, 2 edition, 1997.

[88] DX Yan, Kun Dai, ZD Xiang, and ZM Li. Electrical conductivity and major mechanical and thermal properties of carbon nanotube filled polyurethane foams. *Journal of Applied ...*, 120(5):3014–3019, 2011.

[89] Harry Kesten. What is Percolation. *Notices of the AMS*, pages 572–573, apr 2006.

[90] F Carmona, P Prudhon, F Barreau, Centre De Recherche, Paul Pascal, and Domaine Universitaire. Percolation in short fibres epoxy resin composites: conductivity behavior and finite size effects near threshold. *Solid State Communications*, 51(4):255–257, 1984.

[91] A van Itterbeek and K de Clippeleir. Measurements on the dielectric constant of carbon dioxide as a function of pressure and temperature. *Physica*, 13(8):459–464, 1947.

[92] J. W. Schmidt and M. R. Moldover. Dielectric Permittivity of Eight Gases Measured with Cross Capacitors. *International Journal of Thermophysics*, 24(2):375–403, 2003.

[93] Isabel Molenberg, Isabelle Huynen, Anne-christine Baudouin, Jean-michel Thomassin, and Christophe Detrembleur. Foamed Nanocomposites for EMI Shielding Applications. In *Advanced Microwave and Millimeter Wave Technologies: Semiconductor Devices Circuits and Systems*, pages 453–470. InTech Open Access Publisher, 2010.

[94] Andreas Noll, Klaus Friedrich, Thomas Burkhart, and Ulf Breuer. Effective Multifunctionality of Poly (p -phenylene sulfide) Nanocomposites Filled With Different Amounts of Carbon Nanotubes , Graphite , and Short Carbon Fibers. *Polymer Composites*, 34(9):1405–1412, 2013.

[95] Limeng Chen, Behic K. Goren, Rahmi Ozisik, and Linda S. Schadler. Controlling bubble density in MWNT/polymer nanocomposite foams by MWNT surface modification. *Composites Science and Technology*, 72(2):190–196, jan 2012.

[96] Ken-Hsuan Liao, Yuqiang Qian, and Christopher W. Macosko. Ultralow percolation graphene/polyurethane acrylate nanocomposites. *Polymer*, 53(17):3756–3761, aug 2012.

[97] Mohammad A Rafiee, Javad Rafiee, Zhou Wang, Huaihe Song, Zhong-zhen Yu, and Nikhil Koratkar. Enhanced Mechanical Properties of Nanocomposites at Low Graphene Content. *ACS Nano*, 3(12):3884–3890, 2009.

[98] S. R. Kim. Thermal diffusivity of in-situ exfoliated graphite intercalated compound/polyamide and graphite/polyamide composites. *Express Polymer Letters*, 6(6):476–484, apr 2012.

[99] Raquel Verdejo, Francisco J Tapiador, Lukas Helfen, M Mar Bernal, Natacha Bitinis, and Miguel a Lopez-Manchado. Fluid dynamics of evolving foams. *Physical chemistry chemical physics : PCCP*, 11(46):10860–6, dec 2009.

[100] Changchun Zeng, Nemat Hossieny, Chuck Zhang, and Ben Wang. Synthesis and processing of PMMA carbon nanotube nanocomposite foams. *Polymer*, 51(3):655–664, feb 2010.

[101] Egidio Rizzi, Enrico Papa, and Alberto Corigliano. Mechanical behavior of a syntactic foam: experiments and modeling. *International Journal of Solids and Structures*, 37(40):5773–5794, oct 2000.

[102] Jie Gao, Jibin Wang, Haiyan Xu, and Chifei Wu. Preparation and properties of hollow glass bead filled silicone rubber foams with low thermal conductivity. *Materials and Design*, 46:491–496, apr 2013.

[103] Erwin M. Wouterson, Freddy Y.C. Boey, Xiao Hu, and Shing-Chung Wong. Specific properties and fracture toughness of syntactic foam: Effect of foam microstructures. *Composites Science and Technology*, 65(11-12):1840–1850, sep 2005.

[104] R. R. Nair, M. Sepioni, I-Ling Tsai, O. Lehtinen, J. Keinonen, a. V. Krasheninnikov, T. Thomson, a. K. Geim, and I. V. Grigorieva. Spin-half paramagnetism in graphene induced by point defects. *Nature Physics*, 8(3):199–202, 2012.

[105] William H. Jr. Hayt. *Engineering Electromagnetics*. McGraw-Hill, 5th edition, 1989.

[106] Chris Bishop. The Relationship Between Loss, Conductivity and Dielectric Constant, 2001.